Computer Methods in Applied Mechanics and Engineering 103 (1993) 43–114
North-Holland

CMA 390

Optimization of composite, stiffened, imperfect panels under combined loads for service in the postbuckling regime

David Bushnell
Lockheed Palo Alto Research Laboratory, Palo Alto, CA 94304, USA

Received 16 September 1992
Revised manuscript received 17 November 1992

Local buckling and postbuckling of panels stiffened by stringers and rings and subjected to combined in-plane loads is explored with the use of a single module model that consists of one stringer and a width of panel skin equal to the stringer spacing. The cross-section of the skin-stringer module is discretized and the displacement field is assumed to vary trigonometrically in the axial direction. Local imperfections in the form of local buckling modes and overall initial axial bowing of the panel are included in the numerical model. The local postbuckling theory, based on early work of Koiter, is formulated in terms of buckling modal coefficients derived from integrals of products of the discretized displacement field and its derivatives. The principle of minimum potential energy is used to derive nonlinear algebraic equilibrium equations in terms of four unknowns, the amplitude f of the postbuckling displacement field, a postbuckling 'flattening' parameter a, the slope m of the nodal lines in the postbuckling displacement field, and an axial wavelength parameter N. The nonlinear equations are solved by Newton's method. An elaborate strategy is introduced in which the incidence of non-convergence is minimized by removal and re-introduction of the unknowns f, a, m, N on a one-by-one basis. This nonlinear theory has been implemented in the PANDA2 computer program, which finds minimum-weight designs of stiffened panels made of composite materials. PANDA2 is used to find the minimum weight of a cylindrical panel made of isotropic material with rectangular stringers mounted on thickened bases. The panel is optimized for three load sets, axial compression with negative axial bowing, axial compression with positive axial bowing, and combined axial compression and in-plane shear with no axial bowing. The optimum design is loaded well beyond local buckling for each load set. Critical margins of the optimized design include maximum allowable effective stress, bending-torsion buckling and general instability. The optimum design is evaluated by application of a general-purpose finite element program, STAGS, to finite element models generated by PANDA2 for each of the three load sets. The agreement of results between PANDA2 and STAGS is good enough to qualify PANDA2 as a preliminary design tool.

1. Introduction

There is an extensive literature on the buckling and postbuckling behavior of stiffened plates and shells. This literature covers metallic panels and panels fabricated from laminated composite materials. Leissa [1] has gathered results from almost 400 sources on the buckling

Correspondence to: David Bushnell, Consulting Scientist, Lockheed Palo Alto Research Laboratory, 3251 Hanover St., Palo Alto, CA 94304, USA.

and postbuckling behavior of flat and cylindrical panels made of composite material with various stacking sequences and boundary conditions and subjected to various in-plane loads. The emphasis in his survey is on theoretical results, although some experimental results are included. He includes several examples in which the effect of transverse shear deformation is explored. Emphasis is given also to the effects of anisotropy on bifurcation buckling and on postbuckling behavior. Wiggenraad [2] surveys the literature on design of composite panels permitted to buckle locally under operating loads. Included in his survey are damage tolerance, fatigue and optimization. Arnold and Parekh [3] emphasize in their survey and theoretical development the effect of in-plane shear load on the postbuckling behavior of stiffened, composite cylindrical panels. Surveys of earlier work on buckling of stiffened panels and shells appear in [4–6]. The Baruch–Singer theory [7] for averaging the properties of stiffeners over a shell surface while retaining the important eccentricity effects has been incorporated into many widely used computer programs for the stress, vibration and buckling analysis of stiffened shells.

The literature in the field of buckling of stiffened shells can be divided into three categories, one in which test results are emphasized, a second in which structural analysis is emphasized and a third in which optimum designs are obtained. References [8–18] feature test results for plates, shells and stiffeners made of laminated composite material; [19–27] feature structural analysis with structural properties fixed, and [28–39] feature structural analysis with optimum configurations sought in most cases via the widely used optimizers CONMIN or ADS, written by Vanderplaats and his colleagues [40–43]. This is just a sample of the literature on the subject. The reader is referred to the surveys given in [1–6] and references cited there for other sources.

2. Capabilities of PANDA2

PANDA2 finds minimum weight designs of laminated composite flat or curved cylindrical panels or cylindrical shells with stiffeners in one or two orthogonal directions. Stiffeners can be blades, tees, angles or hats. Truss-core sandwich panels can also be handled. Recently the capability of finding optimum designs of isogrid panels has been added. The panels or shells can be loaded by as many as five combinations of in-plane loads, edge moments, normal pressure and temperature. The material properties can be temperature-dependent. The axial load can vary across the panel. The presence of overall (bowing) imperfections as well as local imperfections in the form of the local buckling mode are included. Constraints on the design include local buckling of the stiffener parts and rolling of the stiffeners, local and general buckling of the panel, maximum displacement under pressure, maximum tensile or compressive stress along the fibers and normal to the fibers in each lamina, and maximum in-plane shear stress in each lamina.

Local and general buckling loads are calculated with use of either closed-form expressions or with use of discretized models of panel cross-sections. The discretized model is based on one-dimensional discretization similar to that used in the BOSOR4 computer code [44]. An analysis branch exists in which local post buckling of the panel skin is accounted for. In this branch a constraint condition that prevents stiffener popoff is introduced into the optimization

calculations. The postbuckling theory incorporated into PANDA2 is similar to that formulated by Koiter for panels loaded into the far-postbuckling regime [45].

PANDA2 can be run in five modes: simple analysis of a fixed design, optimization, test simulation, design sensitivity and load-interaction. Plots of decision variables, margins and weight versus design iterations can be obtained following use of PANDA2 in the optimization mode. Plots of user-selected behaviors versus load can be obtained following use of PANDA2 in the test-simulation mode. Plots of margins versus a user-selected design variable can be obtained following use of PANDA2 in the design sensitivity mode. Plots of in-plane load interaction curves and margins versus load combination number can be obtained following use of PANDA2 in the load-interaction mode.

There is a processor in the PANDA2 system that automatically generates an input file for the STAGS computer program [22, 23]. Thus, STAGS, which is a general purpose nonlinear finite element analyzer, can easily be used to check the load-carrying capacity of panels designed with PANDA2.

Note that the theory on which PANDA2 is based is valid only if the panel is either unstiffened or, if stiffeners exist in either or both coordinate directions, there are several of them within the span of the panel. One cannot accurately determine the behavior of a panel with only one stiffener, for example. The panel, if axially stiffened, for example, has a 'field' of equally spaced, identical stringers.

In PANDA2 local buckling behavior is predicted from analysis of a single module which is assumed to repeat several times over the width of the panel, as shown for example in Fig. 1.

A panel module consists of one stiffener plus skin of width equal to the spacing between stiffeners. The single module is considered to be composed of segments, each of which has its own laminated wall construction. The cross-section of a single panel module is shown in Fig. 2 and the conventions used in PANDA2 for numbering the segments and the nodal points in the module are displayed in Fig. 3. The segments are discretized as shown in Figs. 4(a) and 5(a),

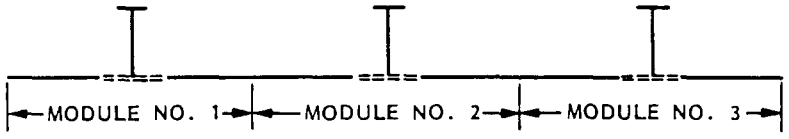

Fig. 1. Tee-stiffened panel with three modules.

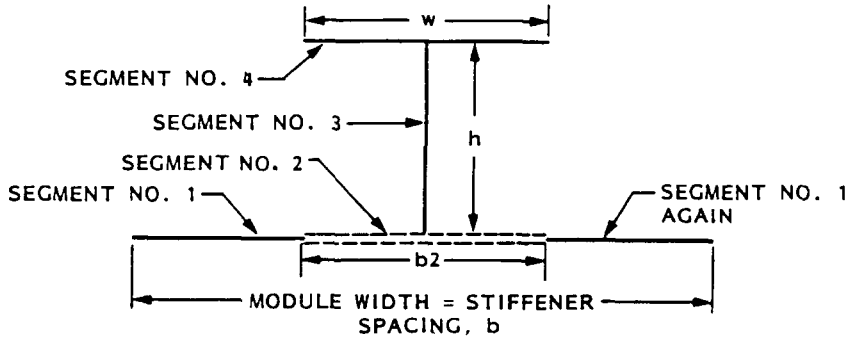

Fig. 2. A single panel module. Each segment may have its own composite laminate.

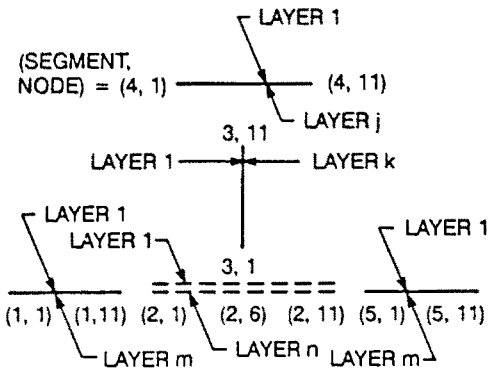

Fig. 3. Segment and nodal point numbering and layer numbering convention for a single panel module.

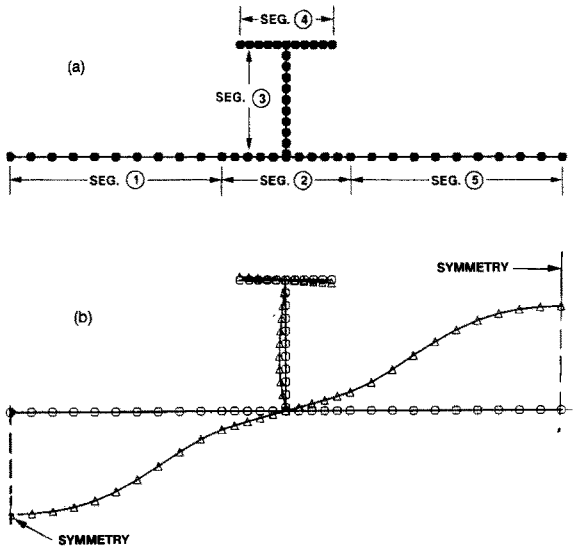

Fig. 4. (a) Discretized single panel module with Tee stiffener. (b) Local buckling mode that is antisymmetric. The power n in (24b) is three for this type of stringer.

for example. Details concerning the one-dimensional discretization (strip method) are provided in [44].

Local buckling modes calculated from the discretized single module models are shown in Fig. 4(b) for a Tee-stiffened panel and in Fig. 5(b) for a hat-stiffened panel. For blade, Tee

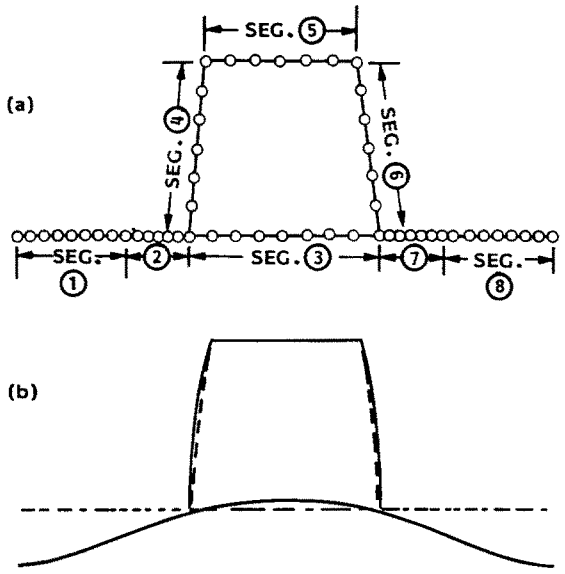

Fig. 5. (a) Discretized single panel module with hat stiffener. (b) Local buckling mode that is symmetric. The power n in (24b) is two for this type of stringer.

and Jay stiffened panels, the local buckling mode in the panel skin is antisymmetric about the line of intersection of the stringer web with the panel skin, as shown in Fig. 4(b), for example. For hat-stiffened panels the local buckling mode is symmetric about the symmetry plane of the panel module, as shown in Fig. 5(b). Local buckling modes for truss-core panels present a special case that is described in [48]. In the axial direction (normal to the plane of the paper) the local buckling modal displacement components u, v, w vary trigonometrically, with an integral number of axial halfwaves between rings. When in-plane shear loading N_{xy} is present, or when one or more segments of the panel module is anisotropic, the nodal lines of the local buckling pattern are generally not parallel to the plane of the panel module cross-section, but are slanted with a slope m with respect to this plane, as is shown in Fig. 9 of [5] and in Fig. 21 of this paper. The nodal line slope m is one of the unknowns of the bifurcation buckling and postbuckling analyses.

General instability is predicted from a model in which the stiffeners are 'smeared' in the manner of Baruch and Singer [7] over the width (stringers) and length (rings) of the panel. As described in [39], the effect of 'softening' of the panel skin and stringer segments due to local buckling is accounted for.

More details about PANDA2 appear in [39, 46–51].

3. Post-local buckling theory used in PANDA2

3.1. Introduction

It is assumed that when the panel is loaded by uniform applied in-plane axial, hoop and shear resultants, N_1, N_2, N_{12}, respectively, it deforms in a uniform manner, that is, its edges remain straight and parallel. The effect of normal pressure or load eccentricity is to create an axial curvature change κ_x that increases with the ratio $\lambda_G/(\lambda_G - 1)$, where λ_G is the load factor corresponding to a preliminary estimate of general instability. The local buckling and postbuckling theory is based on the assumption that the local buckling and postbuckling behavior of a single panel module represents the local buckling and postbuckling behavior of the entire panel.

The cross-section of the single panel module is discretized as shown in Fig. 4(a), and variation of the deformation in the axial direction, that is, normal to the plane of the paper, is trigonometric. The projection of the bifurcation buckling mode ϕ and post-bifurcation deformation on the plane of the panel module cross-section is assumed to be symmetric midway between axial stiffeners (stringers), as shown in Figs. 4(b) and 5(b). The nodal lines of the local buckling mode and postbuckling deformation are assumed to have a slope m that is constant over the panel module cross-section, as shown in Fig. 21, for example.

The expression for the normal displacement distribution in the panel skin, $w(x, y)$ is given by (12) and (24b). The objective of the lengthy derivation in this chapter is to obtain nonlinear algebraic equations for the unknowns, f, a, m, N, where f is the amplitude of the local buckles, a is a local buckling mode modification parameter (eq. (24b)), m is the slope of the nodal lines in the locally buckled panel skin, and N is inversely proportional to the square of the axial wavelength l of the local buckles (eq. (17a)).

The nonlinear theory presented here represents a refinement of that described in [50, 51].

In [50] the effect of rings (stiffeners that are parallel to the y-coordinate in Fig. 7) is not included, and in [51] the axial wavelength of the local buckling pattern is assumed to remain constant as the panel is loaded further and further into the local postbuckling regime. In addition, since [50, 51] were written, a rather elaborate strategy has been developed to ensure convergence to the appropriate nonlinear solution when no 'starting' solution is available. This is often the case in problems involving optimum design of a structure the behavior of which is highly nonlinear. Details of the strategy with examples are presented in this paper.

It is assumed in the theory presented here that the panel is flat. Experience has shown that optimized designs usually have rather closely spaced stringers. Therefore, the effect of panel skin curvature on the local postbuckling behavior is assumed to be small enough to neglect for the purpose of preliminary design, which is what PANDA2 is intended for.

If an axially stiffened panel has a finite imperfection in the form of the local buckling mode, there are no longer any distinct 'prebuckling' and 'postbuckling' phases of behavior. Rather, the panel deforms in a continuous manner as the external loads are increased. This difference in behavior for perfect and imperfect panels is illustrated in Fig. 6. An unstiffened, isotropic plate is subjected to uniform end shortening to an average axial load N_1 four times the load N_{cr} at which the perfect plate buckles locally. The imperfection, in the form of the bifurcation buckling mode of the perfect plate, has five halfwaves along the length and one halfwave across the width. Two cases are shown: one for an almost perfect plate with normalized

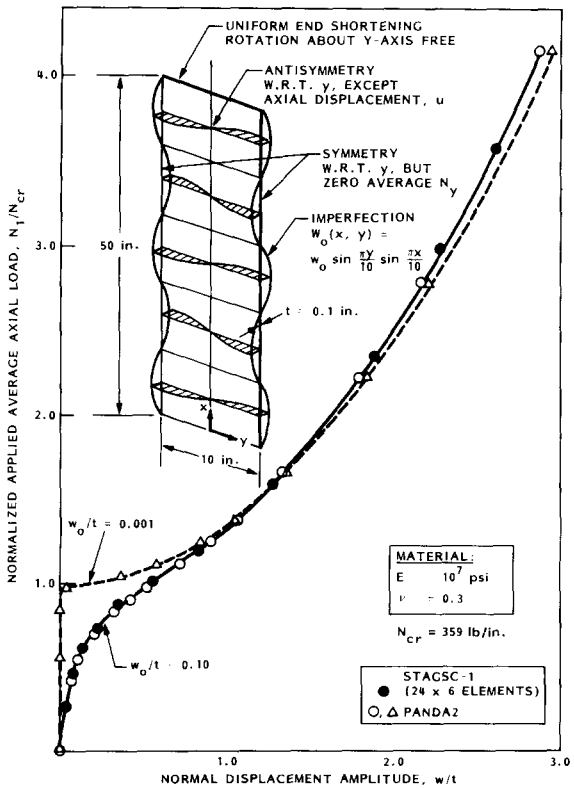

Fig. 6. Axially compressed imperfect flat plate: comparison of results from PANDA2 and STAGSC-1 (from [50]).

imperfection amplitude $w_0/t = 0.001$, and the other for a plate with $w_0/t = 0.1$. The almost perfect plate (imperfection amplitude $w_0/t = 0.001$) exhibits an almost discontinuous behavior at the bifurcation load, whereas the plate with larger imperfection amplitude, $w_0/t = 0.1$, exhibits a continuous softening followed by stiffening behavior. In Fig. 6 results from PANDA2 are compared with those from STAGS.

Two computational advantages result from the inclusion of local imperfections:

1. The behavior of stiffened panels that have been optimized is often sensitive to imperfections. If imperfections are neglected in the theory, the program user must provide a significant factor of safety to compensate for random geometric imperfections that are always present in practical structures. It is difficult to choose an appropriate factor of safety. Introduction of an imperfection in the form of the local buckling mode of the perfect structure partially eliminates this difficulty. While it may still be necessary to introduce a factor of safety larger than unity, the factor can be much closer to unity and can be thought of as a factor to compensate for uncertainties in load, material properties and failure criteria rather than as a factor to compensate for uncertainty in geometry. Uncertainties in load, material properties and failure criteria generally do not affect the behavior with increasing severity, as does uncertainty in geometry, as the structure approaches its optimum configuration. Therefore, it is particularly advantageous to include the effect of uncertainty in geometry in the structural analysis rather than to compensate for it by use of a large, rather arbitrary, factor of safety.
2. Because of discontinuous behavior such as that exhibited in Fig. 6 for the almost perfect panel, design iterations often lead to designs and margins that jump around from iteration to iteration. For example, this behavior occurred during optimization of the ARIANE interstage, and is evident in Figs. 88 and 89 of [39]. Introduction of a local imperfection smooths the behavior, as displayed in Fig. 6 for the panel with the larger imperfection amplitude. Therefore, gradients of behavior of imperfect panels with respect to design perturbations are generally smooth. They do not ordinarily lead to erratic swings in design or in design margins as the optimum configuration is sought.

3.2. Components of strain energy and external work

The following derivation applies to panels that consist of segments each of which has a balanced laminate. Most of the derivation involves the extensional strain energy of the panel skin and stiffener web(s) and flanges. The relevant geometry is shown in Figs. 2 and 7: a single panel module including one stringer and a width of panel skin that represents the spacing b of the stringers. Equilibrium equations are derived from the principle of virtual work and the first variation of the total potential, $U - W$, in which U is the strain energy and W is the work done by average prescribed axial, hoop and in-plane shear external loads, N_1, N_2, N_{12}, respectively.

NOTE. The effect of normal pressure is handled in another part of the PANDA2 code. By the time calculations in PANDA2 have entered the part of the code that is described here (called SUBROUTINE KOIT2 in PANDA2), the effect of normal pressure has been converted into overall bending of the panel as amplified by in-plane destabilizing applied loads (represented here by axial curvature change κ_x) and the associated local redistribution of the internal in-plane loads N_x, N_y, N_{xy} over the cross-section of the skin-stringer module. These

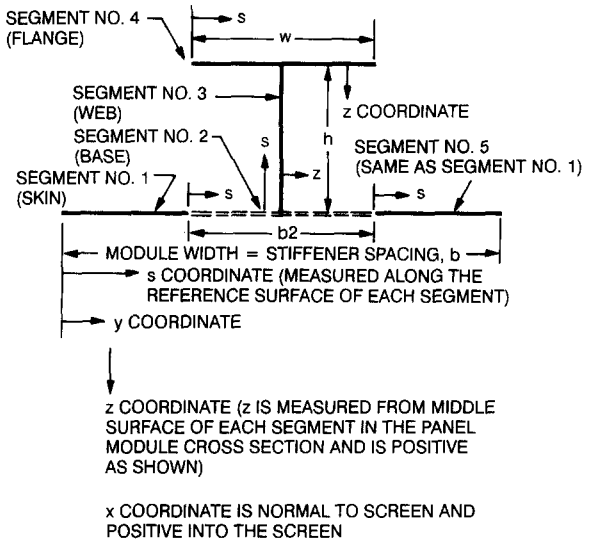

Fig. 7. Local coordinates in a panel module.

internal loads affect the local buckling load factor and mode, also found previously in PANDA2 (in SUBROUTINES LOCAL and MODE). Details about the overall and local static response of the panel to normal pressure appear in [39, 47].

For balanced laminates the components of strain energy are

1. first variation of extensional energy in panel skin (including stringer base):

$$U'_{\text{ext}}(\text{skin}) = \int_0^{2l}\int_0^b (N_x e'_x + N_y e'_y + N_{xy} e'_{xy})\,\mathrm{d}y\,\mathrm{d}x\,; \tag{1}$$

2. first variation of extensional energy in stringer web(s) and flange and ring web(s) and flange:

$$U'_{\text{ext}}(\text{stringer}) = \int_0^{2l}\sum_{i=3}^{4}\int_0^{\text{width}_i} (N_x^i e_x^{i\prime} + N_s^i e_s^{i\prime} + N_{xs}^i e_{xs}^{i\prime})\,\mathrm{d}s\,\mathrm{d}x\,, \tag{2a}$$

$$U'_{\text{ext}}(\text{ring}) = \int_0^{b}\sum_{i=3}^{4}\int_0^{\text{width}_i} (N_x^i e_x^{i\prime} + N_s^i e_s^{i\prime} + N_{xs}^i e_{xs}^{i\prime})\,\mathrm{d}s\,\mathrm{d}x\,; \tag{2b}$$

3. bending and twisting strain energy in the panel skin (including the stringer base):

$$U_{\text{bend}}(\text{skin}) = \frac{1}{2}\int_0^{2l}\int_0^b \{C_{44}w_{,xx}^2 + 2C_{45}w_{,xx}w_{,yy} + C_{55}w_{,yy}^2 + 4w_{,xy}(C_{46}w_{,xx} + C_{56}w_{,yy} + C_{66}w_{,xy})\}\,\mathrm{d}y\,\mathrm{d}x\,; \tag{3}$$

4. bending and twisting strain energy in the stringer web and flange:

$$U_{\text{bend}}(\text{stringer}) = \frac{1}{2}\int_0^{2l}\sum_{i=3}^{4}\int_0^{\text{width}_i}\{C^i_{44}w^2_{,xx} + 2C^i_{45}w_{,xx}w_{,ss} + C^i_{55}w^2_{,ss} + 4w_{,xs}(C^i_{46}w_{,xx} + C^i_{56}w_{,ss} + C^i_{66}w_{,xs})\}\,\mathrm{d}s\,\mathrm{d}x\,. \quad (4)$$

Bending and twisting energy of the rings are ignored. The tacit assumption in the theory presented here is that there are multiple axial halfwaves of the local buckling pattern between adjacent rings. In (1)–(4) $(\ )'$ denotes 'derivative with respect to a degree of freedom' (f, a, m, N, to be defined later); $(\ )_{,xx}$ means $\partial^2(\ )/\partial x^2$; b is the stringer spacing; l is the axial length of one half wave of the local buckling pattern; x is the axial coordinate; y is the transverse coordinate, measured from the left-hand side of the panel module as shown in Fig. 7; $i = 3$ denotes stiffener web (segment 3 in Fig. 7); $i = 4$ denotes outstanding stiffener flange (segment 4 in Fig. 7); width_i means width of the ith stiffener part (e.g. height h for the web and width w for the flange); and s is the local segment coordinate shown in Fig. 7. The C_{ij} in (3) and (4) are the coefficients of the integrated constitutive relationship that appear in (8.1) of [39]. The quantities N_x, N_y, N_{xy} are the stress resultants at x, y in the panel skin, and N^i_x, N^i_s, N^i_{xs} are the stress resultants at x, s in the stiffener web ($i = 3$) and stiffener flange ($i = 4$). The quantities e_x, e_y, e_{xy}, e_s, e_{xs} are the strain components in the reference surface, which herein is the middle surface, of each of the various segments of the panel module.

The first variation of the work done by the uniform external in-plane loads, N_1, N_2, N_{12}, is given by

$$W' = 2lb(N_1e'_1 + N_2e'_2 + N_{12}e'_{12})\,, \quad (5)$$

in which e_1, e_2, e_{12} are the average in-plane strains of the reference surface of the panel skin, and

$$N_1 = \frac{1}{b}\left\{\int_0^b N_x\,\mathrm{d}y + \sum_{i=3}^{4}\int_0^{\text{width}_i} N^i_x\,\mathrm{d}s\right\} \quad (6)$$

and

$$N_2 = \frac{1}{2l}\int_0^{2l} N_y\,\mathrm{d}x + \frac{1}{b_r}\sum_{i=3}^{4}\int_0^{\text{width}_i} N^i_x\,\mathrm{d}s\,, \quad (7)$$

in which b_r is the ring spacing. In (7) N^i_x denotes the stress resultant in the ith ring part along the axis of the ring. The in-plane shear resultant N_{12} is constant and equal to N_{xy} for ring-stringer configurations (not for truss-core sandwich or isogrid wall constructions). The internal axial resultant N_x is assumed to be constant in the x-direction, and the internal hoop resultant N_y is assumed to be constant in the y-direction. Therefore, we can write

$$N_1 = \frac{1}{2l}\int_0^{2l}\frac{1}{b}\left\{\int_0^b N_x\,\mathrm{d}y + \sum_{i=3}^{4}\int_0^{\text{width}_i} N^i_x\,\mathrm{d}s\right\}\mathrm{d}x \quad (8)$$

and

$$N_2 = \frac{1}{2l}\frac{1}{b}\int_0^{2l}\int_0^b N_y\,\mathrm{d}y\,\mathrm{d}x + \frac{1}{b_r}\sum_{i=3}^{4}\int_0^{\text{width}_i} N^i_x\,\mathrm{d}s\,. \quad (9)$$

The derivatives of the strains with respect to the degrees of freedom (as yet unspecified) of the

problem can be expressed as derivatives of uniform average strains and increments, thus

$$e'_x = e'_1 + \Delta e'_x\,, \qquad e'_y = e'_2 + \Delta e'_y\,, \qquad e'_{xy} = e'_{12} + \Delta e'_{xy}\,. \tag{10}$$

In the ring web(s) and flange it is assumed that $\Delta e'_x$, $\Delta e'_y$, $\Delta e'_{xy}$ are zero. Therefore, from (1), (2) and (5), the assumption of uniform in-plane shear resultant N_{xy}, and with use of (8) and (9), it follows that the first variation of the extensional energy of skin and stiffeners minus the first variation of the work done by the prescribed uniform external in-plane loads N_1, N_2, N_{12} is given by

$$(U_{\text{ext}} - W)' = \int_0^{2l} \left\{ \int_0^b (N_x\,\Delta e'_x + N_y\,\Delta e'_y + N_{xy}\,\Delta e'_{xy})\,\mathrm{d}y \right.$$
$$\left. + \sum_{i=3}^{4} \int_0^{\text{width}_i} (N^i_x\,\Delta e^{i\prime}_x + N^i_s\,\Delta e^{i\prime}_s + N^i_{xs}\,\Delta e^{i\prime}_{xs})\,\mathrm{d}s \right\} \mathrm{d}x\,. \tag{11}$$

3.3. Δe_x, Δe_y, Δe_{xy} *in the panel skin*

In the following development it is assumed that the undeformed, perfect panel skin is flat. The formulas in this section, valid for imperfect panels, are analogous to those derived by Koiter [45], who analyzed perfect panels.

The normal displacement $w(x, y)$ in the panel skin is assumed to have the form

$$w(x, y) = W(y)\sin\{\pi(x - my)/l\}\,, \tag{12}$$

in which $W(y)$ is given later (eq. (24b)), m is the slope of the local buckling nodal lines, and l is the axial halfwavelength of the local buckles. The initial imperfection is assumed to have a similar form

$$w_0(x, y) = W_0(y)\sin\{\pi(x - my)/l\}\,, \tag{13}$$

in which $W_0(y)$ is given later (eq. (24a)). In a lengthy derivation, Koiter [45] establishes formulas for perfect panels analogous to the following, which apply to locally imperfect panels:

axial strain increment:

$$\Delta e_x = N(W^2 + 2W_0W)\,; \tag{14}$$

hoop strain increment:

$$\Delta e_y = -\nu\,\Delta e_x + C + \frac{1}{8}\,(WW_{,yy} - W^2_{,y} + WW_{0,yy}$$
$$+ W_0W_{,yy} - 2W_{,y}W_{0,y})\cos\{2\pi(x - my)/l\}\,. \tag{15}$$

In-plane shear strain increment:

$$\Delta e_{xy} = -2Nm \frac{1}{b} \int_0^b (W^2 + 2W_0 W)\, dy\,, \tag{16}$$

in which

$$N = \pi^2/(4l^2)\,; \qquad \nu = C_{12}/C_{22} \tag{17}$$

and

$$C = \frac{1}{b} \int_0^b \{N(\nu + m^2)(W^2 + 2W_0 W) + \frac{1}{4}(W_{,y}^2 + 2W_{0,y}W_{,y})\}\, dy\,. \tag{18}$$

Notice that in the Koiter theory Δe_x is a function of y only and Δe_{xy} is uniform throughout the entire panel skin.

3.4. Δe_x, Δe_s, Δe_{xs} *in the stringer web and outstanding flange*

We assume that in the stringer web and flange the slope of the local buckling nodal lines is zero. (Note: This is not true for truss-core sandwich panels. The truss-core sandwich configuration is treated in a special way, as described in [48]). The displacement components have the form

$$u(x, s) = U(s) \sin\left(\frac{\pi x}{l}\right), \qquad v(x, s) = V(s) \cos\left(\frac{\pi x}{l}\right), \qquad w(x, s) = W(s) \sin\left(\frac{\pi x}{l}\right), \tag{19}$$

in which $U(s)$, $V(s)$, $W(s)$ are the local buckling modal displacement components. The total strain components at any location (x, s) in the stringer web or flange (neglecting thermal strains, which are not functions of the degrees of freedom and therefore do not appear in the derivatives $(\ )'$), are given by
axial strain:

$$e_x^i = e_1 - Z\kappa_x + v_{,x} + \frac{1}{2}(u_{,x}^2 + w_{,x}^2 + 2u_{0,x}u_{,x} + 2w_{0,x}w_{,x})\,; \tag{20}$$

strain in width direction, s:

$$e_s^i = -\nu e_x^i\,; \tag{21}$$

in-plane shear strain:

$$e_{xs}^i = v_{,s} + u_{,x} + w_{,x}w_{,s} + w_{,x}w_{0,s} + w_{0,x}w_{,s}\,; \tag{22}$$

in which Z is the coordinate normal to the panel skin and positive as shown for segment 1 in Fig. 7; κ_x is the change in overall axial curvature due to the applied loads, positive in the sense that the lower surface of the panel skin portrayed in Fig. 7 becomes concave; and ν is defined as in (17b) with the C_{ij} being the constitutive coefficients for the appropriate stringer segment, either web $(i = 3)$ or outstanding flange $(i = 4)$.

The derivatives of the strain increments with respect to the as yet unspecified degrees of

freedom appear in the second line of (11). They are given by

$$\Delta e_x^{i\prime} = v'_{,x} + \frac{1}{2}(u_{,x}^2 + w_{,x}^2 + 2u_{0,x}u_{,x} + 2w_{0,x}w_{,x})' , \qquad \Delta e_s^{i\prime} = -\nu\,\Delta e_x^{i\prime} ,$$
$$\Delta e_{xs}^{i\prime} = v'_{,s} + u'_{,x} + (w_{,x}w_{,s} + w_{,x}w_{0,s} + w_{0,x}w_{,s})' . \tag{23}$$

The κ_x term is absent from (23a) because κ_x is not considered to be a function of any of the degrees of freedom of the nonlinear equilibrium problem. Instead, κ_x is assumed to grow hyperbolically as axial compression increases [50]. An amplitude factor $A = \lambda_G/(\lambda_G - 1)$ for any initial axial bowing, whether it be caused by an initial geometric imperfection, applied pressure, residual deformation due to curing the panel, axial load eccentricity or any combination of these effects, is calculated based on a preliminary estimate λ_G of the general instability load factor. The overall axial curvature change, κ_x, is assumed to be equal to the axial bowing caused by the effects just listed multiplied by the amplitude factor A. This amplitude factor is derived in Section 16 of [50].

3.5. Initial local imperfection and modal displacements

The local imperfection causes no residual stresses, but simply represents modification of the shape of the panel. In the panel skin the initial local imperfection W_0 and additional displacement W caused by loading are assumed to be given by

$$W_0(y) = w_0\phi(y) , \qquad W(y) = f(\phi + a\phi^n) , \tag{24}$$

in which w_0 is a PANDA2-user-supplied amplitude, and $\phi = \phi(y)$ is the critical local buckling mode obtained from the single panel module discretized model, such as shown in Figs. 4(b) and 5(b). The power $n = 3$ if the stringer is not a hat (Fig. 4(b)) and $n = 2$ if the stringer is a hat (Fig. 5(b)). Note that the local buckling mode $\phi(y)$ contains in general not only normal modal displacements W, but also in-plane modal displacements U and V. However, for a flat panel skin, to which this section applies, the in-plane modal displacement components U and V are zero. In the PANDA2 program ϕ is a vector containing displacements at the nodal points in the discretized panel module model.

In the stringer web and outstanding flange the initial local imperfection U_0, V_0, W_0 and additional displacement U, V, W caused by loading are taken as

$$U_0(s), V_0(s), W_0(s) = w_0\phi(s) , \qquad U(s), V(s), W(s) = f\phi(s) . \tag{25}$$

Note that, in the case of the stringer web and outstanding flange, the in-plane modal displacement components U and V are not always zero, especially in the outstanding flange.

The amplitude f, the 'mode shape modification parameter' a (also called the 'flattening parameter'), the slope of the local buckling nodal lines m, and the axial wavelength parameter N (eq. (17a)) are the four degrees of freedom of the nonlinear equilibrium problem established by minimization of the total potential energy, $U - W$, with respect to these degrees of freedom.

3.6. *Internal stress resultants* N_x, N_y, N_{xy}

For a balanced laminate, the internal stress resultants that appear in (11) have the form

$$N_x = C_{11}e_x + C_{12}e_y + N_{x0}\,, \qquad N_y = C_{12}e_x + C_{22}e_y + N_{y0}\,, \qquad N_{xy} = C_{33}e_{xy}\,, \tag{26}$$

in which N_{x0} and N_{y0} are initial resultants from curing the panel, and the reference surface strains are given by

$$e_x = e_1 + \Delta e_x\,, \qquad e_y = e_2 + \Delta e_y\,, \qquad e_{xy} = e_{12} + \Delta e_{xy}\,. \tag{27}$$

With subscript y replaced by subscript s, (26) and (27) apply to the stringer web and outstanding flange also. For the ring, the coordinate x is identified as the coordinate along the axis of the ring, and, as with the stringer, the coordinate y is identified as the coordinate s in the plane of the ring web and flange and perpendicular to the coordinate along the axis of the ring.

3.7. *Extensional strain energy in the panel skin*

In this section we are concerned only with the first line of (11). Insertion of (14)–(16) into (27), and (27) thus modified into (26), and (26) thus modified into the first line of (11), followed by integration over x and some algebra yields

$$\begin{aligned}\frac{(U_{\text{ext}} - W)'}{2lb} = \frac{1}{b}\int_0^b \Big\{ &(C_{11}^* e_1 + N_{x0}^*)N(W^2 + 2W_0W)' + \frac{1}{2}\,C_{11}^*\{(W^2 + 2W_0W)^2N^2\}' \\ &+ \frac{C_{22}}{256}\,\{(WW_{,yy} - W_{,y}^2 + WW_{0,yy} + W_0W_{,yy} - 2W_{,y}W_{0,y})^2\}'\Big\}\,\mathrm{d}y \\ &+ (\bar{C}_{12}e_1 + \bar{C}_{22}e_2^* + \bar{N}_{y0})C' + N_{xy}\,\Delta e_{xy}'\,,\end{aligned} \tag{28}$$

in which

$$\begin{aligned} &C_{11}^* = C_{11} - C_{12}^2/C_{22}\,, \qquad N_{x0}^* = N_{x0} - \nu N_{y0}\,, \\ &\bar{C}_{ij} = \sum_{i=1}^{2} B_{1i}C_{ij}^i\,, \qquad \bar{N}_{y0} = \sum_{i=1}^{2} B_{1i}N_{y0}^i\,, \\ &B_{11} = (b - b_2)/b\,, \qquad B_{12} = b_2/b\,, \qquad e_2^* = e_2 + C\,, \end{aligned} \tag{29}$$

with N and ν given by (17), and C given by (18). The quantity b_2 is the width of the base under the stringer shown in Fig. 2. In (28) ( )′ denotes 'derivative with respect to a degree of freedom'. The degrees of freedom are

1. the amplitude factor f given in (24b) and (25b);
2. the coefficient a that appears in (24b);
3. the slope m of the buckling nodal lines (eqs. (12), (13));
4. The axial wavelength parameter N (eq. (17a)).

3.8. Evaluating e_1 and e_2^*

Equation (28) contains the average strain quantities, e_1 and e_2^*, which must be expressed in terms of the degrees of freedom and other parameters of the equilibrium problem such as the known, prescribed applied average loads, N_1 and N_2. In this section we will derive expressions for e_1 and e_2^*.

Use of the right-hand-sides of (26a, b) in (8) and (9) gives

$$\begin{aligned} N_1 &= \frac{1}{2l}\int_0^{2l}\frac{1}{b}\left\{\int_0^b (C_{11}e_x + C_{12}e_y + N_{x0})\,\mathrm{d}y \right. \\ &\qquad \left. + \sum_{i=3}^{4}\int_0^{\text{width}_i} (C_{11}^i e_x^i + C_{12}^i e_s^i + N_{x0}^i)\,\mathrm{d}s\right\}\mathrm{d}x\,, \\ N_2 &= \frac{1}{2l}\int_0^{2l}\frac{1}{b}\int_0^b (C_{12}e_x + C_{22}e_y + N_{y0})\,\mathrm{d}y\,\mathrm{d}x \\ &\quad + \frac{1}{b_r}\sum_{i=3}^{4}\int_0^{\text{width}_i} (C_{11}^i e_x^i + C_{12}^i e_s^i + N_{x0}^i)\,\mathrm{d}s\,. \end{aligned} \tag{30}$$

The summation in (30a) refers to the stringer web and outstanding flange, and the summation in (30b) refers to the ring web and outstanding flange. Insertion of the right-hand sides of (27) into (26), use of (14), (15), (20) and (21), and integration over x leads to an expression for the average axial resultant N_1:

$$\begin{aligned} N_1 &= \frac{1}{b}\int_0^b \{C_{11}e_1 + C_{12}e_2^* + C_{11}^* N(W^2 + 2W_0W) + N_{x0}\}\,\mathrm{d}y \\ &\quad + \frac{1}{b}\sum_{i=3}^{4}\int_0^{\text{width}_i}\left\{C_{11}^{*\,i}\{e_1 - Z\kappa_x + N(U^2 + W^2 + 2U_0U + 2W_0W)\} + N_{x0}^i\right\}\mathrm{d}s\,, \end{aligned} \tag{31}$$

and for the average hoop resultant N_2:

$$N_2 = \bar{C}_{12}e_1 + C_{s22}e_2^* - (\text{STIFL2})C\,, \tag{32a}$$

in which

$$\text{STIFL2} = k(C_{s22} - C_{s22x})\,, \tag{32b}$$

where C_{s22} is the membrane hoop stiffness of the panel with both stringers and rings smeared out, C_{s22x} is the membrane hoop stiffness of the panel with only the stringers smeared out, and STIFL2 is the contribution to the hoop stiffness of the ring material.

The quantity k in (32b) is a 'knockdown' factor applied to the ring stiffness that compensates for the unconservative assumption in the theory presented here that the ring stiffness is equally effective over the entire span between rings and therefore can be smeared out. Actually, for most practical boundary conditions along the two longitudinal edges of the panel (edges parallel to the stringers), the rings prevent hoop contraction more at the ring

stations than midway between rings. Therefore, there will generally be higher post-local-buckling bending stresses in the panel skin midway between rings than near rings. Just how much higher depends on how wide the panel is, how many stringers there are, how stiff the stringer bases (width b_2 in Fig. 2) are in resisting in-plane bending, and the actual boundary conditions along the two longitudinal edges of the panel.

In PANDA2 k is set equal to 0.1 if the 'inextensional' postbuckling theory is chosen by the user and 0.3 if the 'extensional' postbuckling theory is chosen. By choosing the 'inextensional' postbuckling theory, the user is essentially assuming that the two longitudinal edges of the panel are free to warp in the plane of the undeformed panel skin, therefore diminishing the development of local hoop membrane force midway between rings more than would be the case if the projections of two longitudinal edges onto the plane of the undeformed panel skin were forced to remain straight. In the 'inextensional' postbuckling theory the terms in (28) multiplied by $C_{22}/256$ are omitted.

Note that the hoop residual stress resultants in the panel skin (N_{y0}) and in the ring parts (N^i_{x0} from (30b)) do not appear in (32a) because there is assumed to be zero residual hoop force applied to the edges of the panel normal to the screen. The quantity C in (32a) is given by (18) and e_2^* is given by (29g). In (31) the quantities U and U_0 are the modal displacement component and initial local imperfection component in the s-direction in the stringer web and outstanding flange (Fig. 7). Use of (24) and integration over y in the first integral of (31), and use of (25) and integration over s in the second integral of (31) yields

$$N_1 = \bar{C}_{11}e_1 + \bar{C}_{12}e_2^* + \bar{N}_{x0} + f^2(g_7 + ag_8 + a^2g_9) + f(g_{w7} + ag_{w8})$$
$$+ (\text{STIFL1})e_1 + C_{s14}\kappa_x + \frac{1}{b}\sum_{i=3}^{4}(\text{width}_i)N^i_{x0} + (\text{ASUM6})N(f^2 + 2fw_0)\,, \qquad (33)$$

in which the $\bar{C}_{ij}$ are given by (29c); e_2^* is given by (29g); C_{s14} is the constitutive coefficient for the panel with smeared stringers (between rings) that relates axial load N_1 to the overall change in curvature κ_x, and

$$\bar{N}_{x0} = \sum_{i=1}^{2} B_{1i}N^i_{x0}\,, \qquad g_7 = N\sum_{i=1}^{2} C^{*i}_{11}A^i_1\,, \qquad g_8 = 2N\sum_{i=1}^{2} C^{*i}_{11}A^i_2\,,$$
$$g_9 = N\sum_{i=1}^{2} C^{*i}_{11}A^i_3\,, \qquad g_{w7} = 2w_0g_7\,, \qquad g_{w8} = w_0g_8\,, \qquad (34)$$
$$\text{ASUM6} = \sum_{i=3}^{4} C^{*i}_{11}A^i_{21}\,, \qquad \text{STIFL1} = \frac{1}{b}\sum_{i=3}^{4}(\text{width}_i)C^{*i}_{11}\,.$$

The quantity C^*_{11} is defined in (29a) and the A^i_k are integrals of functions of the local buckling modal displacements U, V, W listed in (35a, b). The A_k listed in (35) that do not appear in (34) arise from other integrals that appear in (28) and that will appear in the expressions for bending energy, to be developed below. The superscript i in the terms A^i_k and C^{*i}_{11} pertains to the segment number of the panel module, with $i = 1$ signifying the thin part of the panel skin, $i = 2$ signifying the thickened base under the stringer, $i = 3$ signifying the stringer web(s), and

$i = 4$ signifying the stringer outstanding flange. Complete lists of the integrals over the cross-section of the panel module, required for the entire nonlinear equilibrium analysis, follow.

If the stringer is *not* a hat configuration, the local buckling mode in the panel skin is antisymmetric with respect to the symmetry plane of the panel module as shown in Fig. 4(b). In (24b) the power $n = 3$. The A_k^i are given by

$$A_1 = \frac{1}{b}\int_{y_1}^{y_2} W^2\,dy\,, \qquad A_2 = \frac{1}{b}\int_{y_1}^{y_2} W^4\,dy\,, \qquad A_3 = \frac{1}{b}\int_{y_1}^{y_2} W^6\,dy\,,$$

$$A_4 = \frac{1}{b}\int_{y_1}^{y_2} W_{,y}^2\,dy\,, \qquad A_5 = \frac{1}{b}\int_{y_1}^{y_2} W^2W_{,y}^2\,dy\,,$$

$$A_6 = \frac{1}{b}\int_{y_1}^{y_2} W^4W_{,y}^2\,dy\,, \qquad A_7 = \frac{1}{b}\int_{y_1}^{y_2} WW_{,yy}\,dy\,,$$

$$A_8 = \frac{1}{b}\int_{y_1}^{y_2} W^8\,dy\,, \qquad A_9 = \frac{1}{b}\int_{y_1}^{y_2} W^{10}\,dy\,, \qquad A_{10} = \frac{1}{b}\int_{y_1}^{y_2} W^{12}\,dy\,,$$

$$A_{11} = \frac{1}{b}\int_{y_1}^{y_2} (WW_{,yy} - W_{,y}^2)^2\,dy\,, \qquad A_{12} = \frac{1}{b}\int_{y_1}^{y_2} 8W^3W_{,yy}(WW_{,yy} - W_{,y}^2)\,dy\,,$$

$$A_{13} = \frac{1}{b}\int_{y_1}^{y_2} \{16W^6W_{,yy}^2 + 6(WW_{,yy} - W_{,y}^2)(W^5W_{,yy} - W^4W_{,y}^2)\}\,dy\,,$$

$$A_{14} = \frac{1}{b}\int_{y_1}^{y_2} 24W^3W_{,yy}(W^5W_{,yy} - W^4W_{,y}^2)\,dy\,, \tag{35a}$$

$$A_{15} = \frac{1}{b}\int_{y_1}^{y_2} 9(W^5W_{,yy} - W^4W_{,y}^2)^2\,dy\,,$$

$$A_{16} = \frac{1}{b}\int_{y_1}^{y_2} W^3W_{,yy}\,dy\,, \qquad A_{17} = \frac{1}{b}\int_{y_1}^{y_2} W^5W_{,yy}\,dy\,,$$

$$A_{18} = \frac{1}{b}\int_{y_1}^{y_2} W_{,yy}^2\,dy\,, \qquad A_{19} = \frac{1}{b}\int_{y_1}^{y_2} W_{,yy}(6W^2W_{,yy} + 12WW_{,y}^2)\,dy\,,$$

$$A_{20} = \frac{1}{b}\int_{y_1}^{y_2} (3W^2W_{,yy} + 6WW_{,y}^2)^2\,dy\,, \qquad A_{21}^i = \frac{1}{b}\int_0^{\text{width}_i} (U^2 + W^2)\,ds\,,$$

$$A_{22}^i = \frac{1}{b}\int_0^{\text{width}_i} (V_{,s} + 2N^{1/2}U)^2\,ds\,, \qquad A_{23}^i = \frac{1}{b}\int_0^{\text{width}_i} V^2\,ds\,,$$

$$A_{24}^i = \frac{1}{b}\int_0^{\text{width}_i} (U^2 + W^2)Z\,ds\,, \qquad A_{25}^i = \frac{1}{b}\int_0^{\text{width}_i} (U^2 + W^2)^2\,ds\,,$$

$$A_{26} = \frac{1}{b}\int_{y_1}^{y_2} 16W^6W_{,yy}^2\,dy\,.$$

If the stringer *is* a hat configuration, the local buckling mode in the panel skin is symmetric

with respect to the symmetry plane of the panel module as shown in Fig. 5(b). In (24b) the power $n = 2$. The A_k^i are given by

$$A_1 = \frac{1}{b}\int_{y_1}^{y_2} W^2\,dy\,, \qquad A_2 = \frac{1}{b}\int_{y_1}^{y_2} W^3\,dy\,, \qquad A_3 = \frac{1}{b}\int_{y_1}^{y_2} W^4\,dy\,,$$

$$A_4 = \frac{1}{b}\int_{y_1}^{y_2} W_{,y}^2\,dy\,, \qquad A_5 = \frac{1}{b}\int_{y_1}^{y_2} WW_{,y}^2\,dy\,, \qquad A_6 = \frac{1}{b}\int_{y_1}^{y_2} W^2W_{,y}^2\,dy\,,$$

$$A_7 = \frac{1}{b}\int_{y_1}^{y_2} WW_{,yy}\,dy\,, \qquad A_8 = \frac{1}{b}\int_{y_1}^{y_2} W^6\,dy\,, \qquad A_9 = \frac{1}{b}\int_{y_1}^{y_2} W^7\,dy\,,$$

$$A_{10} = \frac{1}{b}\int_{y_1}^{y_2} W^8\,dy\,, \qquad A_{11} = \frac{1}{b}\int_{y_1}^{y_2} (WW_{,yy} - W_{,y}^2)^2\,dy\,,$$

$$A_{12} = \frac{1}{b}\int_{y_1}^{y_2} (6W^2W_{,yy} - 4WW_{,y}^2)(WW_{,yy} - W_{,y}^2)\,dy\,,$$

$$A_{13} = \frac{1}{b}\int_{y_1}^{y_2} \{(3W^2W_{,yy} - 2WW_{,y}^2)^2 + 4(WW_{,yy} - W_{,y}^2)(W^3W_{,yy} - W^2W_{,y}^2)\}\,dy\,,$$

$$A_{14} = \frac{1}{b}\int_{y_1}^{y_2} 4(3W^2W_{,yy} - 2WW_{,y}^2)(W^3W_{,yy} - W^2W_{,y}^2)\,dy\,,$$

$$A_{15} = \frac{1}{b}\int_{y_1}^{y_2} 4(W^3W_{,yy} - W^2W_{,y}^2)^2\,dy\,, \qquad A_{16} = \frac{1}{b}\int_{y_1}^{y_2} W^2W_{,yy}\,dy\,, \tag{35b}$$

$$A_{17} = \frac{1}{b}\int_{y_1}^{y_2} W^3W_{,yy}\,dy\,, \qquad A_{18} = \frac{1}{b}\int_{y_1}^{y_2} W_{,yy}^2\,dy\,,$$

$$A_{19} = \frac{1}{b}\int_{y_1}^{y_2} 4W_{,yy}(WW_{,yy} + W_{,y}^2)\,dy\,, \qquad A_{20} = \frac{1}{b}\int_{y_1}^{y_2} 4(WW_{,yy} + W_{,y}^2)\,dy\,,$$

$$A_{21}^i = \frac{1}{b}\int_0^{\text{width}_i} (U^2 + W^2)\,ds\,, \qquad A_{22}^i = \frac{1}{b}\int_0^{\text{width}_i} (V_{,s} + 2N^{1/2}U)^2\,ds\,,$$

$$A_{23}^i = \frac{1}{b}\int_0^{\text{width}_i} V^2\,ds\,, \qquad A_{24}^i = \frac{1}{b}\int_0^{\text{width}_i} (U^2 + W^2)Z\,ds\,,$$

$$A_{25}^i = \frac{1}{b}\int_0^{\text{width}_i} (U^2 + W^2)^2\,ds\,, \qquad A_{26} = \frac{1}{b}\int_{y_1}^{y_2} (3W^2W_{,yy} - 2WW_{,y}^2)^2\,dy\,,$$

$$A_{27} = \frac{1}{b}\int_{y_1}^{y_2} W^5\,dy\,.$$

In (35a, b) the limits y_1 and y_2 depend on which segment of the panel module cross-section is involved in the integral. When (35) are applied to the stringer web and flange the independent variable called y should be re-interpreted as the coordinate s along the web or flange, as shown in Fig. 7.

From (32a) we have

$$e_2^* = \{N_2 - \bar{C}_{12}e_1 + (\text{STIFL2})C\}/C_{s22}\,. \tag{36}$$

Insertion of the right-hand side of (36) into (33) and solution for e_1 yields

$$\begin{aligned} e_1 = \{&N_1 - C_s(1,4)\kappa_x - \bar{\nu}N_2 - f^2(g_7 + N(\text{ASUM6}) + ag_8 + a^2g_9) \\ &- f(g_{w7} + 2w_0N(\text{ASUM6}) + ag_{w8}) - \bar{\nu}(\text{STIFL2})C\}/(\bar{C}_{11} - \bar{\nu}\bar{C}_{12} + \text{STIFL1})\,. \end{aligned} \tag{37}$$

It should be emphasized that the axial residual stress resultant terms that occur in (33) must add to zero:

$$\bar{N}_{x0} + \frac{1}{b}\sum_{i=3}^{4}(\text{width}_i)N_{x0}^i = 0\,, \tag{38}$$

since the residual stress over the entire panel module cross-section must be self-equilibrating.

The average strain components, which appear in (28), can now be expressed in the form

$$\begin{aligned} e_1 &= F_1 + f^2(g_{11} + ag_{12} + a^2g_{13}) + f(g_{w11} + ag_{w12}) + \bar{S}_2C\,, \\ e_2^* &= F_2 + f^2(g_{21} + ag_{22} + a^2g_{23}) + f(g_{w21} + ag_{w22}) + \{(\text{STIFL2})/C_{s22} - \bar{\nu}\bar{S}_2\}C\,, \end{aligned} \tag{39}$$

in which

$$\begin{aligned} &F_1 = (N_1 - C_s(1,4)\kappa_x - \bar{\nu}N_2)/A_{x11}\,, \qquad F_2 = N_2/C_{s22} - \bar{\nu}F_1\,, \\ &\bar{\nu} = \bar{C}_{12}/C_{s22}\,, \qquad \bar{S}_2 = -\bar{\nu}(\text{STIFL2})/A_{x11}\,, \\ &(g_{21}, g_{22}, g_{23}, g_{w21}, g_{w22}) = -\bar{\nu}(g_{11}, g_{12}, g_{13}, g_{w11}, g_{w12})\,, \end{aligned} \tag{40}$$

and $g_{11}, g_{12}, g_{13}, g_{w11}, g_{w12}$ can be derived from (37). The quantity A_{x11} is the denominator of the right-hand side of (37).

3.9. *Extensional strain energy in stringer web and flange*

The extensional strain energy in the stringer web and outstanding flange is expressed in the term with the summation in (11), with the strain increments given in (23) and the stress resultants given by (26) (replace y by s in the subscripts). Noting that the resultant $N_s = 0$, we obtain for the derivative of the extensional strain energy density

$$\begin{aligned} \frac{(U_{\text{ext}} - W)'}{2lb} = \frac{1}{2l}\int_0^{2l}\frac{1}{b}\sum_{i=3}^{4}\int_0^{\text{width}_i} &\{\{C_{11}^{*\,i}(e_1 - Z\kappa_x + \Delta e_x^i) + N_{x0}^{*\,i}\}\,\Delta e_x^{i\prime} \\ &+ C_{33}^i e_{xs}^i\,\Delta e_{xs}^{i\prime}\}\,\mathrm{d}s\,\mathrm{d}x\,, \end{aligned} \tag{41}$$

in which Δe_x and Δe_{xs} are given by (23a, c) without the primes, C_{11}^* and N_{x0}^* are given by (29a, b), and ( )′ denotes differentiation with respect to the amplitude parameter f or the axial wavelength parameter N. Use of the right-hand sides of (23) with and without the primes, as appropriate, use of (25), and integration over x yields

$$\begin{aligned}\frac{(U_{\text{ext}}-W)'}{2lb} &= N\{e_1(\text{ASUM6})-\kappa_x(\text{ASUM6P})+\text{TSUM6}\}(f^2+2fw_0)' \\ &\quad +\{N(\text{ASUM7})+(\text{A6SUM2})/4\}(f^2\}' \\ &\quad +\{3N^2(\text{ASUM4})/4+N(\text{A6SM10})/4\}\{(f^2+2fw_0)^2\}'\,, \end{aligned} \tag{42}$$

in which

$$\begin{aligned}&\text{TSUM6}=\sum_{i=3}^{4} N_{x0}^{*i}A_{21}^i\,, \qquad \text{ASUM6}=\sum_{i=3}^{4} C_{11}^{*i}A_{21}^i\,, \\ &\text{ASUM6P}=\sum_{i=3}^{4} C_{11}^{*i}A_{24}^i\,, \qquad \text{ASUM4}=\sum_{i=3}^{4} C_{11}^{*i}A_{25}^i\,, \\ &\text{ASUM7}=\sum_{i=3}^{4} C_{11}^{*i}A_{23}^i\,, \qquad \text{A6SUM2}=\sum_{i=3}^{4} C_{33}^{i}A_{22}^i\,, \\ &\text{A6SM10}=\sum_{i=3}^{4} C_{33}^{i}A_{5}^i\,. \end{aligned} \tag{43}$$

3.10. *Further development of extensional strain energy in skin*

Using (16), (18), (24), (32), and (35a or 35b) in (28), and integrating over the spacing b between stringers, one obtains

$$\begin{aligned}\frac{(U_{\text{ext}}-W)'}{2lb} = \sum_{i=1}^{2}\Big\{ & NC_{11}^{*i}e_1\{f^2(A_1^i+2aA_2^i+a^2A_3^i)+fw_0(2A_1^i+2aA_2^i)\}' \\ & + NN_{x0}^{*i}\{f^2(A_1^i+2aA_2^i+a^2A_3^i)+fw_0(2A_1^i+2aA_2^i)\}' \\ & + \bar{N}_2[N\nu^i\{f^2(A_1^i+2aA_2^i+a^2A_3^i)+fw_0(2A_1^i+2aA_2^i)\}' \\ & \quad +\tfrac{1}{4}\{f^2(A_4^i+6aA_5^i+9a^2A_6^i)+fw_0(2A_4^i+6aA_5^i)\}'] \\ & + \tfrac{1}{2}C_{11}^{*i}N^2\{f^4(A_2^i+4aA_3^i+6a^2A_8^i+4a^3A_9^i+a^4A_{10}^i)\}' \\ & + \frac{C_{22}^i}{256}\{f^4(A_{11}^i+aA_{12}^i+a^2A_{13}^i+a^3A_{14}^i+a^4A_{15}^i)\}' \\ & + C_{11}^{*i}N^2w_0\{f^3(2A_2^i+6aA_3^i+6a^2A_8^i+2a^3A_9^i)\}' \\ & + \frac{C_{22}^i w_0}{256}\{f^3(4A_{11}^i+3aA_{12}^i+2a^2A_{13}^i+a^3A_{14}^i)\}' \\ & + C_{11}^{*i}N^2w_0^2\{f^2(2A_2^i+4aA_3^i+2a^2A_8^i)\}' \end{aligned}$$

$$+\frac{C^i_{22}w_0^2}{256}\{f^2(4A^i_{11}+2aA^i_{12}+a^2A^i_{26})\}'$$
$$+N[\{(\bar{N}_2m^2-2mN_{xy}\}\{f^2(A^i_1+2aA^i_2+a^2A^i_3)$$
$$+fw_0(2A^i_1+2aA^i_2)\}]'\Big\}, \tag{44a}$$

in which the A^i_k are integrals of the type listed in (35a, b), e_1 is given by (37), and $\bar{N}_2$ is given by

$$\bar{N}_2 = N_2 - (\text{STIFL2})(e^*_2 + C), \tag{44b}$$

with e^*_2 given by (39b) and C given by (18).

3.11. Bending-twisting strain energy density of the panel skin and stringer parts

If (12), (13), (24), and (35a) or (35b) are used with (3), and integration is performed with respect to x and y, the following expression results for the bending and twisting strain energy density of the panel skin:

$$\frac{U_{\text{bend}}(\text{skin})}{2lb} = f^2\sum_{i=1}^{2}\Big\{4N^2D^{*i}_{11}(A^i_1+2aA^i_2+a^2A^i_3)$$
$$+ND^{*i}_{12}\{A^i_7+a(4A^i_{16}+6A^i_5)+a^2(3A^i_{17}+6A^i_6)\}$$
$$+ND^{*i}_{22}(A^i_4+6aA^i_5+9a^2A^i_6)+\tfrac{1}{4}C^i_{55}(A^i_{18}+aA^i_{19}+a^2A^i_{20})\Big\}, \tag{45}$$

in which

$$D^{*i}_{11} = C^i_{44}+2C^i_{45}m^2+C^i_{55}m^4-4C^i_{46}m-4C^i_{56}m^3+4C^i_{66}m^2,$$
$$D^{*i}_{12} = -2C^i_{45}-2C^i_{55}m^2+4C^i_{56}m, \qquad D^{*i}_{22} = 4C^i_{55}m^2-8C^i_{56}m+4C^i_{66}. \tag{46}$$

The C^i_{ij} are the bending and twisting components of the thickness-integrated constitutive relationship given by (8.1) of [39]; m is the slope of the local buckling nodal lines; $i=1$ denotes the part of the panel skin that does not form the stringer base of width b_2; and $i=2$ denotes the stringer base of width b_2 (Fig. 2).

The bending/twisting strain energy density of the stringer web and outstanding flange are calculated in an analogous manner through use of (19b), (25) and (35a) or (35b) in (4). The final expression is

$$\frac{U_{\text{bend}}(\text{stringer})}{2lb} = f^2\sum_{i=3}^{4}\Big\{4N^2C^i_{44}A^i_1-2NC^i_{45}A^i_7+4NC^i_{66}A^i_4+\frac{1}{4}C^i_{55}A^i_{18}\Big\}. \tag{47}$$

The stringer bending/twisting energy does not depend on the slope m of the local buckling nodal lines nor on the buckling mode modification parameter, a. (However, see item 30 of [47], which describes a more sophisticated bending-twisting model implemented in PANDA2.)

The bending/twisting energy of the rings is neglected in this part of the PANDA2 code. (It is included in the calculation of general instability load factors.)

3.12. Final equilibrium equations

The nonlinear equilibrium equations contain contributions from the extensional energy terms, eqs. (42) and (44), and the bending/twisting energy terms, eqs. (45) and (47). The average axial strain e_1 that occurs in (42) is expressed in terms of f, a, m and stiffness parameters (eq. (37)). Like powers of the amplitude factor f, the buckling mode shape modification parameter a and the buckling nodal line slope m are appropriately collected.

Four governing nonlinear algebraic equations of the local postbuckling problem are derived from the first variation of the total potential with respect to f or a or m or N. All four equations are represented by

$$
\begin{aligned}
(U-W)' = {} & \{f^2(C_1 + aC_2 + a^2C_3) + f(C_4 + aC_5)\}'\{f^2(C_{42} + aC_{43} + a^2C_{44}) \\
& + f(C_{45} + aC_{46})\} \\
& + \{f^2\{(C_6 + aC_7 + a^2C_8) + m^2(C_9 + aC_{10} + a^2C_{11}) + \mathrm{SBPB}(m, a, N)\} \\
& + f\{(C_{12} + aC_{13}) + m^2(C_{14} + aC_{15})\} + [f^2\{(C_{16} + aC_{17} + a^2C_{18}) \\
& + m(C_{19} + aC_{20} + a^2C_{21}) + m^2(C_{22} + aC_{23} + a^2C_{24})\} \\
& + f\{(C_{25} + aC_{26}) + m(C_{27} + aC_{28}) + m^2(C_{29} + aC_{30})\}]_{\text{eigenvalue terms}} \\
& + f^4\{C_{31} + aC_{32} + a^2C_{33} + a^3C_{34} + a^4C_{35}\} \\
& + f^3\{C_{36} + aC_{37} + a^2C_{38} + a^3C_{39}\}\}' \\
& + \bar{S}_2C\{f^2(C_1 + aC_2 + a^2C_3) + f(C_4 + aC_5)\}' \\
& + \bar{S}_3\{f^2(C_{42} + aC_{43} + a^2C_{44}) + f(C_{45} + aC_{46})\}C' + \bar{S}_4CC' = 0\,, \qquad (48)
\end{aligned}
$$

in which SBPB(m, a, N) represents the bending/twisting strain energy of the panel skin [eqs. (45), (46)], $\bar{S}_2$ is given by (40d), and

$$
\bar{S}_3 = \bar{\nu}(\mathrm{STIFL2})\,, \qquad \bar{S}_4 = (\mathrm{STIFL2})(\bar{C}_{12}\bar{S} + \bar{C}_{22})/C_{s22}\,,
$$

$$
C_1 = N\sum_{i=1}^{2} C_{11}^{*i}A_1^i + N(\mathrm{ASUM6})\,, \qquad C_2 = 2N\sum_{i=1}^{2} C_{11}^{*i}A_2^i\,,
$$

$$
C_3 = N\sum_{i=1}^{2} C_{11}^{*i}A_3^i\,, \qquad C_4 = 2w_0C_1\,, \qquad C_5 = w_0C_2\,,
$$

$$
\begin{aligned}
C_6 = {} & g_{010} + 4w_0^2\sum_{i=1}^{2}\left(\frac{1}{2}N^2C_{11}^{*i}A_2^i + \frac{1}{256}C_{11}^iA_{11}^i\right) \\
& + F_{1B}C_1 - N(\mathrm{ASUM6P})\kappa_{xB} + \mathrm{USTBPB}(f, N) + N(\mathrm{TSUM6} + \mathrm{ASUM7}) \\
& + \frac{1}{4}(\mathrm{A6SUM2}) + 4w_0^2N\left\{\frac{3}{4}N(\mathrm{ASUM4}) + \frac{1}{4}(\mathrm{A6SM10})\right\},
\end{aligned}
$$

$$C_7 = g_{011} + 2w_0^2 \sum_{i=1}^{2} \left(2N^2 C_{11}^{*i} A_3^i + \frac{1}{256}\, C_{22}^i A_{12}^i\right) + F_{1B} C_2 ,$$

$$C_8 = g_{012} + w_0^2 \sum_{i=1}^{2} \left(2N^2 C_{11}^{*i} A_8^i + \frac{1}{256}\, C_{22}^i A_{26}^i\right) + F_{1B} C_3 ,$$

$$C_9 = g_4 \bar{N}_{2B} , \qquad C_{10} = g_5 \bar{N}_{2B} , \qquad C_{11} = g_6 \bar{N}_{2B} ,$$

$$C_{12} = 2w_0 g_{010} + F_{1B} C_4 + 2w_0 N\{(\text{TSUM6}) - (\text{ASUM6P})\kappa_{xB}\} ,$$

$$C_{13} = w_0 g_{011} + F_{1B} C_5 , \qquad C_{14} = 2w_0 C_9 , \qquad C_{15} = w_0 C_{10} ,$$

$$C_{16} = g_{10} + F_{1A} C_1 - N(\text{ASUM6P})\kappa_{xA} , \qquad C_{17} = g_{11} + F_{1A} C_2 ,$$

$$C_{18} = g_{12} + F_{1A} C_3 , \qquad C_{19} = -2g_4 N_{xyA} ,$$

$$C_{20} = -2g_5 N_{xyA} , \qquad C_{21} = -2g_6 N_{xyA} ,$$

$$C_{22} = g_4 \bar{N}_{2A} , \qquad C_{23} = g_5 \bar{N}_{2A} , \qquad C_{24} = g_6 \bar{N}_{2A} ,$$

$$C_{25} = 2w_0 g_{10} + F_{1A} C_4 - 2w_0 N(\text{ASUM6P})\kappa_{xA} , \qquad C_{26} = w_0 g_{11} + F_{1A} C_5 , \tag{49}$$

$$C_{27} = 2w_0 C_{19} , \qquad C_{28} = w_0 C_{20} , \qquad C_{29} = 2w_0 C_{22} , \qquad C_{30} = w_0 C_{23} ,$$

$$C_{31} = \sum_{i=1}^{2} \left(\frac{1}{2}\, N^2 C_{11}^{*i} A_2^i + \frac{1}{256}\, C_{22}^i A_{11}^i\right) + N\left\{\frac{3}{4}\, N(\text{ASUM4}) + \frac{1}{4}\,(\text{A6SM10})\right\} ,$$

$$C_{32} = \sum_{i=1}^{2} \left(2N^2 C_{11}^{*i} A_3^i + \frac{1}{256}\, C_{22}^i A_{12}^i\right) , \qquad C_{33} = \sum_{i=1}^{2} \left(3N^2 C_{11}^{*i} A_8^i + \frac{1}{256}\, C_{22}^i A_{13}^i\right) ,$$

$$C_{34} = \sum_{i=1}^{2} \left(2N^2 C_{11}^{*i} A_9^i + \frac{1}{256}\, C_{22}^i A_{14}^i\right) , \qquad C_{35} = \sum_{i=1}^{2} \left(\frac{1}{2}\, N^2 C_{11}^{*i} A_{10}^i + \frac{1}{256}\, C_{22}^i A_{15}^i\right) ,$$

$$C_{36} = 4w_0 C_{31} , \qquad C_{37} = 3w_0 C_{32} , \qquad C_{38} = 2w_0 C_{33} , \qquad C_{39} = w_0 C_{34} ,$$

$$C_{40} = \text{not needed} , \qquad C_{41} = \text{not needed} , \qquad C_{42} = -\frac{C_1}{A_{x11}} ,$$

$$C_{43} = -\frac{C_2}{A_{x11}} , \qquad C_{44} = -\frac{C_3}{A_{x11}} , \qquad C_{45} = 2w_0 C_{42} , \qquad C_{46} = w_0 C_{43} .$$

The axial wavelength parameter N is given by (17a), C_{11}^* by (29a), A_k^i by (35a) or (35b), and ASUM6, ASUM6P, TSUM6, ASUM7, A6SUM2, ASUM4 and A6SM10 by (43). The quantity USTBPB(f, N) represents the bending/twisting strain energy of the stringer web and outstanding flange, and is given by (47). Subscripts A and B in the quantities F_{1A} and F_{1B}, κ_{xA} and κ_{xB}, $\bar{N}_{2B}$ and $\bar{N}_{2A}$, and N_{xyA} denote 'load set A' and 'load set B', where 'load set A' means those loads to be multiplied by a load factor (eigenvalue) and 'load set B' means those loads

that are simply parameters of the problem and are not to be multiplied by a load factor. (A buckling quantity would thus be given by $N_{cr} = N_B + \lambda N_A$, in which λ is the load factor or eigenvalue.) The quantities F_{1A} and F_{1B} are given by (40a, b). Other quantities that appear in (49) are

$$
\begin{aligned}
g_{010} &= \sum_{i=1}^{2} \left\{ \left(N\nu^i A_1^i + \frac{1}{4} A_4^i \right) \bar{N}_{2B} + N N_{x0}^{*i} A_1^i \right\}, \\
g_{011} &= \sum_{i=1}^{2} \left\{ \left(2N\nu^i A_2^i + \frac{3}{2} A_5^i \right) \bar{N}_{2B} + 2N N_{x0}^{*i} A_2^i \right\}, \\
g_{012} &= \sum_{i=1}^{2} \left\{ \left(N\nu^i A_3^i + \frac{9}{4} A_6^i \right) \bar{N}_{2B} + N N_{x0}^{*i} A_3^i \right\}, \\
g_{10} &= \sum_{i=1}^{2} \left\{ \left(N\nu^i A_1^i + \frac{1}{4} A_4^i \right) \bar{N}_{2A} \right\}, \qquad g_{11} = \sum_{i=1}^{2} \left\{ \left(2N\nu^i A_2^i + \frac{3}{2} A_5^i \right) \bar{N}_{2A} \right\}, \\
g_{12} &= \sum_{i=1}^{2} \left\{ \left(N\nu^i A_3^i + \frac{9}{4} A_6^i \right) \bar{N}_{2A} \right\}, \qquad g_4 = \sum_{i=1}^{2} N A_1^i, \qquad g_5 = \sum_{i=1}^{2} 2N A_2^i, \\
g_6 &= \sum_{i=1}^{3} N A_3^i, \qquad \bar{N}_{2A} = N_{2A} \left\{ 1 - \frac{\text{STIFL2}}{C_{s22}} \right\} + (\text{STIFL2}) \bar{\nu} F_{1A}, \\
\bar{N}_{2B} &= N_{2B} \left\{ 1 - \frac{\text{STIFL2}}{C_{s22}} \right\} + (\text{STIFL2}) \bar{\nu} F_{1B}, \qquad A_{x11} = \bar{C}_{11} - \bar{\nu} \bar{C}_{12} + \text{STIFL1},
\end{aligned}
\tag{50}
$$

in which $\bar{C}_{ij}$ is given in (29c); STIFL2 is given in (32b); $\bar{\nu}$ is given in (40c); and STIFL1 is given in (34). The Poisson ratio ν^i is given by (17b) applied to either segment 1 or 2 of the panel module (Fig. 2). Note that most of the C_i in (49) and all of the g_k in (50) are functions of the axial wavelength parameter N.

3.13. *Local buckling load factor λ from this theory*

The load factor corresponding to initiation of local buckling is obtained from (48) modified as follows:

1. The initial local imperfection amplitude is set to $w_0 = 0$.
2. The mode shape modification parameter is set to $a = 0$.
3. Terms with cubic and quartic powers of f are neglected.
4. The axial wavelength parameter N is treated as constant.

The resulting two equilibrium equations corresponding to the variation of the total potential with respect to f and m are represented by

$$
(U - W)' = \{ f^2 \{ [C_6 + m^2 C_9 + SBPB(m)\} + \lambda [C_{16} + m C_{19} + m^2 C_{22}] \} \}' = 0 . \tag{51}
$$

The 'f' equation yields

$$
\lambda = -(\text{NUM})/(\text{DEN}) , \tag{52}
$$

in which

$$\text{NUM} = C_6 + m^2 C_9 + \text{SBPB}(m)\,, \qquad \text{DEN} = C_{16} + mC_{19} + m^2 C_{22}\,, \tag{53}$$

and the 'm' equation yields

$$2mC_9 + (\text{SBPB})_{,m} - \frac{\text{NUM}}{\text{DEN}}\,(C_{19} + 2mC_{22}) = 0\,, \tag{54}$$

where $(\ )_{,m}$ indicates partial differentiation with respect to m. Equation (54) is solved for the slope of the local buckling nodal lines m by Newton's method, and the result is inserted into the right-hand side of (52) to yield the load factor λ for local bifurcation buckling corresponding to a given value for the axial wavelength parameter N. In PANDA2 the critical (lowest) eigenvalue λ with respect to N is sought by varying the number of axial halfwaves between rings until a minimum λ is found. This critical λ is called in the PANDA2 output 'local buckling load factor from Koiter theory'.

4. Strategy for solving the nonlinear equations

The four nonlinear equilibrium equations represented by (48) are solved for f, a, m, N by the Newton method. The equations are set up and solved in SUBROUTINE KOIT2. In SUBROUTINE KOIT2 a sophisticated strategy is pursued in order to achieve convergence, which is often difficult for the following reasons.

1. There is often no adequate starting vector available because the design has changed significantly since the last time a converged solution was obtained. The new design may not behave in a manner similar to that of the previous design. For example, the previous design may have been such that local buckling does not occur at the applied load, whereas the current design may be in the locally postbuckled regime at the applied load. Although the transition from prebuckled state to postbuckled state is smoothed by introduction of an initial imperfection in the form of the critical local buckling mode, as demonstrated in Fig. 6, it is still often difficult to obtain a converged solution of the nonlinear equations (48) in the early post-local-buckling regime.
2. It often happens that near-optimum designs correspond to loading in the EARLY post-local-buckling regime, a state for which critical stresses are likely to be very sensitive to changes in design variables because the amount of local bending in the early post-local-buckling regime is strongly dependent on the values of the design variables. Therefore, a solution for a previous design state, even if this design state is rather close to the current design state, may represent a poor starting vector for the solution at the current design state.
3. Because the equilibrium problem is nonlinear, the solution f, a, m, N is not unique, and it may happen that the Newton method converges to a solution that is unacceptable from a common-sense point of view.
4. The 'flattening' parameter a and the buckling nodal line slope m often seem to be responsible for failure of convergence of the Newton iterations.

Experience over the past several years has shown that an unsophisticated strategy fails often enough to prevent the evolution of an optimum design that is reasonably conservative. Therefore, the elaborate strategy described next has evolved over the past several years. To oversimplify, the basic strategy is to attempt a solution with a full set of unknowns f, a, m, N, and to remove unknowns one by one if convergence fails until a simpler problem converges. Then the unknowns that were removed are re-introduced one-by-one until a solution of the full problem with f, a, m, N as unknowns has been achieved. The strategy is outlined in Table A.1, which contains a simplified list of SUBROUTINE KOIT2. (All tables are given in Appendix A.)

There are two formulations of the nonlinear problem handled by SUTROUTINE KOIT2:

1. A formulation in which only the three variables f, a, m are unknowns and the axial wavelength parameter N [eq. (17a)] is held constant. In this formulation the nonlinear equations are solved in SUBROUTINE NEWTON. The version of PANDA2 described in [39, 50, 51] contained only this version.
2. A formulation in which the four variables f, a, m, N are unknowns and the nonlinear equations are solved in SUBROUTINE ENERGY.

4.1. *Strategy pursued in SUBROUTINE NEWTON*

A solution is initially attempted in SUBROUTINE NEWTON. The three nonlinear equations represented by variation of the total potential energy [eq. (48)] with respect to the unknowns f, a, m are solved by Newton's method with use of the following strategy:

1. If the applied load exceeds the critical local bifurcation buckling load of the locally perfect shell ($\lambda < 1$), then a solution is first obtained with the local imperfection amplitude w_0 set to zero and with initial values $f = 0$, $a = 0$ and $m = m_0$, where m_0 is the slope of the local buckling nodal lines obtained from the Koiter theory eigenvalue analysis [eq. (52)]. If convergence with $w_0 = 0$ is achieved within 45 iterations, the resulting f, a and m are then used as starting values for the case with $w_0 > 0$. If convergence is not achieved with $w_0 = 0$, the convergence is attempted with $w_0 > 0$ with zero starting values for f and a and with $m = m_0$.
2. If the applied load is less than the critical local bifurcation buckling load of the locally perfect shell ($\lambda > 1$), then convergence is first attempted with $w_0 > 0$, as described in the last sentence of Strategy 1.
3. If convergence fails in Strategy 1 or Strategy 2, then either of two following strategies will be chosen:
   a. If optimization is being performed and if more than five design iterations have been completed in the current set of design iterations, then the converged solution for the previous design iteration will be used as a starting value and convergence will be attempted again.
   b. Strategy 4 will be pursued.
4. If convergence continues to fail, the slope of the local buckling nodal lines m will be fixed at m_0 and the 'm' equation will be removed from the set of three equations to be solved iteratively, leaving only the 'f' and the 'a' equations to be solved iteratively, an easier problem for which to find a converged solution. If this reduced problem converges within 45 iterations, then the nodal line slope m will be re-introduced as an unknown with a

starting value $m = m_0$, along with the values of f and a determined from the reduced problem, and the three-variable problem f, a, m will be attempted again.
5. If convergence continues to fail, m will be fixed at m_0 and a will be set equal to zero and both the 'm' and 'a' equations will be removed, leaving only the 'f' equation to be solved iteratively. In this case the three-variable problem is not attempted again.
6. If convergence continues to fail, f and a are set equal to zero and m is set equal to m_0, the value obtained from solution of the eigenvalue problem (eq. (52)).

4.2. Strategy pursued in SUBROUTINE ENERGY

Actually, the strategy is implemented outside of SUBROUTINE ENERGY, in SUBROUTINE KOIT2, from which SUBROUTINE ENERGY is called, as seen from the list in Table A.1. This strategy is similar to that described for SUBROUTINE NEWTON: As long as convergence fails, unknowns are removed one-by-one, then re-introduced one-by-one if a converged solution to each simpler problem has been achieved. Whenever a converged solution via SUBROUTINE ENERGY is achieved, solutions are next attempted via the more robust SUBROUTINE NEWTON with the axial wavelength parameter N fixed at its converged value from SUBROUTINE ENERGY. The SUBROUTINE NEWTON part of the computations is embodied in SUBROUTINE BLOCK, which is listed at the end of Table A.1.

In order to save space, certain additional refinements in the strategy have been omitted from Table A.1. These include certain adjustments to the overall change in axial curvature κ_x caused by redistribution of the stiffness of the panel that occurs when the skin is loaded into its post-locally buckled state, strategy elements related to problems that arise when the axial wavelength parameter N tries to reach a value that corresponds to one or less than one axial halfwave between adjacent rings, and strategy elements brought into play when the modal modification parameter a exceeds certain lower and upper bounds.

4.3. Examples

Tables A.2 and A.3 contain examples for the case of an isotropic flat plate loaded in combined axial compression N_1 or N_x and in-plane shear N_{12} or N_{xy}. Table A.2 represents an example in which no convergence difficulties are encountered. Table A.3 represents an example in which certain convergence difficulties are encountered and overcome by successive removal and re-introduction of the frequently troublesome unknowns a and m.

5. Numerical results

Figure 8 shows the axially stiffened panel, boundary conditions, material properties, loading and decision variables b, b_2, h, t_1, t_2, t_3. Starting values of b, b_2, h, t_1, t_2, t_3 and values obtained after optimization are also given in Fig. 8. General instability load factors for the panel are computed with use of the wide column model: the panel is assumed to be flat and infinitely wide. (In PANDA2 the user can choose whether or not to use the wide column model for buckling between rings.) In the DECIDE processor, where decision variables and their lower and upper bounds are selected by the PANDA2 user, the minimum stringer

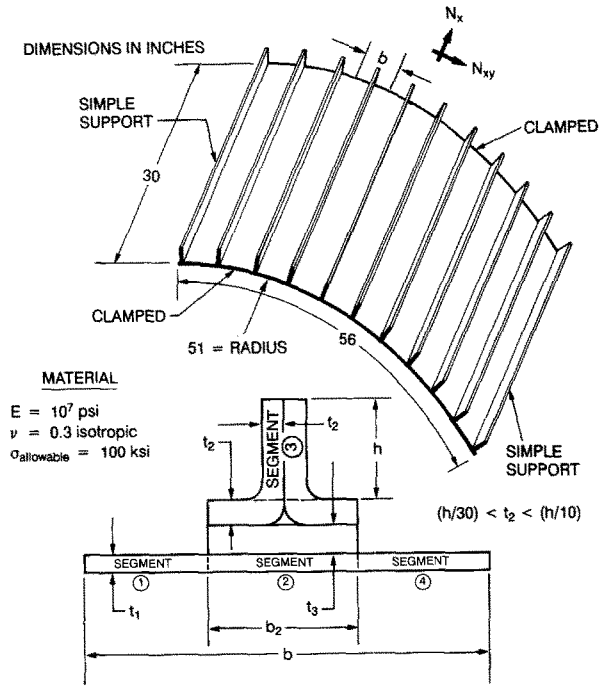

	DECISION VARIABLES					
	b	b_2	h	t_1	t_2	t_3
STARTING VALUES	8.0	1.0	2.0	0.080	0.030	0.040
OPTIMUM VALUES	5.0	1.0	1.4	0.054	0.0663	0.0231

Fig. 8. Blade stiffened cylindrical panel and decision variables.

spacing was set to 5.0 in. Previous work showed that for stringer spacings in the range 3.5–5.0 in the optimum weight is almost constant. The panel with the most widely spaced stringers is the most economical to fabricate, exhibits the most interesting post-local-bucking behaviour, and is the most interesting and practical to study with the use of STAGS because

(1) the design load factor, PA = 1.0, corresponds to a load level well above that corresponding to local buckling, and
(2) the characteristic axial wavelength of the local buckling pattern is not so short compared to the length of the panel as to require an impractically large STAGS finite element model for adequately converged behavior in the post-locally-buckled regime.

The panel is optimized for three sets of loads, each set applied independently.

Load set 1. Uniform axial compression $N_x = -3000$ lb/in, negative axial bowing with amplitude 0.1 in. With negative axial bowing, the panel is initially bowed so that at the midlength of the panel the surface of the panel skin opposite to the surface to which the stringers are attached is concave. Therefore, as the axial compression N_x is applied, the panel skin in the neighborhood of the midlength of the panel becomes axially compressed more than the tips of the stringers. Negative axial bowing of a flat panel generates positive change in axial curvature κ_x at the midlength of the panel.

Load set 2. Uniform axial compression $N_x = -3000\,\text{lb/in}$, positive axial bowing with amplitude 0.1 in. With positive bowing at the midlength of the panel the stringer tips become compressed more than the panel skin, and torsion-bending buckling of the stringers becomes more likely as the panel is axially compressed than it would if there were no positive axial bowing.

Load set 3. Uniform axial compression $N_x = -1000\,\text{lb/in}$ and in-plane shear loading, $N_{xy} = +1000\,\text{lb/in}$, no axial bowing.

In all three load sets the amplitude of the local initial imperfection, assumed to be in the shape of the local buckling mode for each load set, is one tenth of the thickness of the panel skin. Although this example involves isotropic material, it is emphasized that PANDA2 will handle laminated composite materials, as described in [18, 39]. In problems for which there is no pressure loading PANDA2 optimizes for conditions only at the midlength of the panel. The local buckling and postbuckling analyses are based on the assumption that the conditions existing at the panel midlength extend along the entire length of the panel.

5.1. *PANDA2 runstream*

The PANDA2 runstream used for this case is listed in table A.4. PANDA2 consists of a number of processors, BEGIN, SETUP, DECIDE, MAINSETUP, PANDAOPT, CHANGE, CHOOSEPLOT, DIPLOT and STAGSMODEL, that are invoked by the commands listed in the left-hand column of Table A.4. The results described in this section are obtained by first running PANDA2 in the optimization mode and then running PANDA2 in the test simulation mode. In the test simulation mode the optimized panel is 'tested' by subjecting it to a sequence of monotonically increasing loads corresponding to one of the three load sets listed above.

After PANDA2 is run in the test simulation mode, input files for the STAGS computer program [22, 23, 52–56] are produced via the PANDA2 processor called STAGSMODEL. STAGS is then executed in various sequences of bifurcation and nonlinear collapse runs in order to ascertain the behavior of the optimized panel as predicted by this widely used general-purpose nonlinear finite element program.

5.2. *Results from PANDA2 optimization runs*

Table A.5 and Figs. 9–14 pertain to this section. The optimum design is found by several executions of PANDAOPT, as listed in Table A.4. Table A.5 presents a summary of results. For each PANDAOPT run, results for the current starting design (which is the same as the final design in the previous run) and five iterations are listed. The entire analysis was performed with use of the model control index IQUICK = 0. That is, local buckling loads and postbuckling behavior were determined with use of a discretized panel module model analogous to that shown in Fig. 4(a). Table A.5 lists the number of critical margins for each iteration for each of the three load sets. A margin is defined as critical if it is less than 0.05. Designs that are NOT FEASIBLE have one or more margins that are less than −0.05; designs that are ALMOST FEASIBLE have one or more margins that are between −0.05 and −0.01; and designs that are FEASIBLE have no margins less than −0.01.

Note from Table A.5 that the weight corresponding to Iterations 17–36 is very close to 18.6 lb. It therefore appears that an optimum design has been found. In order to check

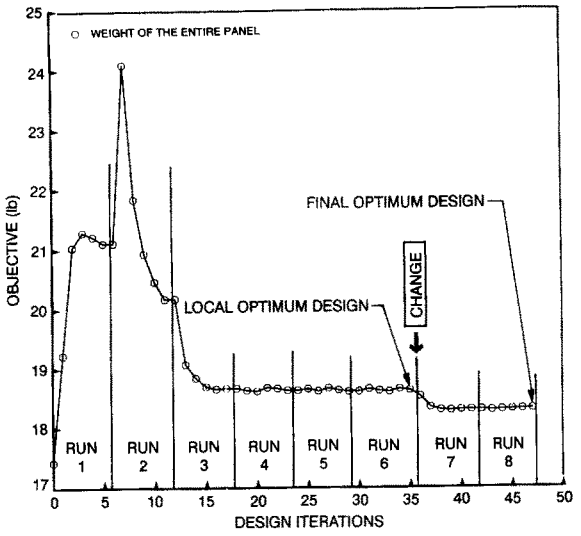

Fig. 9. Weight of the blade stiffened panel for all design iterations. The PANDA2 processor CHANGE was used after Run 6.

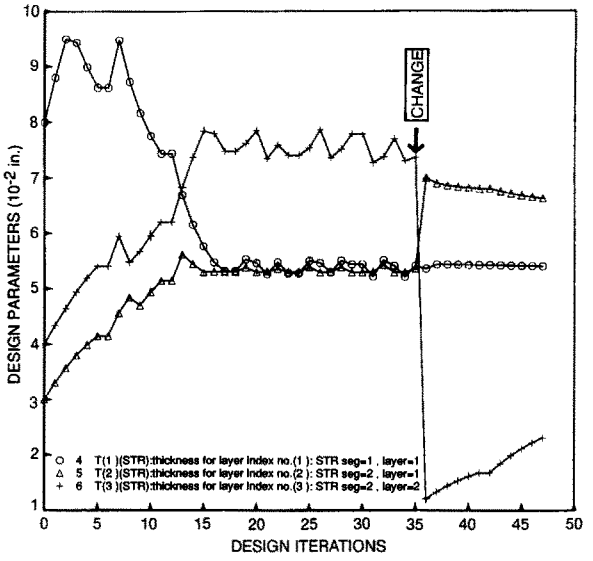

Fig. 10. Thicknesses t_1, t_2, t_3 for all design iterations.

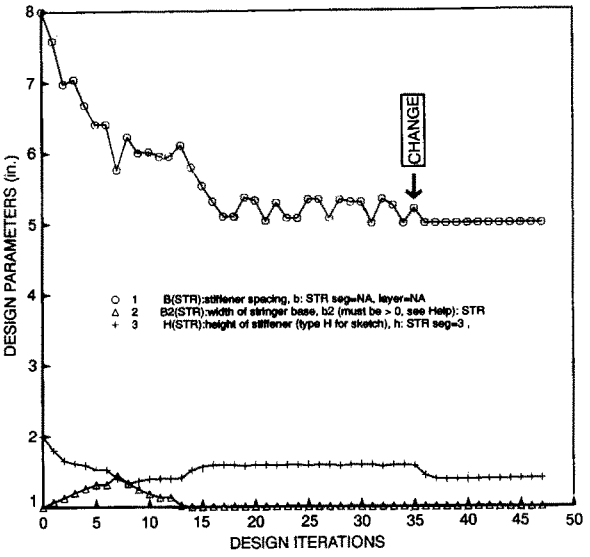

Fig. 11. Widths b, b_2 and height h for all design iterations.

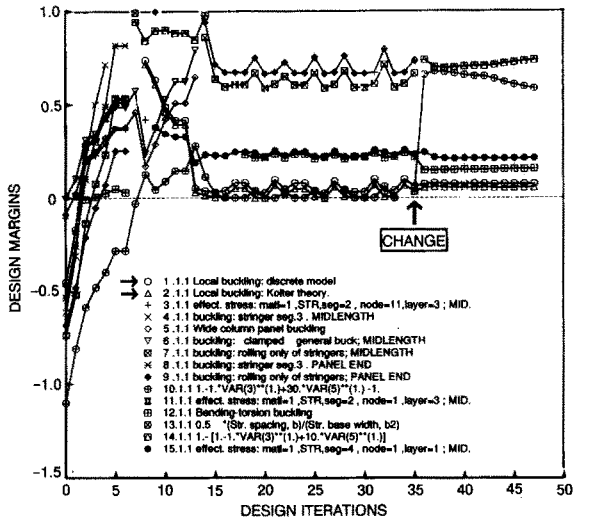

Fig. 12. Margins corresponding to Load set 1: $N_x = -3000$ lb/in, negative axial bowing.

whether or not this optimum is a global optimum, the PANDA2 processor CHANGE is used after Iteration 36 in order to change some of the values of the decision variables b, b_2, t_1, t_2, t_3. Iterations are then continued. This time the design settles to a somewhat lower weight of about 18.3 lb. Even though the weight is lower there are fewer critical margins, an unusual but possible result. The design corresponding to Iteration 48 is accepted as the optimum. It often happens that iterations lead to a local optimum design that can be improved by repeated

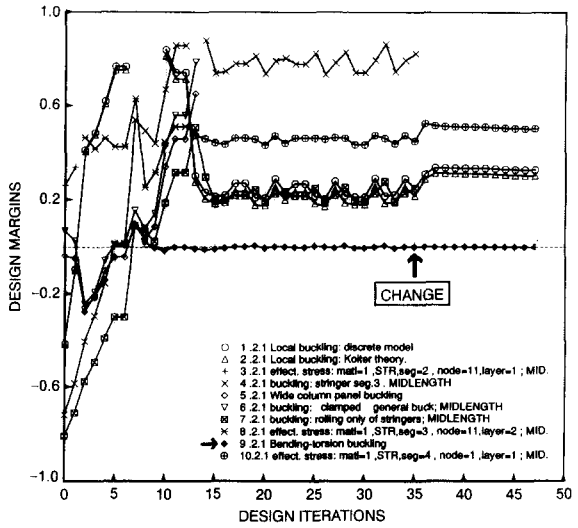

Fig. 13. Margins corresponding to Load set 2: $N_x = -3000$ lb/in, positive axial bowing.

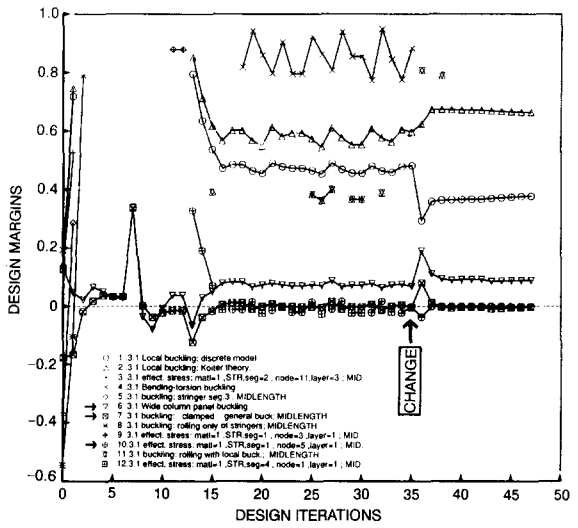

Fig. 14. Margins corresponding to Load set 3: $N_x = -1000$ lb/in, $N_{xy} = +1000$ lb/in, no axial bowing.

application of the CHANGE processor, each application of CHANGE followed by several executions of PANDAOPT.

The reader might notice that even though the design is labelled FEASIBLE for Iterations 44–48, the weight increases slightly from iteration to iteration. This trend results from the fact that designs with very small negative margins (−0.01) are labelled FEASIBLE. For Iterations 44–48 there are one or two margins that are less than zero and greater than −0.01 and that increase from iteration to iteration while remaining negative and very small.

Figures 9–14, which show the evolution of the design and the margins corresponding to the three load sets, were generated by the CHOOSEPLOT/DIPLOT processors. From Figs. 10 and 11 one can see how CHANGE was used to change the values of t_2 and t_3 and b and h. Note that upon further iteration via PANDAOPT, these CHANGEd decision variables did not return to their old values. Figures 12–14 show the design margins corresponding to Load sets 1–3, respectively. Note from Fig. 12 that after the application of CHANGE the inequality constraint corresponding to the requirement that $h/30$ be less than t_2 (VAR(3) = h, VAR(5) = t_2, see Fig. 8) is no longer critical. It appears that the criticality of this inequality constraint causes the design to become trapped at a local rather than at a global optimum for Iterations 17–36.

For Load set 1, the first two margins listed in the legend in Fig. 12, 'Local buckling: discrete model' and 'Local buckling: Koiter theory', are almost critical at the final optimum design. Being slightly larger than 0.05, they are not listed as critical at the bottom of Table A.5. These two local buckling margins are calculated from the following:

$$\text{margin} = (\text{local buckling load factor})/(\text{factor of safety}) - 1.0\,. \tag{55}$$

In this case the factor of safety is set equal to 0.3. By setting the factor of safety for local buckling to a number considerably less than unity, the user accepts designs for which local

buckling may occur at a load well below the design load. In the present example, for Load set 1 the local buckling load factor from the discrete model is 0.32252 at the optimum design, and the local buckling load factor from Koiter theory is 0.31637. In other words, local buckling occurs at a little less than one third of the applied load in Load set 1, or at about 950 lb/in axial compression. PANDA2 predicts that the number of axial halfwaves in the local buckling pattern is 10.

The first margin, 'Local buckling: discrete model', is computed directly from the BOSOR4-type strip theory [44] for the single panel module discretized in a manner analogous to that shown in Fig. 4(a). The second margin, 'Local buckling: Koiter theory', is computed as set forth in (51)–(54). The coefficients in these equations depend on the A_k and A_k^i listed in (35a), which are calculated from the critical local buckling mode obtained from the BOSOR4-type strip theory for the single panel module. In this case there is good agreement of the local buckling load factor as calculated by the two methods.

From Fig. 13 one can see that the only critical margin in Load set 2 is bending-torsion buckling, incurred because in Load set 2 the panel is bowed positively so that at the midlength of the panel the tips of the stringers are compressed more than the panel skin. From Fig. 14 one can see that for Load set 3 there are two critical margins, general instability and effective stress, and one margin that is almost critical, wide column buckling (another model of general instability).

5.3. *Results from PANDA2 test simulation runs*

Results from Load set 1 are displayed in Figs. 15–19; results from Load set 2 appear in Fig. 20; and results from Load set 3 are plotted in Figs. 21–26.

5.3.1. *Load set 1: axial compression N_x, negative bowing*

Figure 15 shows a post-locally-buckled state at axial load $N_x = -6000$ lb/in for a single panel module. Only part of the length is shown, an amount that corresponds to one full axial wave of the postbuckled pattern. According to PANDA2 there are about 12 axial halfwaves over the 30 in length of the locally buckled panel at $N_x = -6000$ lb/in (Fig. 19). Hence, the plot in Fig. 15 covers one sixth of the panel length. The overall axial bowing component of displacement is not shown in this view.

Figure 16 gives a view of the panel module cross-section at the axial station where the

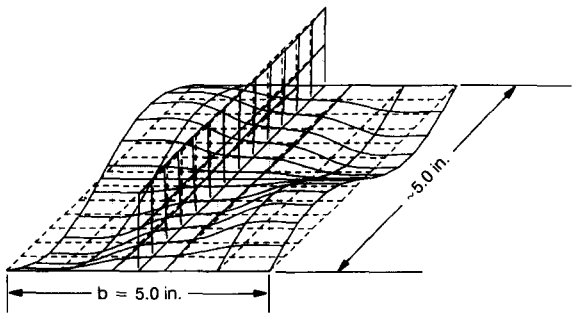

Fig. 15. PANDA2 prediction of deformation of locally postbuckled panel module for Load set 1 with axial load $N_x = -6000$ lb/in.

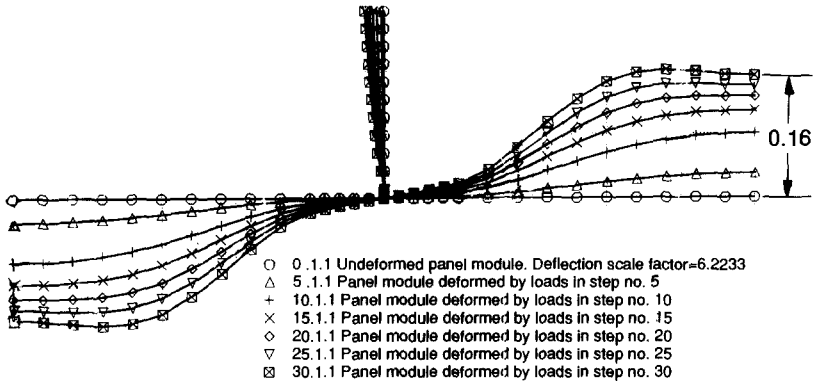

Fig. 16. PANDA2 prediction of deformation of locally postbuckled panel module for Load set 1 with axial load $N_x = 0, -1000, -2000, -3000, -4000, -5000, -6000$ lb/in.

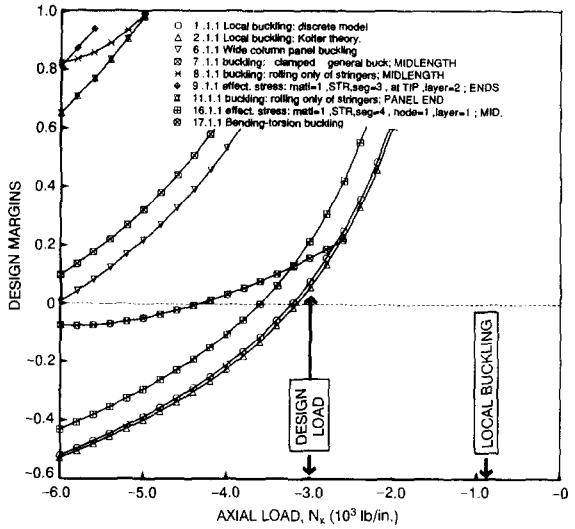

Fig. 17. Margins versus axial load N_x for Load set 1.

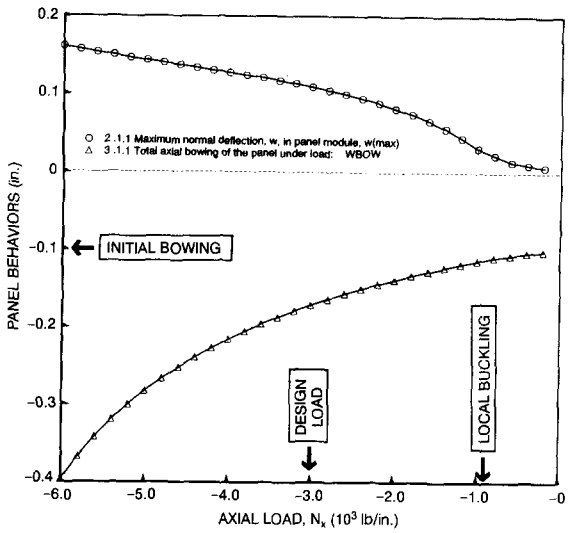

Fig. 18. Local postbuckling normal displacement w between stringers and overall axial bowing for Load set 1.

post-local-buckling normal displacement is maximum. (The overall axial bowing component of w not included in Fig. 16). Load step 5 corresponds approximately to the local buckling load and Load step 15 corresponds to the design load $N_x = -3000$ lb/in. The load increment dN_x is 200 lb/in for all 30 load steps. Note that the normal displacement distribution in the panel skin is antisymmetric about the line of attachment of the blade to the stringer base, that the extra thickness of the stringer base diminishes the rotation of the stringer about its axis, and that the modal 'flattening' parameter a [eq. (24b)] has increasing influence on the deflected shape as the panel is loaded further and further into its postbuckling regime. The fact that the postbuckling deformation pattern in Fig. 16 for load steps 25 and 30 has a maximum normal deflection w which is not at the symmetry plane midway between stringers (longitudinal edges of the single module model) indicates the need for inclusion of higher order terms in eq. (24b)

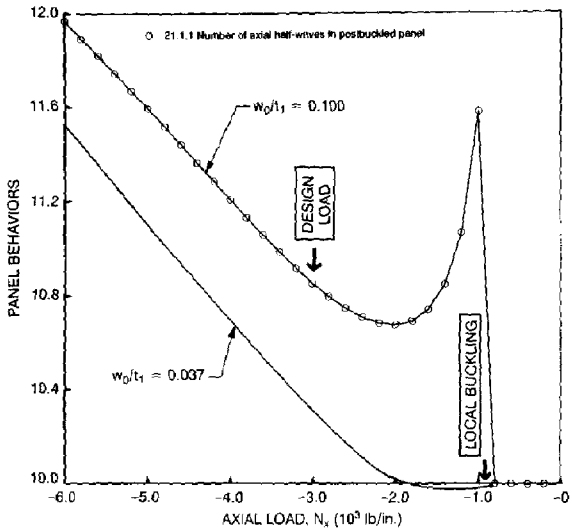

Fig. 19. Change in number of axial halfwaves in postbuckling regime with two different local initial imperfection amplitudes, Load set 1.

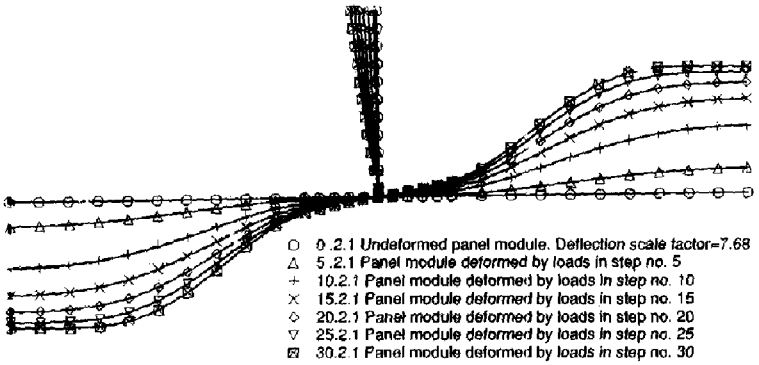

Fig. 20. PANDA2 prediction of deformation of locally postbuckled panel module for Load set 2 with axial load $N_x = 0, -1000, -2000, -3000, -4000, -5000, -6000$ lb/in.

for panels loaded very far into their postbuckled states. However, note that at the design load $N_x = -3000$ lb/in (Load step 15) the maximum normal displacement w is at the longitudinal symmetry plane.

Figure 17 shows margins as functions of the axial load N_x. At the design load $N_x = -3000$ lb/in the two local buckling margins

$$\text{margin} = (\text{local buckling load factor})/0.3 - 1.0 \tag{56}$$

are nearly critical. For the negatively bowed panel, bending-torsion buckling, which according to PANDA2 has five axial halfwaves over the panel length of 30 in, does not become critical until the axial load N_x is 25 percent higher than the design load $N_x = -3000$ lb/in.

Figure 18 depicts the growth in amplitude of the local buckles and of the overall axial

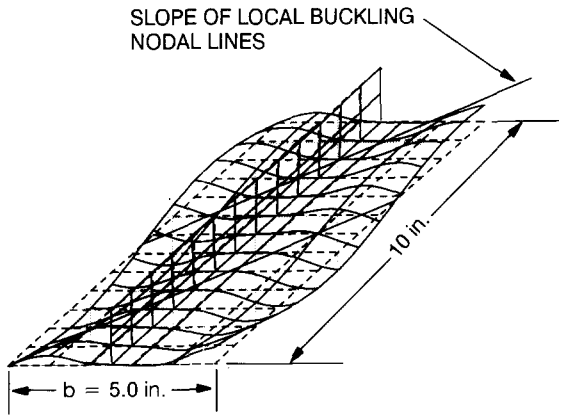

Fig. 21. PANDA2 prediction of deformation of locally postbuckled panel module for Load set 3 with axial load $N_x = -1100$ lb/in, in-plane shear load $N_{xy} = +1100$ lb/in.

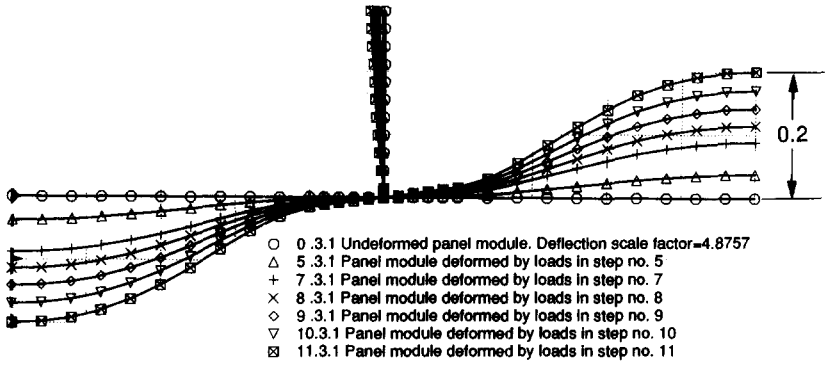

Fig. 22. PANDA2 prediction of deformation of locally postbuckled panel module for Load set 3 with axial load $N_x = 0$, -500, -700, -800, -900, -1000, -1100 lb/in, and shear load $N_{xy} = 0$, 500, 700, 800, 900, 1000, 1100 lb/in.

bowing as N_x is increased. Note that at the local buckling load from Koiter theory, $N_{xcr} = -949$ lb/in, there is already a finite amount of local bending because the panel has an initial imperfection in the form of the local bifurcation buckling mode. This imperfection grows as soon as *any* axial load is applied to the panel, as is demonstrated for the simple example of an axially compressed flat plate in Fig. 6.

Figure 19 shows the change in the number of axial halfwaves in the post-locally-buckled panel skin as the axial compression N_x is increased. This change is continuous in the PANDA2 post-local-buckling theory because the panel is assumed to be infinitely long for the purpose of calculating local buckling and postbuckling behavior. In tests actual panels often experience 'mode jumping' as the applied load is increased well beyond the initial local bifurcation buckling load: the number of axial waves changes suddenly, often with a loud 'bang'.

The peculiar behavior of the curve in Fig. 19 labelled '$w_0/t_1 = 0.1$' in the neighborhood of the local buckling load is an artifact resulting from the analysis strategy and the local initial imperfection: for loads at or below the local buckling load according to the Koiter theory

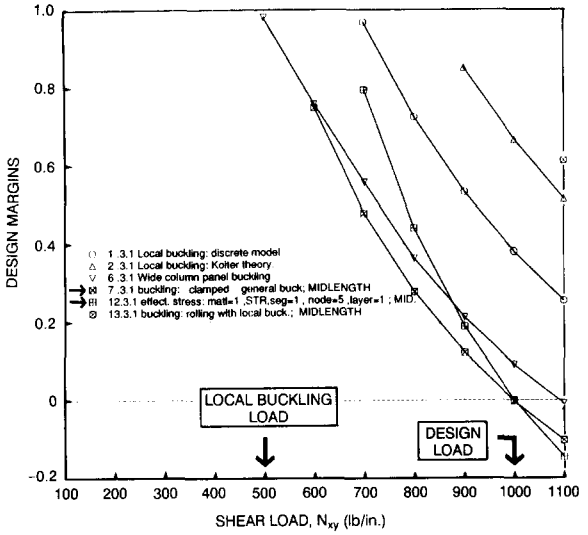

Fig. 23. Margins versus in-plane shear load N_{xy} for Load set 3. Note: the axial compression N_x varies in proportion to N_{xy}.

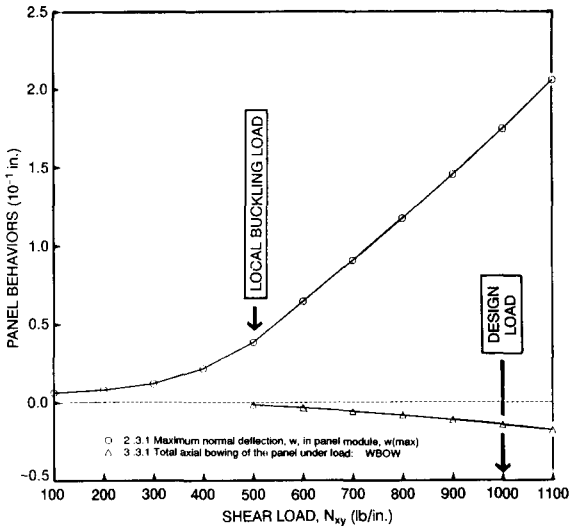

Fig. 24. Local postbuckling normal displacement w between stringers and overall axial bowing for Load set 3. Note: the axial compression N_x varies in proportion to N_{xy}.

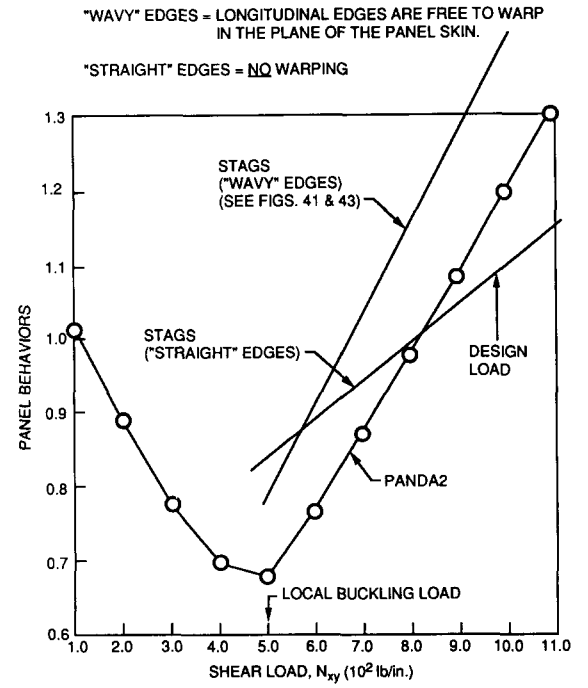

Fig. 25. Slope of the local buckling nodal lines versus N_{xy}. Note: N_x varies in proportion to N_{xy} in Load set 3.

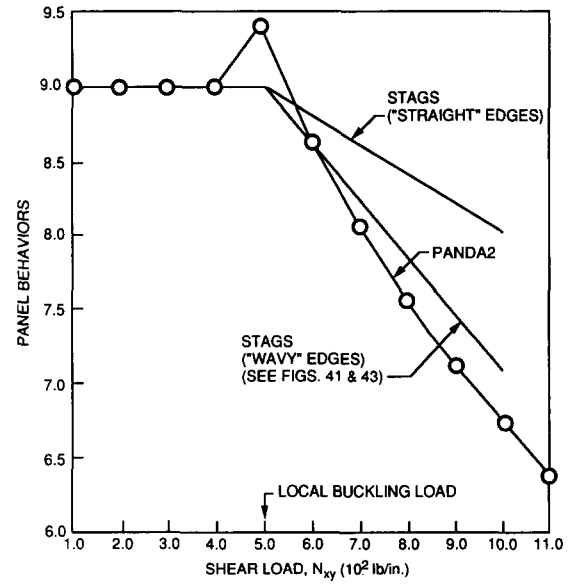

Fig. 26. Number of axial halfwaves versus N_{xy}. Note: N_x varies in proportion to N_{xy} in Load set 3.

(EKOITR ≥ 1.0 in Table A.1) only the postbuckling variables f, a, m are unknowns; the axial wavelength parameter N is fixed at its value at bifurcation. At loads above the local buckling load (EKOITR < 1.0) N becomes one the unknowns and is therefore allowed to vary. The sudden jump in the number of axial halfwaves after local buckling is caused by the presence of the initial imperfection. When the normalized imperfection amplitude w_0/t_1 is set to a very small number the sudden jump in number of axial halfwaves after local buckling disappears, as demonstrated in Fig. 19 for the curve labelled '$w_0/t_1 = 0.037$'.

5.3.2. Load set 2: axial compression N_x, positive bowing

The results for Load set 2 are similar to those for Load set 1. As seen from Fig. 13, bending-torsion buckling of the stringer becomes critical as the design is optimized because the stringer tips are compressed more than the panel skin at the panel midlength in the positively bowed panel. By comparing Fig. 20 with Fig. 16, one can see that as the axial compression N_x is increased, the sidesway of the blade tip becomes somewhat more pronounced and the flattening of the postbuckling normal modal deflection in the panel skin near the midline between stringers becomes less pronounced than in the case of the negatively bowed panel.

5.3.3. Load set 3: combined axial compression N_x and in-plane shear N_{xy}, no bowing

Figure 21 is analogous to Fig. 15. The axial halfwavelength in the local postbuckling pattern is about twice as long in this case. Therefore, Fig. 21 represents about one third of the total length of the panel. The slope of the local buckling nodal lines at the maximum load combination N_x, N_{xy} reached in the test simulation ($N_x = -1100$ lb/in; $N_{xy} = +1100$ lb/in) is indicated in Fig. 21. Figure 22 is analogous to Fig. 16. There is less flattening of the local buckles midway between stringers in Load set 3 than in Load set 1.

Figure 23 is analogous to Fig. 17. In this case general buckling and maximum effective stress become critical at the design load combination $N_x = -1000$ lb/in; $N_{xy} = +1000$ lb/in. Note that although the margins in Fig. 23 are plotted versus the in-plane shear load N_{xy}, the axial load N_x is varied in proportion to N_{xy}.

Figure 24 is analogous to Fig. 18. In this case there is no initial axial bowing. The axial bowing shown in Fig. 24 arises from the redistribution of loads over the various segments of the panel module as the panel is loaded into its locally postbuckled state.

Figure 25 shows the slope of the post-local-buckling nodal lines with increasing load combination N_x and N_{xy}. The trend predicted by PANDA2 is verified by that of STAGS in the post-local buckling regime. Figure 26 is analogous to Fig. 19. Again, the peculiar result in the neighborhood of the local buckling load results from the analysis strategy and local imperfection, as discussed above. Predictions from STAGS, taken from Figs. 41 and 43 and to be discussed in the next section, exhibit the same trend as those from PANDA2.

5.4. Evaluation of the PANDA2 results from STAGS models

The strategies used in PANDA2 [39, 46, 47] involve many 'tricks' and approximations that permit, with modest computer resources, the generation of optimum designs in load ranges for which the behavior is very nonlinear. For example, in PANDA2 the behavior of a single panel module in local buckling and postbuckling phases of the analysis is assumed to repeat over the number of modules in the entire panel; conditions that exist at the midlength of the panel are

assumed to exist along the entire length of the panel; the nonlinear post-local-buckling analysis is reduced to a problem with at most four unknowns, f, a, m, N; the effect of in-plane shear on buckling and postbuckling behavior is predicted with use of the unknown m, the slope of the buckling nodal lines; the axial bowing amplitude is assumed to grow hyperbolically as the load factor approaches that corresponding to a preliminary estimate of the general instability load factor; use is made of the concept of wide column buckling; the unconservative nature of using 'smeared' stringer models for general instability is compensated by using an empirically derived 'knockdown' factor to account in an approximate way for the discreteness of the stringers [47].

To verify the appropriateness of these simplifications, it is essential that the designs generated by PANDA2 be evaluated by application of a general-purpose computer program capable of predicting accurately what happens when a stiffened panel is loaded far into its post-local-buckling regime. The STAGS program was selected because of the close proximity of the developers and because much effort has been expended during the past few years to improve the capability of STAGS to predict the behavior of shells that experience arbitrarily large local rotations.

5.4.1. Capability of STAGS

STAGS (STructural Analysis of General Shells) is a finite element code for general-purpose nonlinear analysis of stiffened shell structures of arbitrary shape and complexity [22, 23]. Its capabilities include stress, stability, vibration and transient analyses with both material and geometric nonlinearities permitted in all analysis types. Currently a new version of STAGS is under development [52]. Enhancements include more advanced nonlinear solution strategies [53], a higher order thick shell element [54–56], accumulation of buckling modal imperfection shapes from previous linear or nonlinear runs [49], and more comprehensive post-processing features such as a link with PATRAN [57] and a sophisticated x–y plotting package called STAGSPP [58]. More details about STAGS are given in [49] and in the STAGS literature [52].

5.4.2. PANDA2-to-STAGS model generation

A PANDA2 processor, executed by the command 'STAGSMODEL', creates input files for STAGS corresponding to panel configurations optimized with PANDA2. With STAGSMODEL and STAGS the load-carrying capacity of optimum designs obtained by PANDA2 can be checked without the user having to spend time setting up elaborate finite element models for STAGS from directions in the STAGS user's manual. The STAGSMODEL processor can be used to create a succession of STAGS models by means of which bifurcation buckling behavior and nonlinear post-local-buckling behavior of a panel optimized by PANDA2 can be determined from a rigorous nonlinear finite element model.

The STAGSMODEL processor creates a finite element model of the part of a panel between adjacent rings. The panel can be loaded by any combination of uniform axial load N_x, uniform hoop load, N_y, uniform in-plane shear N_{xy}, and uniform normal pressure p.

Depending on a user-selected index, the normal projection of the two edges parallel to the stringers on the undeformed panel skin may be forced to remain straight or may be allowed to undergo in-plane warping (nonlinearly varying circumferential displacement v, that is, displacement in the y-direction). At the axially loaded ends of the panel the cross-sections of the

stringers are not allowed to warp. In non-bifurcation phases of analyses the axial displacement u is zero at one end of the STAGS model and is uniform at the other end. The user chooses whether or not stringer sidesway is permitted at the axially loaded ends of the panel.

The entire STAGS model is created in what in STAGS jargon is called an 'element unit'. The stringer web(s) and outstanding flange, if any, are also modelled with finite elements. In STAGSMODEL the user chooses how many skin-stringer modules to include in the STAGS model of the panel. For certain problems, such as a panel subjected only to uniform axial compression, a one-module model is sufficient to predict local buckling and post buckling as well as wide column general instability. Such a model is shown in Fig. 27, for example. This is achieved by imposition of symmetry conditions along the two longitudinal edges of the one-module model, in a manner analogous to that shown in Fig. 4(b). These two edges are located midway between stringers. In other cases, such as panels in which in-plane shear loading is significant, a multi-module model such as that shown in Fig. 40 is required. Even if a multi-module model is required, it is often acceptable to include in the STAGS model fewer modules than exist in the actual panel.

LIMITATIONS IN STAGSMODEL. Thermal loading and edge moments cannot yet be included. Truss-core sandwich panels cannot be handled. Also, if the panel is axially stiffened the axially loaded edges cannot rotate in either the prebuckling or bifurcation buckling phases of the analysis. The material must remain elastic. The loading/end shortening must be uniform. Ring stiffeners cannot yet be included.

5.4.3. Predicting the behavior of stiffened, locally buckled panels via finite element analysis can be difficult

The objective of the STAGS runs is to simulate a test of a panel optimized with PANDA2. In this 'test' the panel must be loaded at least up to the design load and probably beyond the

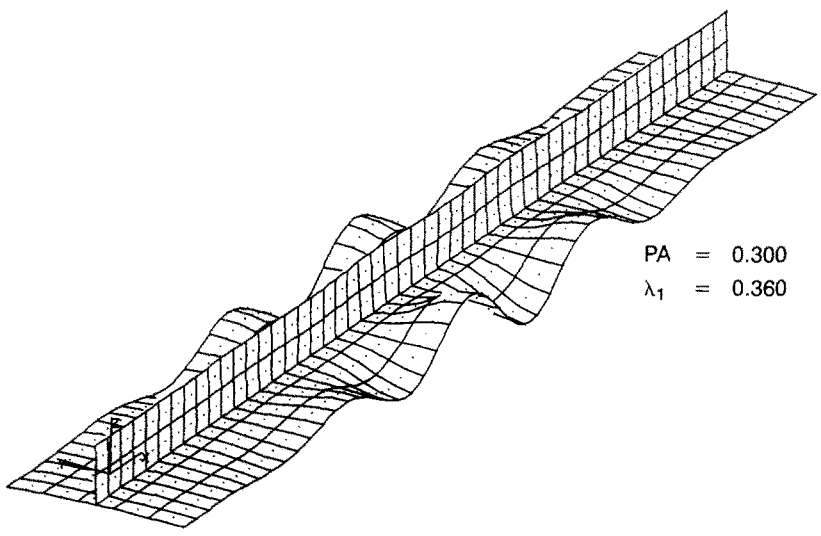

Fig. 27. Bifurcation buckling mode from a STAGS single module finite element model of the optimized panel as loaded by Load set 1. This mode, with an amplitude of +0.002 inches, is used as an initial imperfection in the STAGS collapse run that follows.

design load by at least ten percent. (In this work the design load is associated with a load factor PA = 1.0.) This objective is often not easily obtained if the panel buckles locally at a load factor PA considerably less than unity. This is a difficult problem for a nonlinear finite element program, even if the program includes rather elaborate strategies such as the Riks continuation method [59], which has been implemented in STAGS.

In actual panels loaded well into the postbuckling regime there is a tendency for 'mode jumping' to occur. The wave pattern in the locally postbuckled panel suddenly changes, often with a loud noise. An example of this behavior is given in [39]. The mode jumping phenomenon is evidence of near singularity of the postbuckled equilibrium state. Numerical models of structures that display mode jumping in tests will therefore be difficult to solve.

The problem may become especially difficult if there are many axial halfwaves in the local buckling mode and if the STAGS model of the panel contains several modules. Cases of this sort require a fine mesh so that the local buckling and postbuckling behavior can be captured with reasonable accuracy. The extremely nonlinear behavior associated with local buckling and postbuckling, coupled with the requirement for a large number of degrees of freedom, result in long run times on the computer. When several modules are used in the STAGS model of the panel there tend to be many bifurcations and near-bifurcations on the primary equilibrium (load-deflection) path in the locally postbuckled regime.

As the load factor (called 'PA' in the STAGS output) approaches that corresponding to a bifurcation point on the primary equilibrium path, more iterations are required to obtain convergence to a solution of the nonlinear equations. The Riks [59] path increment parameter (called 'DETA' in the STAGS analysis) is therefore set by STAGS to a smaller and smaller number as the bifurcation point or near-bifurcation region is approached in successive load steps.

It may happen that the path increment DETA becomes so small that the STAGS run terminates. It often happens that when DETA gets very small, the run does not terminate automatically but 'Riks path reversal' occurs, that is, the panel starts to unload along the primary equilibrium path or along an equilibrium path very close to the primary path. This unloading will often continue until the load factor is zero or negative if the user does not intervene to terminate the STAGS run. In some cases 'Riks path oscillation' occurs: over many load steps the load factor PA 'hovers' around a value for which bifurcations or near bifurcations exist, the panel unloading, reloading and unloading again. These behaviors, many of which are illustrated in [46], can prevent the load factor PA from attaining the design load, PA = 1.0.

5.4.4. Solving the problem by introduction of bifurcation buckling modal imperfections

The difficulties just described are often (but unfortunately not always) overcome if the user does the following:

(a) performs a nonlinear equilibrium run of a panel with local imperfection shapes obtained from previous linear or nonlinear bifurcation buckling runs of the same case;

(b) performs one or more nonlinear bifurcation buckling runs corresponding to points on the primary equilibrium path obtained from run (a) at loads for which the Riks path length parameter DETA is very small;

(c) selects as additional initial imperfection shapes one or more eigenmodes from the nonlinear bifurcation buckling runs (b);
(d) assigns an appropriate amplitude factor (positive or negative) to each modal imperfection (eigenmode) selected in (c);
(e) reruns the nonlinear equilibrium analysis, usually starting from a load factor of zero in order to avoid lack of convergence at the first load step.

The new nonlinear equilibrium analysis may well fail as before, this time at a different load factor PA. The user should repeat the procedure just outlined, adding new imperfection shapes to those present in the previous nonlinear equilibrium run.

The process should be repeated until the load factor PA exceeds that corresponding to the design load, PA = 1.0. An example appears in [49]. Fan et al. [60] employ a similar method.

Another example of this repetitive procedure is given in [46]. Figures 39–54 present final

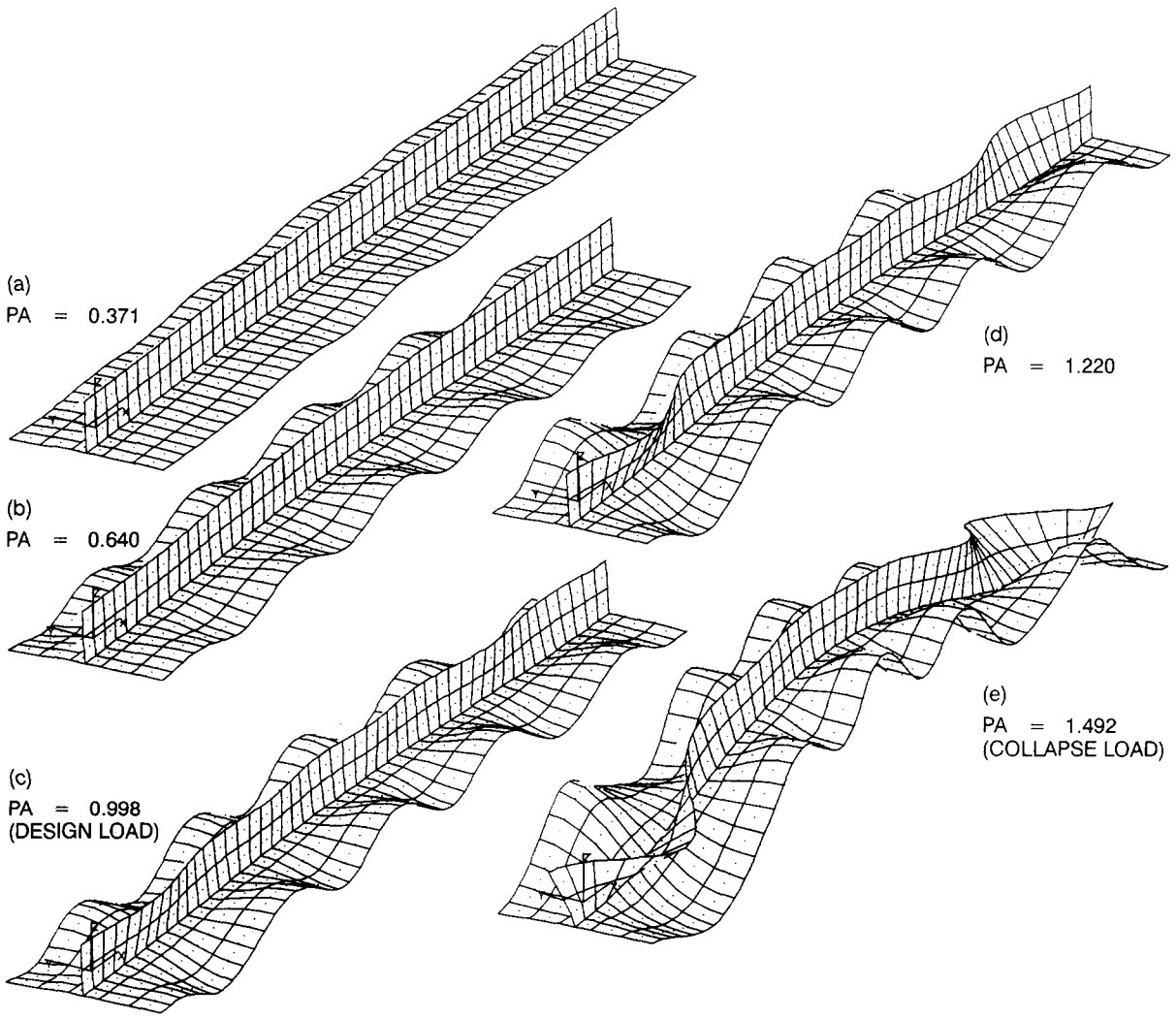

Fig. 28. State of the panel at various load factors PA for Load set 1 (negative axial bowing). PA = 1.0 is the design load.

results from that difficult case. Sixteen STAGS runs were required, and as many as 20 imperfection shapes obtained from nonlinear bifurcation buckling runs at various loads were included in the final nonlinear equilibrium model. Each nonlinear equilibrium run required from 1000 to 2000 minutes of CPU time on the STARDENT P3 computer, which translates to 24–36 hours of wall time. Hence, this case was almost continuously in process from 5 to 28 December 1991.

A new method of solving the mode jumping problem is currently being explored by Rankin et al. [61]. This method involves mixed static and dynamic nonlinear continuation.

In the next section results are given from application of STAGS to the curved, blade-stiffened panel optimized with PANDA2 as loaded by Load sets 1–3. The runstream is listed in the last part of Table A.4. Figures 27–32 pertain to Load set 1; Figs. 33–38 pertain to Load set 2; and Figs. 39–55 pertain to Load Set 3. The ANS finite element (nine nodes, transverse shear deformation included [54–56]) is used in this and all of the STAGS finite element models described in this paper.

5.4.5. STAGS results for Load set 1: axial compression of panel with negative axial bowing

With negative axial bowing the panel skin is compressed more than the stringer tips at the panel midlength. Figure 27 shows the buckling mode shape and load factor obtained from the one-module STAGS model. Buckles appear only in the midlength region because the local prebuckling axial compression N_x in the panel skin is greater there than near the ends because of the negative axial bowing. According to PANDA2 the local buckling load factor from Koiter theory [eqs. (51)–(54)] is 0.316. The PANDA2 value 0.316 is less than the STAGS value 0.360 because of the negative axial bowing. In the STAGS analysis a load factor PA = 0.3 is applied and the local buckling load factor (eigenvalue) is determined from the prebuckled state at that value of PA. In the PANDA2 analysis the local buckling load factor is

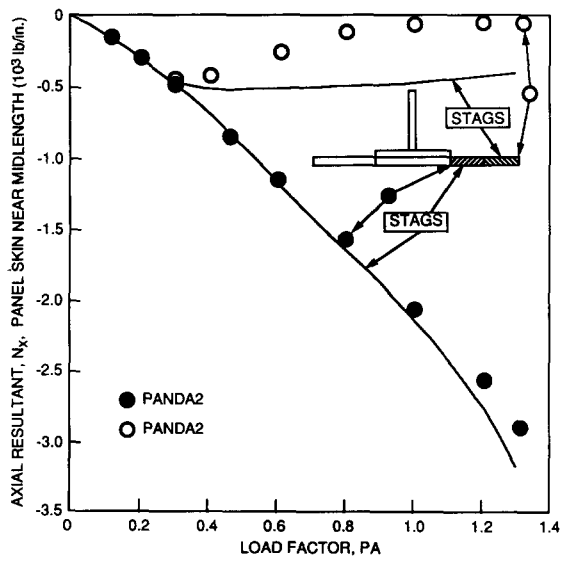

Fig. 29. Redistribution of internal axial load N_x near the panel midlength in the panel skin in the post-local-buckling regime for Load set 1.

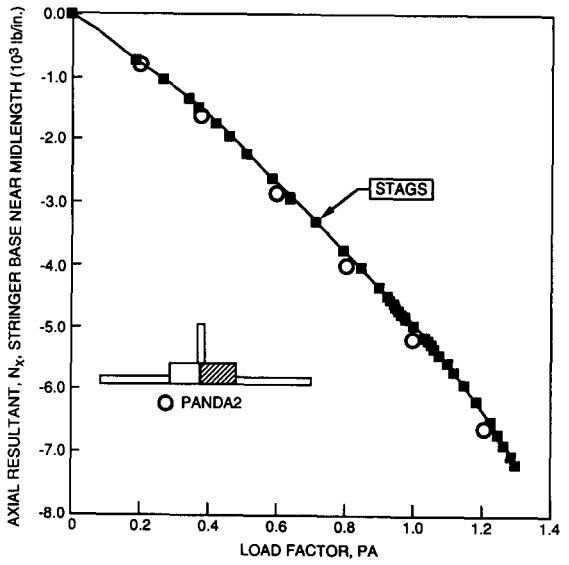

Fig. 30. Redistribution of internal axial load N_x near the panel midlength in the stringer base in the post-local-buckling regime for Load set 1.

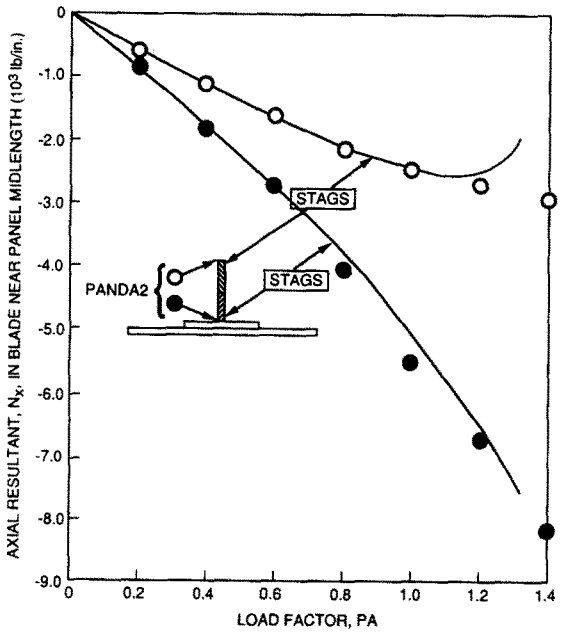

Fig. 31. Redistribution of internal axial load N_x near the panel midlength in the stringer blade in the post-local-buckling regime for Load set 1.

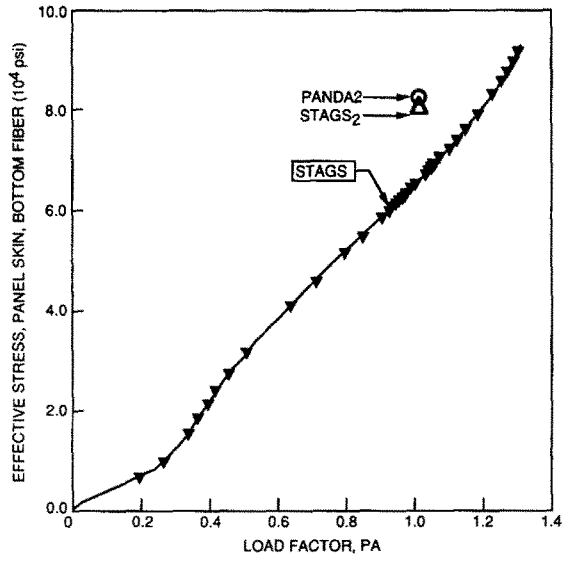

Fig. 32a. Effective stress in the panel skin near the panel midlength, near and at the junction between the panel skin and stringer base for Load set 1.

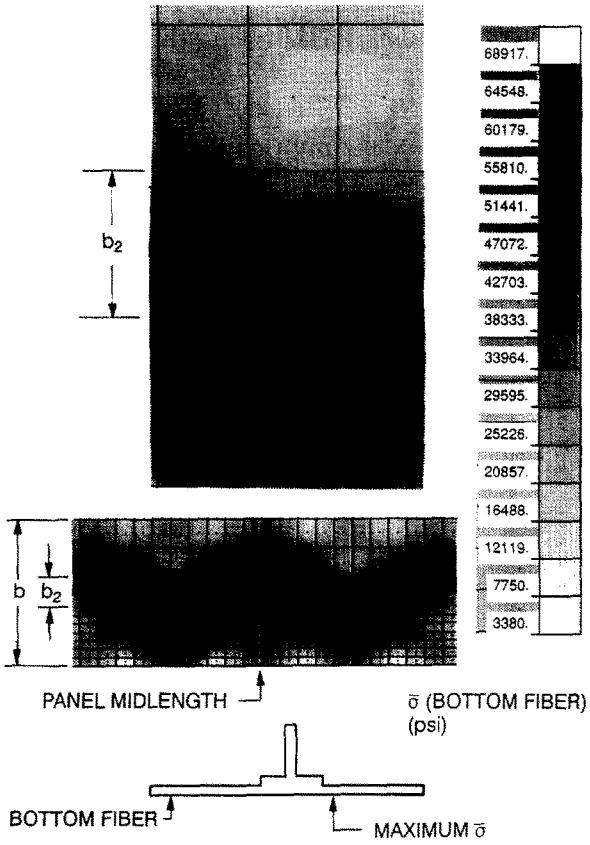

Fig. 32b. PATRAN plot of effective stress at the bottom fiber in a STAGS model in which the number of finite elements in the panel skin on one half of the module has been increased by more than a factor of three from that on the other half of the module. Load factor PA = 1.0, Load set 1.

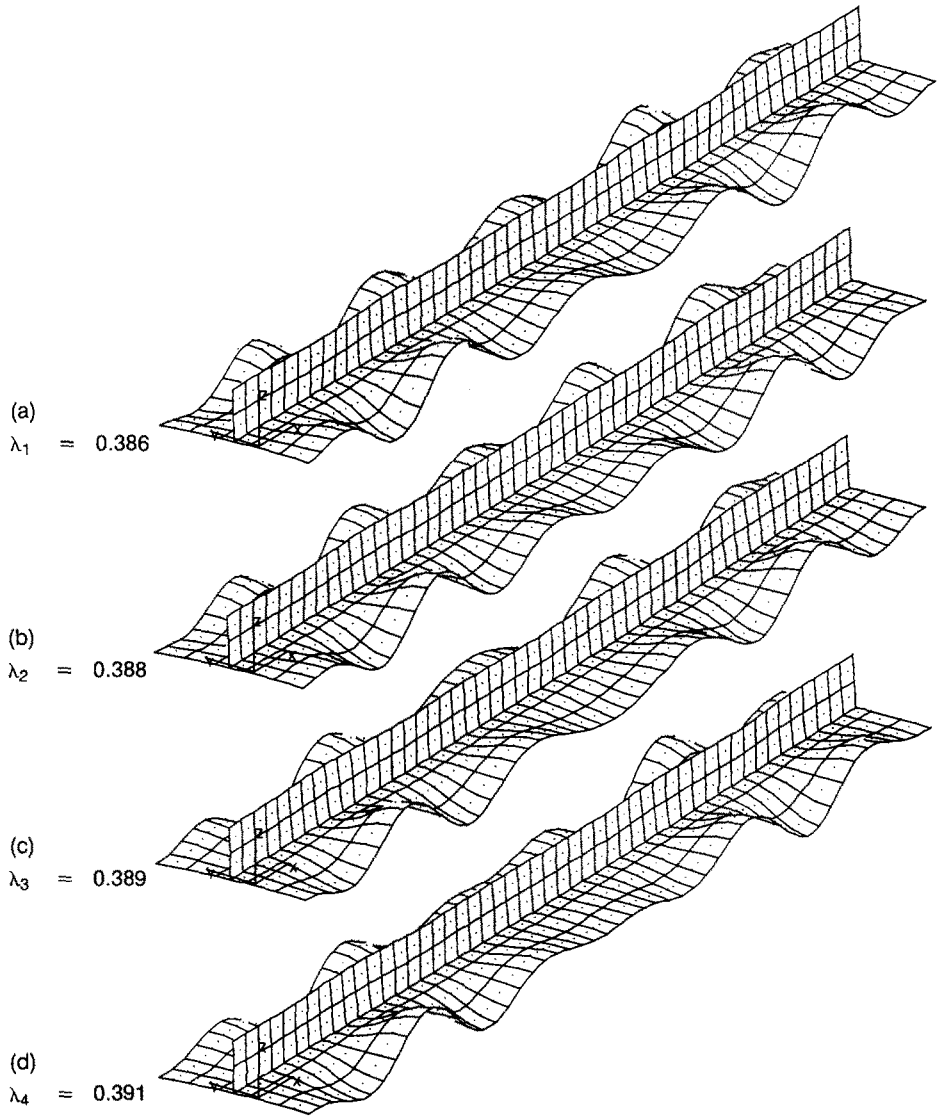

Fig. 33. Bifurcation buckling modes from a STAGS single module finite element model of the optimized panel as loaded by Load set 2. These modes, each with an amplitude of +0.001 in, are used as initial imperfections in the STAGS collapse run that follows.

obtained from the panel as loaded by the design load, PA = 1.0. At PA = 1.0 there is considerable amplification of the negative axial bowing, which increases the local prebuckling axial compression N_x in the panel skin at the midlength of the panel. (With axial bowing set equal to zero, PANDA2 obtains a local buckling load factor of 0.360.)

The mode shape shown in Fig. 27 is introduced as an initial imperfection for the next STAGS run, which corresponds to Step (a) in Section 5.4.4. A modal amplitude of +0.002 in is assigned. This is 3.7 percent of the panel skin thickness t_1.

The nonlinear equilibrium STAGS run with the single modal imperfection is successful: the panel loads to PA = 1.492 before collapsing as shown in Fig. 28. According to PANDA2, the

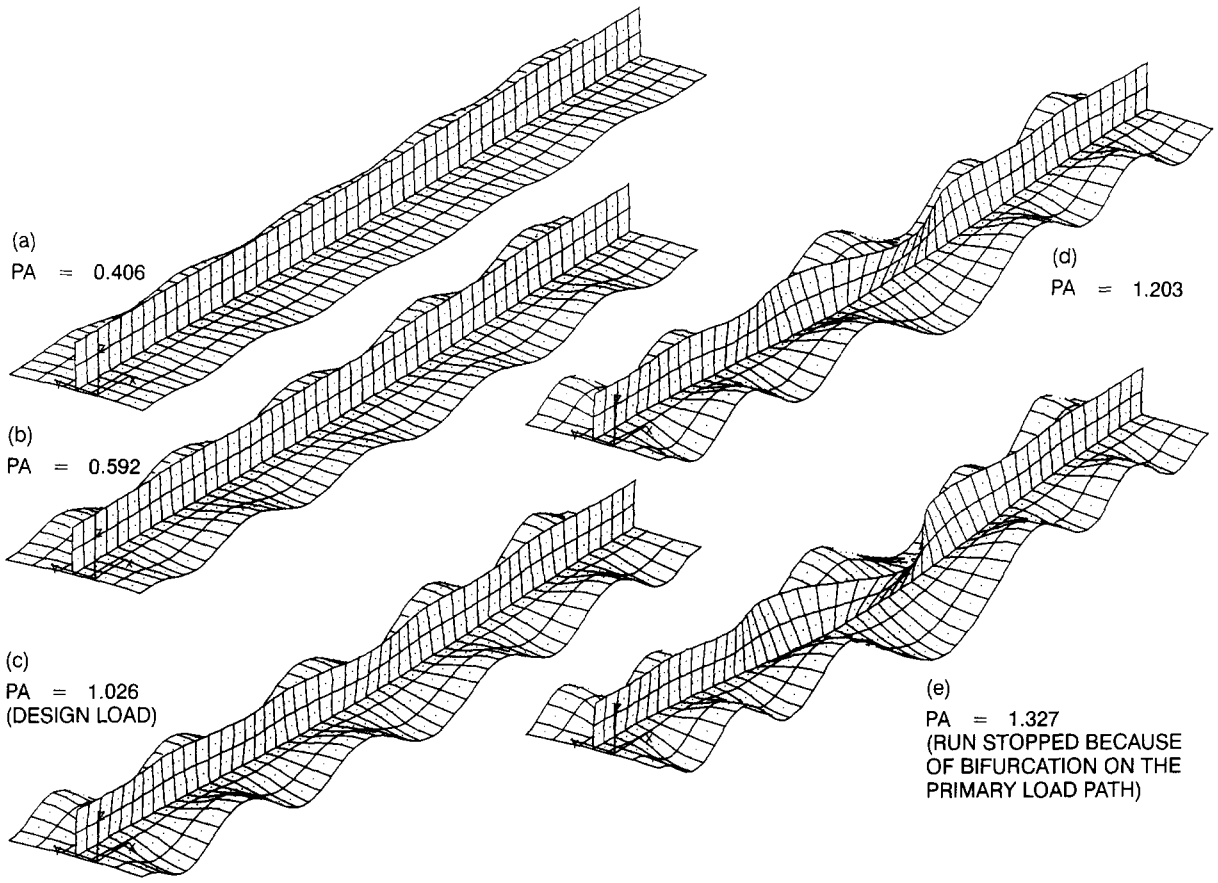

Fig. 34. State of the panel at various load factors PA for Load set 2 (positive axial bowing). PA = 1.0 is the design load.

wide column load factor is PA = 2.218, considerably above the wide column collapse load PA = 1.492 found by STAGS. It is likely that the discrepancy is caused by bending-torsion buckling of the stringer near the ends of the panel, evident in Fig. 28(e). In this problem PANDA2 checks only for conditions at the midlength of the panel, where the stringer does not undergo bending-torsion buckling because of the negative axial bowing. Bending-torsion buckling has been included in the design phase, however, because Load set 2 has positive axial bowing, that is, axial bowing which causes the stinger tips at the panel midlength to be compressed more than the panel skin. Hence, the bending-torsion buckling evident at the ends of the panel in Fig. 29(e) is accounted for in an approximate sense during optimization with PANDA2 through the margins associated with Load set 2. Note from Fig. 13 that according to PANDA2 bending-torsion buckling is critical for the optimized design subjected to Load set 2.

Figures 29–32 give comparisons between PANDA2 and STAGS results corresponding to conditions near the midlength of the panel as loaded by Load set 1.

Figure 29 shows the redistribution of the axial resultant N_x in the thin part of the panel skin at the midlength of the panel in the post-local-buckling regime. Local buckling corresponds to the load at which the two STAGS curves bifurcate. (Actually, the bifurcation of the two

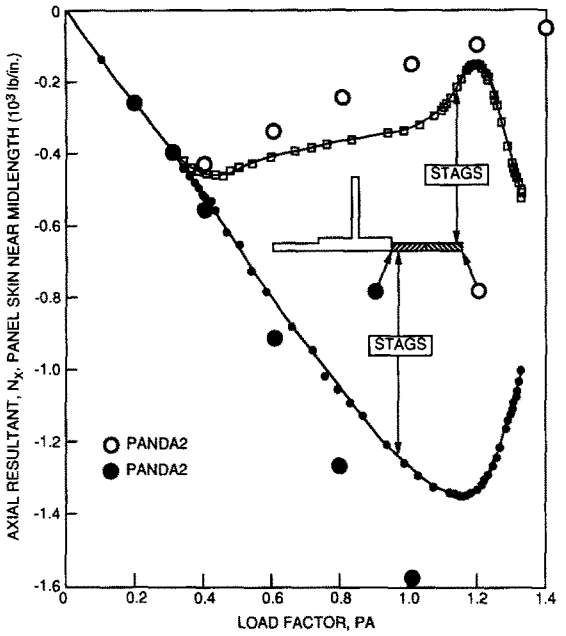

Fig. 35. Redistribution of internal axial load N_x near the panel midlength in the panel skin in the post-local-buckling regime for Load set 2.

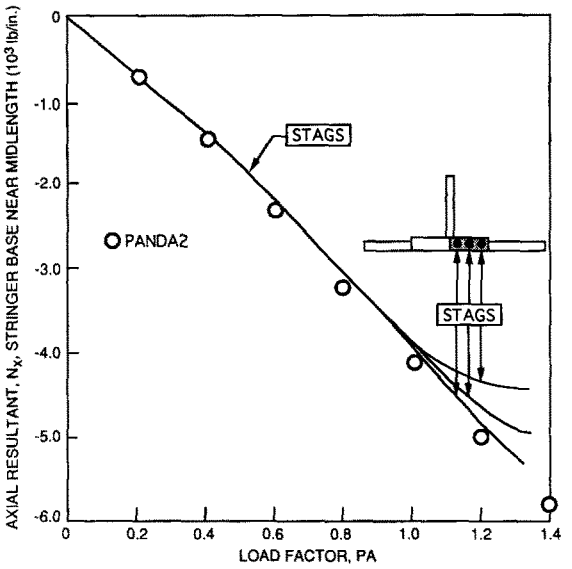

Fig. 36. Redistribution of internal axial load N_x near the panel midlength in the stringer base in the post-local-buckling regime for Load set 2.

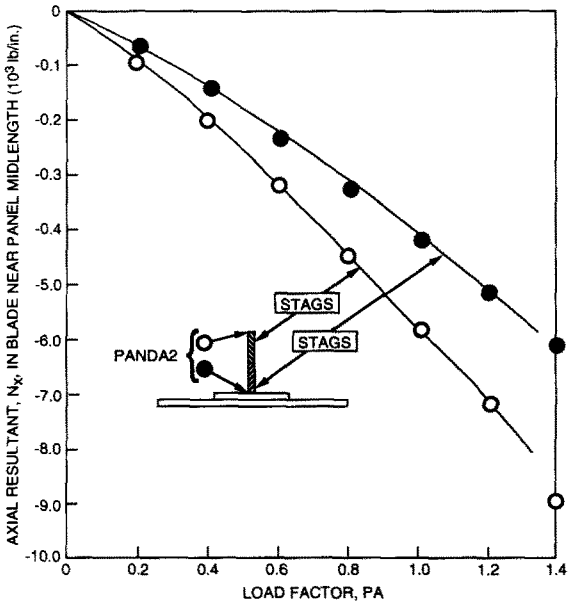

Fig. 37. Redistribution of internal axial load N_x near the panel midlength in the stringer blade in the post-local-buckling regime for Load set 2.

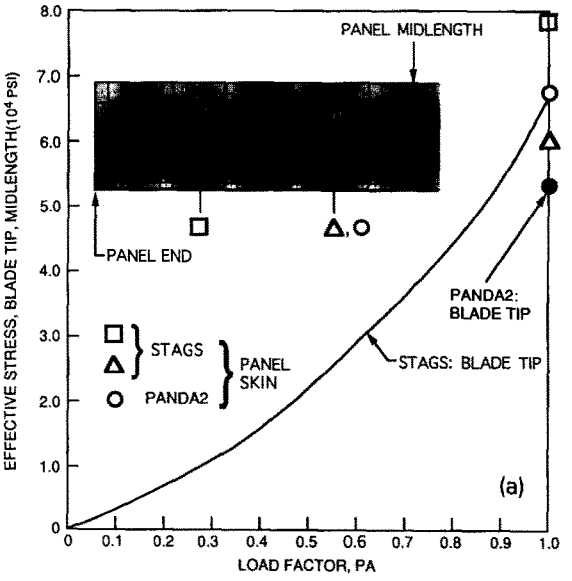

Fig. 38a. Maximum effective stresses in the panel for Load set 2 as predicted from the STAGS model with a dense finite element grid over half of the panel skin. Inset fringe pattern corresponds to effective stress at the bottom fiber of the panel skin at the design load PA = 1.0. All PANDA2 points correspond to predictions at the panel midlength at PA = 1.0.

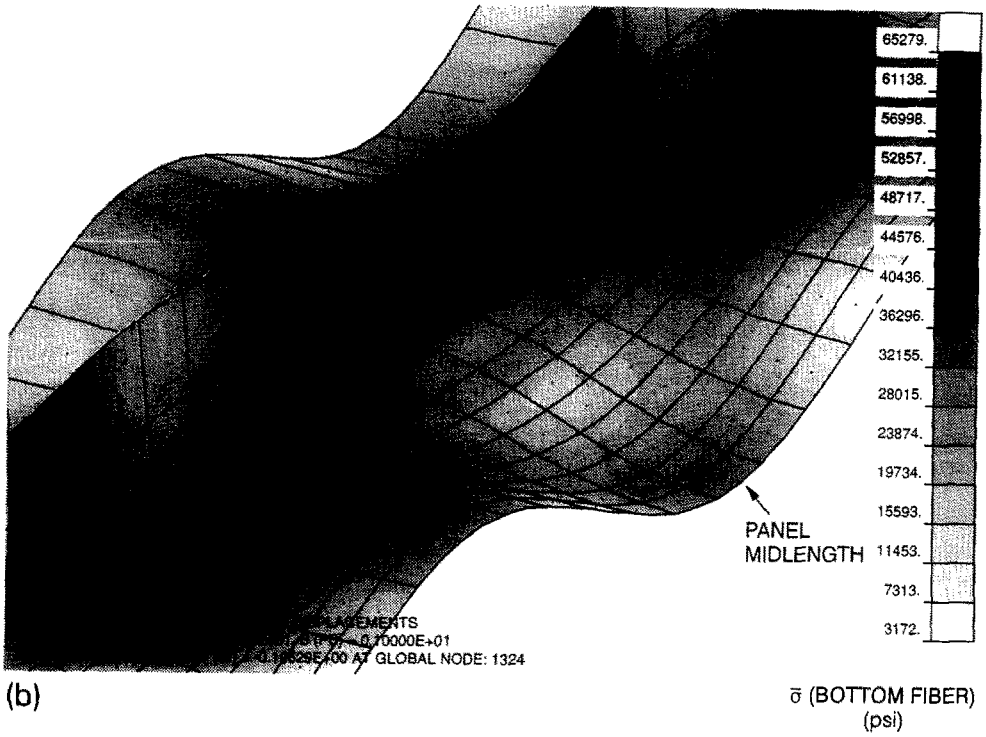

Fig. 38b. Fringe pattern of effective stress in the neighborhood of the panel midlength from the STAGS model as deformed by Load set 2 at the design load PA = 1.0.

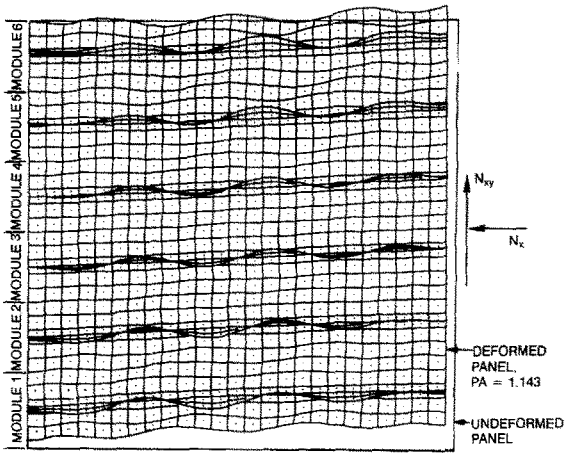

Fig. 39. Six-module STAGS model of the optimized panel for study with Load set 3.

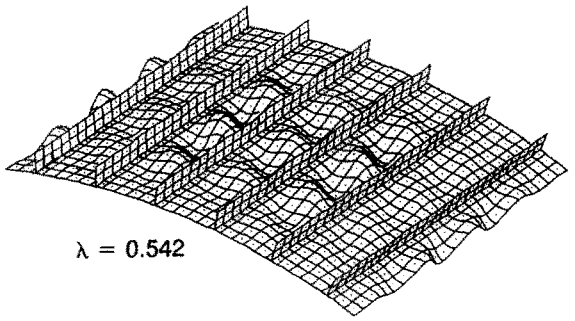

Fig. 40. Bifurcation buckling mode from Load set 3.

curves occurs near the load factor PA = 0.30, somewhat lower than the eigenvalue predicted by STAGS, PA = 0.36, because of the presence of the initial imperfection shown in Fig. 27). At the design load PA = 1.0 the panel is loaded well into the postbuckling regime. Most of the axial load has been shed to the stringer bases and blades. Note that the PANDA2 points in

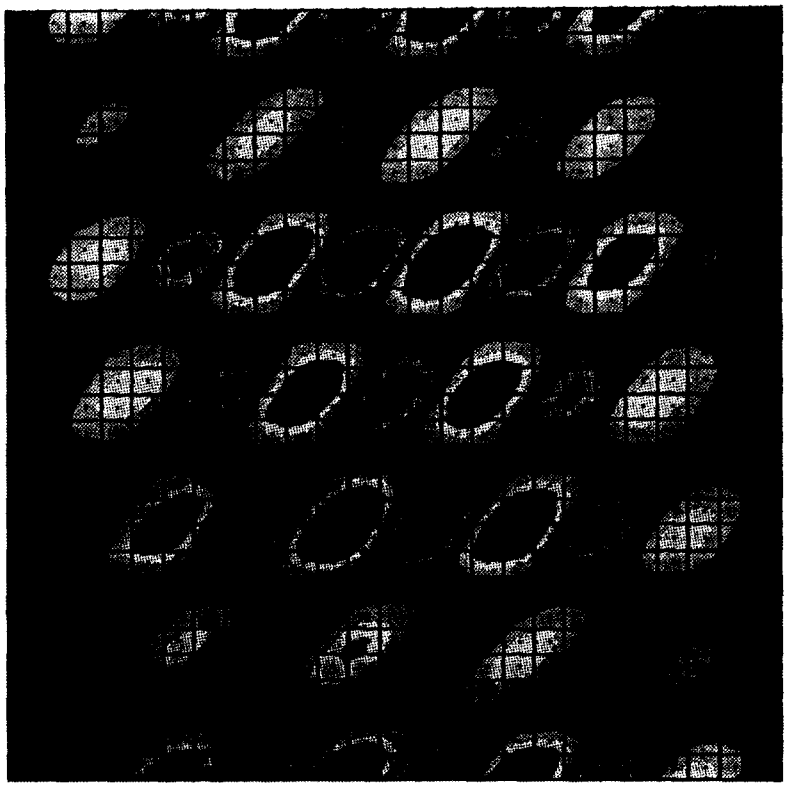

Fig. 41. Fringe plot of bifurcation buckling mode. The slope of the buckling nodal lines plotted at the left-hand end of the line in Fig. 25 labelled 'STAGS result for wavy edges' was measured from this plot.

Fig. 29 correspond to the axial load in the thin part of the panel skin exactly at the skin-base junction and at the midplane between stringers, whereas the STAGS points correspond to the leftmost integration point in the finite element adjacent to the stringer base and to the centroid of the finite element adjacent to the midplane between stringers. There are nine integration points in each of the nine-node quadrilateral finite elements shown in Fig. 27. Therefore, in the panel module cross-section sketched in Fig. 29 there are three integration points along the widths (y direction) of each of the two finite elements that represent the thin part of the panel skin shown shaded in the sketch.

Figure 30 shows the axial load N_x in the stringer base at the midlength of the panel. By looking along the curve toward the origin from a point just above the plane of the paper, one can see the rather sharp break in the slope of this curve near the local buckling load factor PA = 0.30 to 0.36. The steepening slope for PA $\geq$ 1.0 is caused primarily by amplification of the negative axial bowing as the axial load N_x approaches the collapse load.

Figure 31 shows the axial load N_x at the root and tip of the stringer. For load factor PA $\geq$ 1.0 the STAGS curves diverge more abruptly than the PANDA2 curves because the collapse load according to STAGS is PA = 1.492, whereas the wide column buckling load factor according to PANDA2 is PA = 2.218, a discrepancy caused by bending-torsion buckling of the stringers at the ends of the panel, as explained above.

Figure 32a shows the maximum effective (Von Mises) stress $\bar{\sigma}$ in the region near the

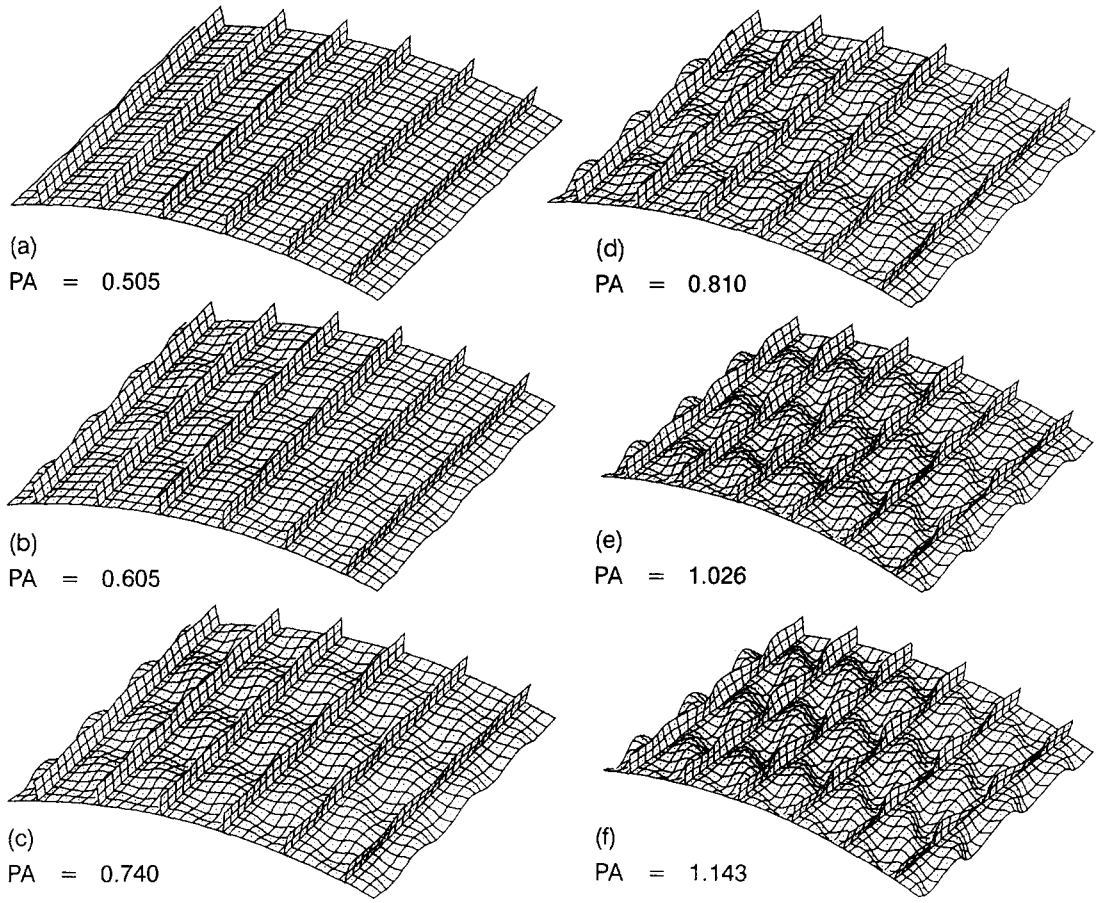

Fig. 42. State of the panel at various load factors PA for Load set 3. PA = 1.0 is the design load.

midlength of the panel. The curve labelled 'STAGS' in Fig. 32a is generated from the single module model shown in Fig. 28c (PA = 0.998, very near the design load) by first obtaining for the load factor PA = 0.998 a fringe plot from PATRAN [57] of the effective stress fields for top and bottom fibers, choosing the finite element(s) that contain the maximum value(s) at PA = 0.998, and then plotting the effective stress versus load factor PA at the integration points in the chosen element with use of the STAGS postprocessor STAGSPP [58]. Both PANDA2 and STAGS predict that this maximum stress occurs at the bottom fiber in the panel skin at the junctions between the stringer bases and the panel skin.

The largest component of stress at these locations is the hoop stress σ_y caused by local hoop bending w_{yy}. For example, according to PANDA2, at the design load PA = 1.0, at the top fiber, in the panel skin, at the junction of panel skin and stringer base where the local postbuckling normal displacement w is downward (left-hand portion of Fig. 16), the axial stress $\sigma_x = -22224$ psi, the hoop stress $\sigma_y = +67918$ psi, and the shear stress $\tau_{xy} = -4890$ psi. The STAGS results at the design load PA = 1.0 are considerably below the PANDA2 results because the STAGS finite element model shown in Fig. 28 is too crude to capture accurately the steeply varying hoop curvature change w_{yy} near the junction of panel skin and stringer base.

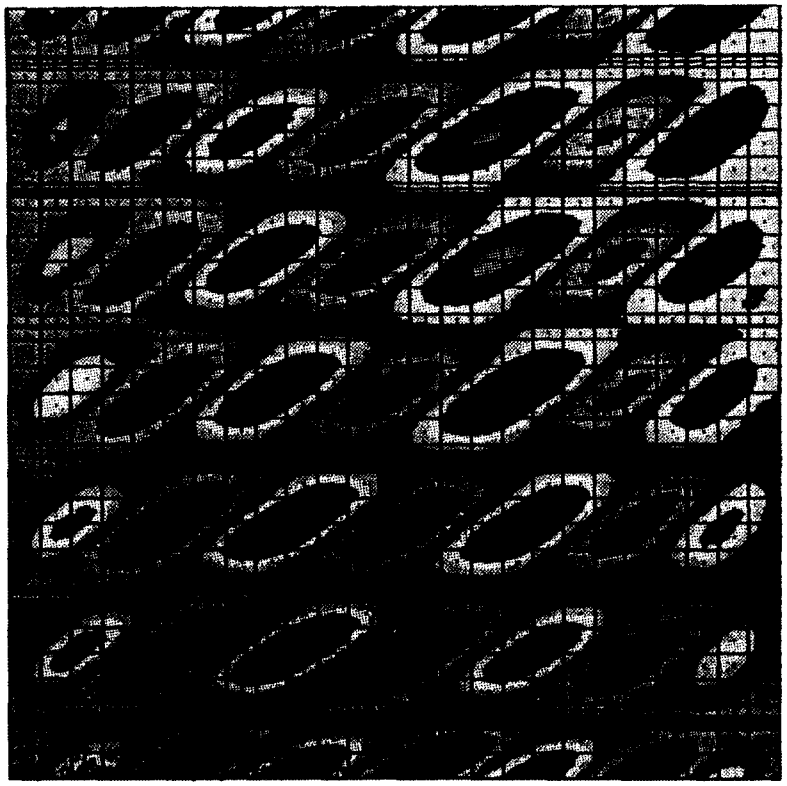

Fig. 43. Fringe plot of the postbuckled state at load factor PA = 1.143. The slope of the buckling nodal lines plotted at the right-hand end of the line in Fig. 25 labelled 'STAGS result for wavy edges' was measured from this plot.

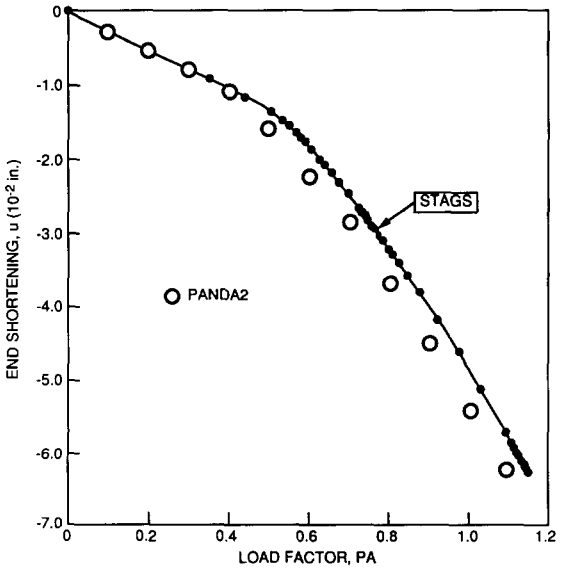

Fig. 44. End shortening u versus load factor PA for Load set 3.

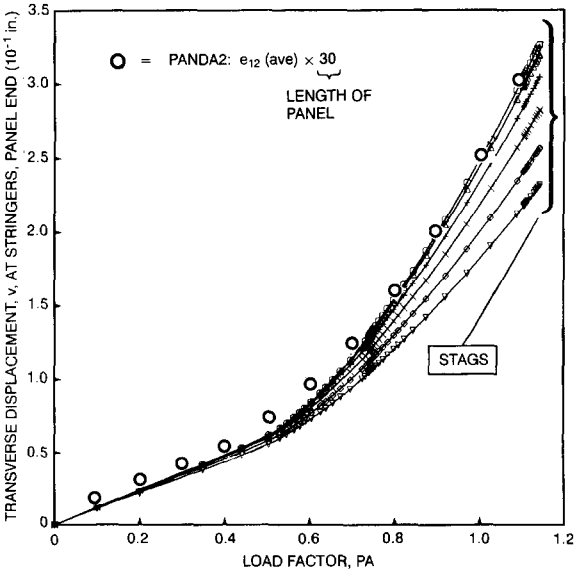

Fig. 45. Average circumferential displacement $\bar{v}$ from PANDA2 and circumferential displacements v_i at the ends of the six stringers from STAGS, Load set 3.

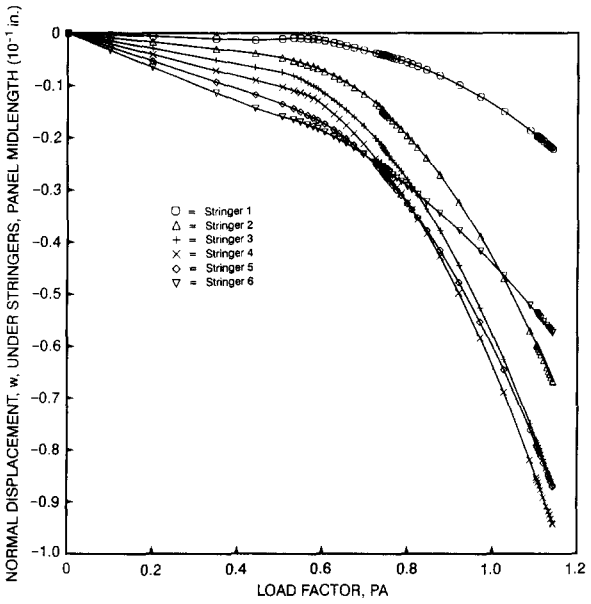

Fig. 46. Axial bowing at the midlength of the panel as obtained from the STAGS model, Load set 3.

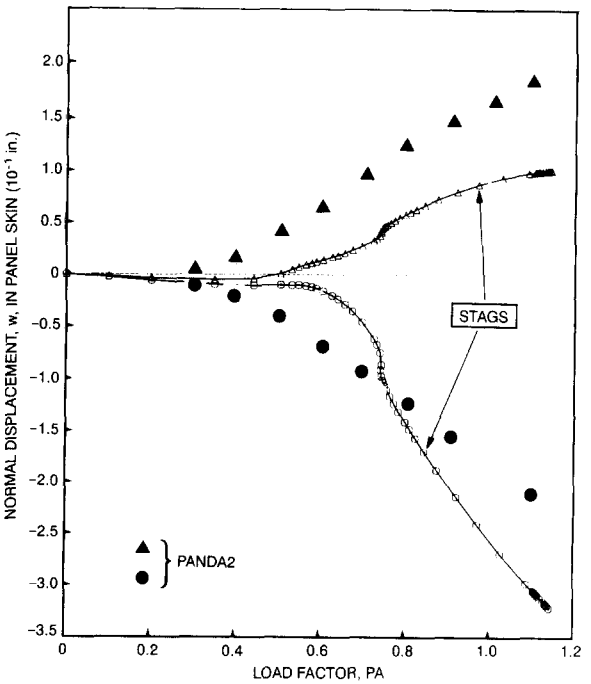

Fig. 47. Amplitude of local buckles from PANDA2 and from the six-module STAGS model in the center bay near the panel midlength, Load set 3.

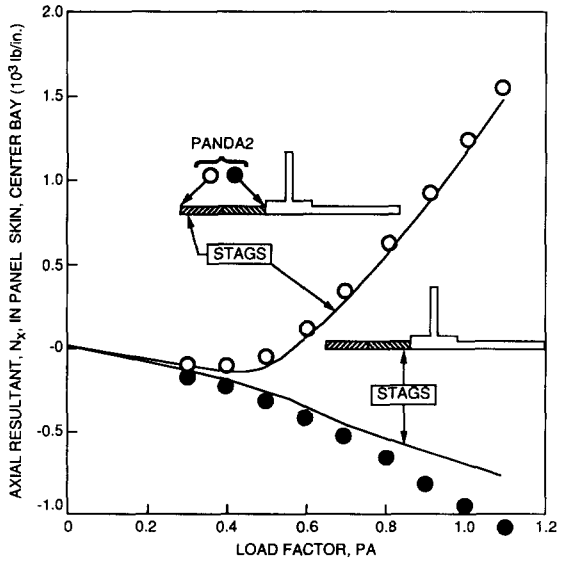

Fig. 48. Redistribution of internal axial load N_x near the panel midlength in the panel skin in the post-local-buckling regime for Load set 3. The STAGS results are from the center bay of the six-module model.

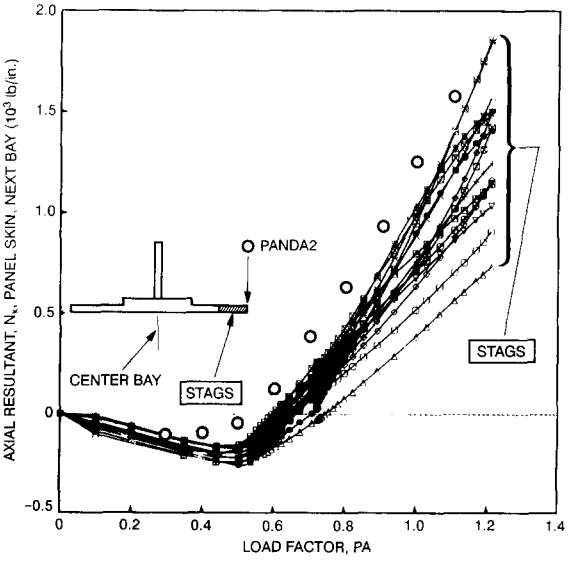

Fig. 49. Variation of internal axial load N_x in the axial direction, Load set 3. The STAGS results correspond to N_x at the centroids of a string of 15 finite elements that straddle the midlength of the panel. The elements are those nearest the midbay in one of the bays next to the center bay of the six-module model.

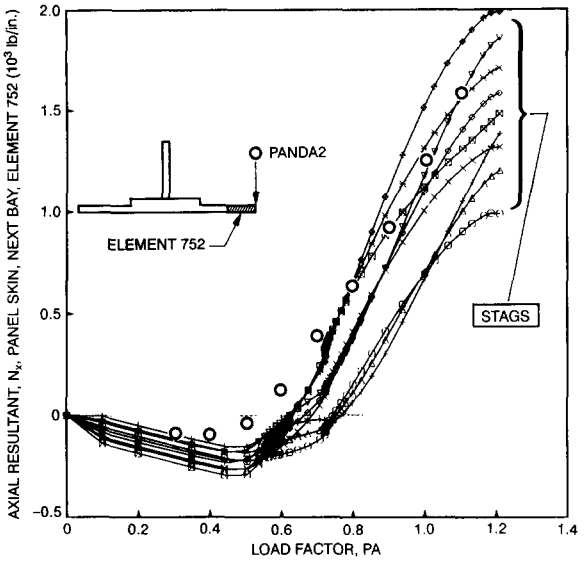

Fig. 50. Variation of internal axial load N_x in a single finite element. Element 752 was chosen because it has the highest tensile N_x at the centroid at the design load PA = 1.0 of all the elements the centroidal N_x values of which are plotted in the previous figure.

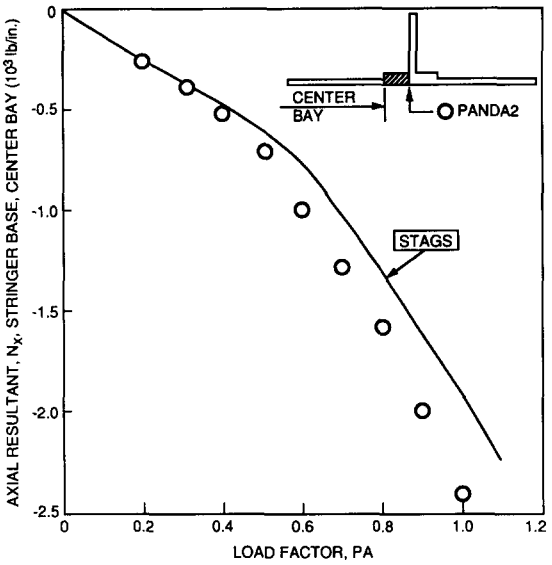

Fig. 51. Redistribution of N_x in the stringer base, Load set 3.

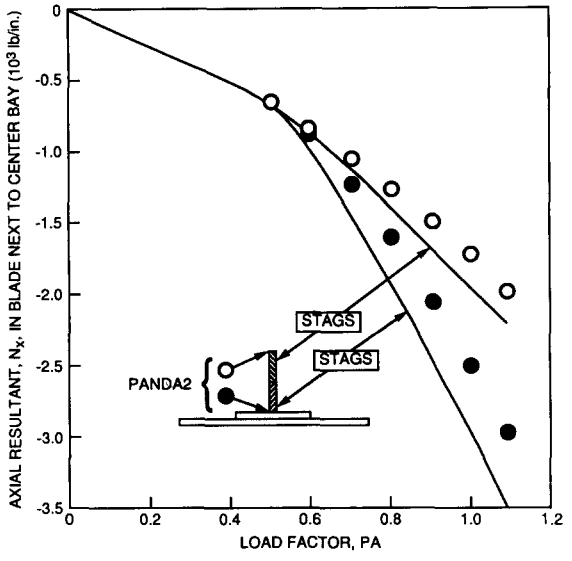

Fig. 52. Redistribution of N_x in the stringer blade, Load set 3.

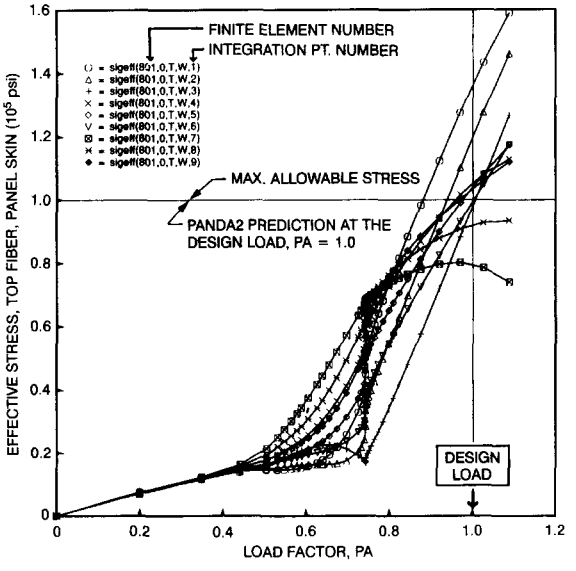

Fig. 53. Load set 3. Effective stress at the nine integration points in the finite element near the panel midlength, one bay from the center bay, that a PATRAN fringe plot showed contained the maximum effective stress anywhere in the six-module model of the panel. In-plane warping of the two longitudinal edges is permitted.

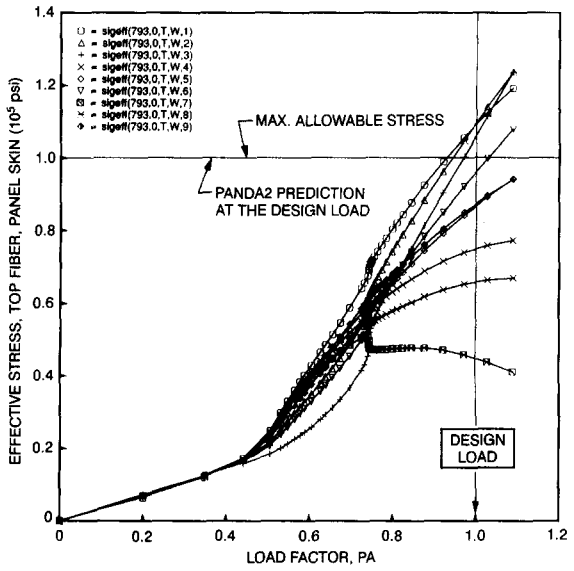

Fig. 54. Load set 3. Effective stress at the nine integration points in the finite element near the panel midlength, in the center bay, that a PATRAN fringe plot showed contained the maximum effective stress anywhere in the center bay of the six-module model of the panel. In-plane warping of the two longitudinal edges is permitted.

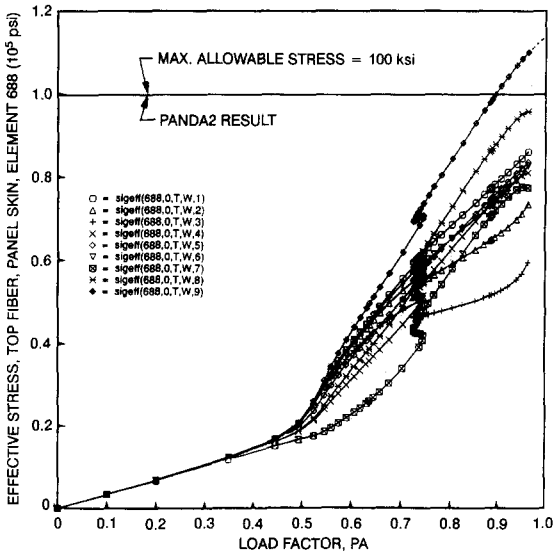

Fig. 55. Load set 3. Effective stress at the nine integration points in the finite element near the panel midlength that a PATRAN fringe plot showed contained the maximum effective stress anywhere in the six-module model of the panel. In this case in-plane warping of the two longitudinal edges of the panel was *not* permitted. The design load corresponds to PA = 1.0.

The point in Fig. 32a labelled $STAGS_2$ corresponds to a more refined STAGS model in which the number of nine-node ANS finite elements in the panel skin on one half of the panel module is increased from two to seven across the width. Figure 32b shows PATRAN plots in which the local bending stress concentration in the panel skin at the junction of the skin with the stringer base is clearly revealed on the half of the panel module with the more refined mesh. Note that the highest effective stress indicated by the PATRAN plot is 68917 psi, whereas the point labelled $STAGS_2$ in Fig. 32a, obtained from a STAGSPP plot [58], is at about 82000 psi. PATRAN plots underestimate maximum stresses because averaging methods that smooth the peaks are used by PATRAN, whereas the STAGSPP result corresponds to the maximum effective stress at any of the nine integration points in the finite element that contains the stress concentration revealed in Fig. 32b.

5.4.6. STAGS results for Load set 2: axial compression of panel with positive axial bowing

Figures 33–38 give comparisons between PANDA2 and STAGS results corresponding to conditions near the midlength of the panel as loaded by Load set 2.

Figure 33 is analogous to Fig. 27. Instead of one buckling mode being used for the initial imperfection in the STAGS nonlinear collapse run, in this case the first four modes are used. The amplitude of each of these four modes chosen for the following nonlinear collapse

analysis with STAGS is $w_0 = +0.001$ in. The buckling load factor of the first STAGS mode is 0.386, which agrees very well with the PANDA2 prediction of 0.390.

Figure 34 is analogous to Fig. 28. Note that in this case of positive bowing, bending-torsion buckling of the stringer appears to initiate near the load factor PA = 1.0 and is very pronounced at the highest load factor reached in this STAGS run, PA = 1.327.

Figure 35 is analogous to Fig. 29. In Fig. 35 the upper 'STAGS' curve corresponds to the right-most integration point in the finite element nearest the longitudinal symmetry plane midway between stringers rather than at the element centroid, as in the case for Fig. 29. For small PA above that corresponding to local buckling and less than the design load PA = 1.0, the panel skin sheds axial load to the stringer base and blade in a manner similar to that exhibited in Load set 1. The skin deforms much more than the blade. In this range of load factor PA, results from STAGS and PANDA2 are in reasonably good agreement; the postbuckling deformations depicted in Figs. 20 and 34 are similar for the panel module cross-section at the midlength of the panel. For load factor PA greater than 1.0 the behavior of N_x in the panel skin as predicted by STAGS at the midlength of the panel is quite different from that predicted by PANDA2. For PA $\geq$ 1.0 the stringer undergoes bending-torsion buckling (Fig. 34(c–e)). The axial wavelength of the local postbuckling deformation in the panel skin near the panel midlength lengthens.

The post-local-buckling theory in PANDA2 is not general enough to predict this change in mode of local deformation over the entire range of load factor PA. However, this lack of rigor should never be significant for the purpose of obtaining optimum designs with PANDA2 because in PANDA2 bending-torsion buckling is always associated with a factor of safety of unity. That is, PANDA2 will not permit designs in the 'post-bending-torsion-buckling' regime. Therefore, it is expected that optimum designs obtained with PANDA2 will always display behavior that is in reasonably good agreement with STAGS predictions up to initial bending-torsion buckling, which will always occur at or above the design load PA = 1.0. What happens for loads above the design load is of less importance to the designer than what happens for loads less than or equal to the design load. In brief, the fact that PANDA2 cannot predict accurately post-bending-torsion-buckling behavior is expected to have little effect on the generation of good optimum designs.

Figure 36 is analogous to Fig. 30. In Fig. 36 STAGS results are shown for three integration points across the width of one of the finite elements in the stringer base. As with Fig. 30, if the reader looks along the curve toward the origin from a viewpoint slightly above the plane of the page, he or she will see the rather sharp break in the slope of the neighborhood of the local buckling load, when axial load N_x from the panel skin starts to be redistributed to the stringer base.

Figure 37 is analogous to Fig. 31. In this case the axial load in the blade as predicted by STAGS and by PANDA2 is in good agreement over the entire range of PA.

Figures 38a and 38b are analogous to Figs. 32a and 32b. The finite element plots shown in the insert in Figs. 38a and 38b correspond to the deformed state as shown in Fig. 34c, except in the case of Figs. 38a and 38b the number of elements has been increased in one half of the panel skin order to capture the bending stress concentrations at the junction of the panel skin and stringer base, as with Figs. 32a and 32b.

In Fig. 38a the open point labelled 'PANDA2' and the curve labelled 'STAGS' both correspond to the maximum effective stress found in the panel in the region near the panel

midlength. However, in this case the point labelled 'PANDA2' corresponds to the same location in the panel as with Load set 1: at the bottom fiber of the panel skin at its junction with the stringer base. In contrast, the curve labelled 'STAGS' corresponds to the extreme leftmost fiber at the tip of the blade at the panel midlength. At the tip of the blade and maximum effective stress at the design load PA = 1.0 as predicted by PANDA2 is $\bar{\sigma}$ = 53300 psi, about 22 percent lower than the STAGS prediction. PANDA2 underpredicts the maximum effective stress at the tip of the blade because in the PANDA2 model the amount of sidesway of the blade at the panel midlength is underestimated for loads higher than the local buckling load, which for Load set 2 (positive bowing) occurs at a load factor PA = 0.386 (see Fig. 33). The underestimation of blade sidesway in the postbuckling regime in the PANDA2 model results from the use of the bifurcation buckling mode with no modification of this mode to account for axial localization of the local buckling behavior nor for the fact that axial load has been shifted from the panel skin to the stringer base and blade as the buckles in the panel skin deepen in the postbuckling regime.

The STAGS points in Fig. 38a at the design load PA = 1.0 correspond to the maximum effective stress in the bottom fiber in the panel skin at the junction with the stringer base near the panel midlength and near one panel end, as shown in the insert. It is emphasized that the PANDA2 model does not check for conditions near the panel ends unless there is normal pressure present. However, as mentioned above in connection with the results for Load set 1, because both positive and negative axial bowing are included in the load sets under which the panel has been optimized via PANDA2, the stress margins generated by PANDA2 during optimization are sufficient to keep the optimum design safe in this case. The high effective stress in the panel skin near the panel end in the STAGS model as loaded by Load set 2 (positive axial bowing) is encountered near the panel midlength in the STAGS model as loaded by Load set 1 (negative axial bowing). As seen from Fig. 32a, the PANDA2 and STAGS predictions for this maximum effective stress are in very good agreement for the STAGS model with the refined finite element grid over half of the panel skin.

5.4.7. STAGS results for Load set 3: combined axial compression and in-plane shear of panel with no axial bowing

Figures 39–55 give comparisons between PANDA2 and STAGS results corresponding to conditions near the midlength of the panel as loaded by Load set 3.

Most of Vol. 2, Part 2 of [46] is devoted to this problem. In [46] STAGS models with three modules and with six modules are analyzed, and results are compared with PANDA2 predictions. Details of the process described above in Section 5.4.4 are given in [46] for most STAGS runs. The effect of allowing and preventing in-plane warping of the longitudinal edges is explored for both the three-module model and the six-module model. Color PATRAN plots are given in [46] of the distributions of internal axial load N_x, hoop load N_y, and in-plane shear load N_{xy} and extreme fiber effective stress $\bar{\sigma}$ over the entire model at the design load PA = 1.0. In this paper only a few of the results will be presented for the six-module model, all of them except the last corresponding to the option in which the two longitudinal edges are allowed to warp in the plane of the panel skin.

Figure 39 shows a plan view of the six-module model as deformed at a load factor PA = 1.14. The applied axial load N_x and in-plane shear load N_{xy} are indicated. Details about the boundary conditions imposed in the STAGS models are given in Fig. 23 of [49]. Briefly,

along the axially loaded (curved) edges uniform axial displacement u is imposed at one end and $u = 0$ at the other. The normal displacement w in the panel skin and stringer bases is zero along the curved edges. Warping of the ends of the stiffeners at the curved edges in the plane of the outstanding flange, if any, is prevented. Along each of the four edges, points are allowed to slide freely in the direction tangent to that edge and in the plane of that edge. If the panel has three or more skin-stringer modules, three rotation components and the normal displacement w along each of the two longitudinal edges are set equal to the corresponding values at the same axial coordinate x two bays removed from that longitudinal edge. This is done for every nodal point along the two longitudinal edges. If the user chooses to prevent warping of the two longitudinal edges in the plane of the panel skin, Lagrange constraints are introduced into the STAGS model that force the circumferential displacement v to vary linearly with axial coordinate x. This last constraint greatly increases the computer time required to solve large problems because it causes the bandwidth of the stiffness matrix approximately to double.

Figure 40 is analogous to Fig. 27. According to STAGS the critical buckling load factor is 0.542, whereas PANDA2 predicts a value of 0.499. Figure 41 is a contour plot of the buckling mode shown in Fig. 40. The slope of the buckling nodal lines, measured graphically from Fig. 41, is plotted in Fig. 25 as the left-hand end of the line labelled 'STAGS results for wavy edges'. While Fig. 41 appears to show eight axial halfwaves over the 30 in length of the panel, PANDA2 predicts bifurcation buckling with nine axial halfwaves, as seen in Fig. 26. However, in the STAGS model the curved edges of the panel are clamped, whereas in the PANDA2 model of local buckling the curved edges are simply supported. Clamping tends to reduce the number of axial halfwaves visible in the contour plot because very little normal deflection w occurs near the clamped edges. Also, the critical loads predicted by PANDA2 for eight and nine waves are very close. In Fig. 26 the left-hand end of the line labelled 'STAGS (wavy edges)' is plotted as nine rather than as eight axial halfwaves because the length of the panel divided by the axial halfwavelength of a buckle near the midlength of the panel measured from Fig. 41 is closer to nine than eight.

Figure 42 is analogous to Fig. 28. The results shown in this and the following figures were obtained after 15 STAGS runs, some of them nonlinear bifurcation buckling runs and others nonlinear 'collapse' runs. The strategy outlined in Section 5.4.4 was pursued. It was possible to obtain converged results for load factor PA greater than unity only after about 20 buckling eigenmodes had been included as initial imperfection shapes, these eigenmodes corresponding to nonlinear bifurcation buckling analyses at several values of PA. Details, including mode shapes, appear in [46].

Figure 43 is a contour plot of the normal deflection w at the maximum load factor, PA = 1.14. The points at the right-hand ends of the lines in Figs. 25 and 26 labelled 'STAGS results for wavy edges' were derived from this contour plot.

Figures 44–46 display overall behavior of the panel with increasing load factor PA. There is reasonably good agreement between PANDA2 and STAGS for the end shortening u and transverse (circumferential) displacement v. The PANDA2 points in Fig. 45 represent an average circumferential displacement v over the entire curved edge: the values corresponding to these points are the average in-plane shear strain e_{12} in the panel skin and stringer bases multiplied by the length of the panel. The STAGS points correspond to the circumferential displacements v at the ends of the six stringers.

Figure 46 shows the axial bowing of each of the six stringers at the midlength of the panel. The two stringers nearest the longitudinal edges, Stringers 1 and 6, behave differently from the four interior stringers. Comparing this figure with the PANDA2 prediction of WBOW in Fig. 24, one sees that at the design load PA = 1.0 STAGS predicts more than twice as much axial bowing for the four interior stringers. The reason for the discrepancy and its effect on prediction of maximum stress is not known. It appears that the axial bowing of the four interior stringers indicates the growth of a general instability mode. However, this mode is difficult to see in Fig. 42(f) because the amplitude of the local buckles is much larger than the amplitude of the stringer bowing. At the maximum load factor PA = 1.14 the general instability mode represents a minor part of the total deformation.

The maximum positive and negative normal displacements w between stringers in the center bay of the six-module model near the panel midlength are plotted in Fig. 47. The PANDA2 points plotted in Fig. 47 contain no component of overall panel bending but the STAGS points do. Therefore, the PANDA2 results should be compared with the difference between the STAGS points in Fig. 47 and the STAGS points in Fig. 46 corresponding to one of the stringers adjacent to the center bay of the six-module STAGS model (Stringers 3 or 4). This subtraction shifts the STAGS curves in Fig. 47 upwards, so that the agreement with PANDA2 for the growth in amplitude of the local buckles as the panel is loaded into the postbuckling regime is reasonably good. Note that even with the subtraction STAGS predicts more inward displacement of the local buckles than outward displacement. This is because the panel is curved. In the local buckling and postbuckling analysis performed in PANDA2 the curvature of the panel skin is neglected. Note that PANDA2 predicts finite local buckles at load factors PA well below the bifurcation buckling load of 0.499. Because of the initial local imperfection, assumed in the PANDA2 analysis to have an amplitude of one tenth of the panel skin thickness, there is a growth in the local buckling pattern as soon as *any* load is applied to the panel.

Figure 48 is analogous to Fig. 29. As before, there is reasonably good agreement between PANDA2 and STAGS for the redistribution of internal axial load N_x in the post-buckling regime. A rather large axial tension has developed midway between stringers at the design load PA = 1.0.

In the PANDA2 theory it is assumed that the internal axial load N_x in the locally postbuckled panel is a function of y only [eq. (8)]. As demonstrated in Fig. 49, in which are plotted the values of N_x at the centroids of an axial string of 15 adjacent finite elements in the panel skin straddling the midlength of the panel in the STAGS model, this is not true. There is considerable variation of the local value of N_x in the axial direction midway between stringers. The STAGS points are lower than the PANDA2 points because the PANDA2 points correspond to the location midway between stringers, whereas the STAGS points correspond to the centroids of the elements adjacent to the line midway between stringers. The maximum postbuckling axial tension occurs midway between stringers.

Figure 50 displays the variation of internal axial load N_x within a single element. The PANDA2 points are the same as those plotted in Fig. 49. The STAGS points correspond to N_x at the nine integration points in Element 752. Element 752 was chosen for this plot because at the design load PA = 1.0 the internal axial load N_x at this element centroid is maximum with respect to axial coordinate x (Fig. 49). The STAGS predictions bracket the PANDA2 predictions for load factor PA greater than about 0.8.

Figures 51 and 52 are analogous to Figs. 30 and 31, respectively. PANDA2 and STAGS predict the same trends for the redistribution of axial load N_x to the stringer bases and blades.

Figures 53 and 54 are plots of the effective stresses at the nine integration points in the elements near the panel midlength and midwidth that contain the maximum values according to PATRAN plots given in [46]. Figure 53 corresponds to an element in the panel skin in a bay adjacent to the center bay and Fig. 54 to an element in the center bay. At the design load PA = 1.0 there is a very large variation of the effective stress within a single element. This result points to the need for an analysis with a more refined grid. The maximum stress at PA = 1.0 predicted by STAGS exceeds that predicted by PANDA2 by about 35 percent (Fig. 53) for this six-module model in which in-plane warping of the two longitudinal edges is permitted. The curves are rather contorted in the neighborhood of PA = 0.75 because of small shifts in the local buckles that are not not visible in Fig. 42. The PANDA2 prediction corresponds to the allowable effective stress $\bar{\sigma} = 100000$ psi because in Load set 3 the design margin corresponding to effective stress is critical (Figs. 14 and 23).

Figure 55 is analogous to Fig. 54. The maximum effective stress is plotted versus load factor PA for the nine integration points in the finite element which contains, according to a PATRAN fringe plot, the maximum extreme fiber effective stress anywhere in the panel for a case in which in-plane warping of the two longitudinal edges is prevented. At the design load PA = 1.0, which the STAGS run did not quite reach, the maximum effective stress according to STAGS is about 13 percent higher than predicted by PANDA2.

6. Conclusions

Details have been presented on the local buckling and postbuckling theory implemented in PANDA2. The elaborate strategy explained in Section 4 and Tables A.1–A.3 greatly increases the probability that a converged solution to the nonlinear postbuckling equilibrium equations will be found, even when no starting vector is available. This is important in optimization problems, especially for early design iterations in which the decision variables and therefore the panel behaviors are changing significantly from iteration to iteration, or for designs for which the applied load is near the local buckling load.

Comparisons of results from PANDA2 and STAGS for a stringer stiffened cylindrical panel optimized by PANDA2 for three load sets and evaluated by STAGS appear to qualify PANDA2 as a preliminary design tool. The agreement between STAGS and PANDA2 results are better for STAGS models in which in-plane warping of the two longitudinal edges is prevented than for models in which in-plane warping is permitted.

To obtain safe optimum designs, the PANDA2 user should include in the load sets for which a panel is optimized, load sets that contain both positive and negative axial bowing, especially for those load sets with significant axial compression.

In order to obtain reliable results from general-purpose finite element codes, the analyst must include a fine enough finite element grid to capture local bending stress concentrations that occur near segment junctions at loads above that corresponding to local buckling.

Finding the behavior of a stiffened panel loaded well beyond the local buckling load is often a very difficult problem for a general-purpose finite element code to solve. A method in which multiple imperfections in the form of bifurcation buckling modes obtained at various load

levels is outlined in Section 5.4.4. This method is often very tedious, as in the case of the six-module model subjected to combined axial compression and in-plane shear. Simple problems, such as a uniformly axially compressed isotropic unstiffened plate, have been found for which the method does not work. Therefore, it is hoped that the efforts of Rankin et al. [61], in which combined static and dynamic solutions are used, will prove successful.

Appendix A

Table A.1
Flow of logic in SUBROUTINE KOIT2

```
C     Begin calculations of local buckling load factor from Koiter theory:
C
            CALL EIGKOI(IMOD, NPRT, IFILE, N, M, CX, EKOITR, MWAVE, ITER)
C
C     Begin calculation of post-local-buckling equilibrium state from
C     Koiter theory:
C
            IF (ABS(EKOITR).LT.1.0) THEN
C     Obtain nonlinear solution for the three unknowns f, a, m in the
C     nonlinear post-local buckling problem.
C
C     In SUBROUTINE NEWTON the axial wavelength parameter N is held
C     constant. In this call to NEWTON, the amplitude W0 of the initial
C     local imperfection, which is assumed to be in the form of the
C     critical local buckling mode, is set equal to zero.
C
  8002        CALL NEWTON(. . . . . .
            ENDIF     $(EKOITR.LT.1.0)
C
C     Refine the solution f, a, m, this time including the user-provided
C     amplitude W0 of the local imperfection:
C
  8004        CALL NEWTON(. . . . . .
C
  8005        IF (ABS(EKOITR).LT.1.0.AND.ISTIF(1).NE.5.AND.F.NE.0.0
            1  .AND.ICONVS.EQ.1.AND.MWAVE.GT.1) THEN
C
C     If local buckling load factor EKOITR is less than unity, and the
C     panel is not truss-core configuration, and the amplitude f as
C     found by NEWTON is not equal zero, and NEWTON yielded a converged
C     solution (ICONVS = 1), and the number of axial halfwaves MWAVE is
C     greater than 1, then do the nonlinear analysis with the axial
C     wavelength parameter N taken as an additional unknown in the
C     nonlinear local postbuckling problem. NOTE: the "ENDIF" for
C     "IF" statement 8005 is near the end of this file, many pages
C     further on.
            ICONV = 0
C     Try for solution with all four variables f, a, m, N free to change.
C     As initial values for f, a, m use the results from SUBROUTINE NEWTON.
C
```

Table A.1 (Continued)

```
 8010      CALL ENERGY(ICONV,.....
 8012      IF (ICONV.EQ.0) THEN
C     Solution failed to converge.
C     Convergence with f, a, m, N free failed. Keep f, a, N free and fix m:
 8030          CALL ENERGY(ICONV1,.....
           ELSE     $(8012:  ICONV1)
C     Convergence with f, a, m, N free succeeded.
               ISAVE = 1;  GO TO 130
           ENDIF    $(8012:  ICONV1)
 8034      IF (ICONV1.EQ.1) THEN
C     Convergence with f, a, N free and m fixed succeeded. Now free m:
               F00 = F;  A00 = AL;  M00 = M;  N0 = N
C     Re-solve the nonlinear problem using the f, a, m formulation in NEWTON:
               CALL BLOCK(IA, 8040, 8050)
               ICONV2 = 0
C     Next, attempt the four-variable (f, a, m, N) problem with f, a, m, N free:
 8060          CALL ENERGY(ICONV2,.....
               IF (ICONV2.EQ.0) THEN
C     Convergence with f, a, m, N free failed again. Accept the solution
C     provided by NEWTON.
                   F = F00;  AL = A00;  M = M00;  N = N0
               ENDIF
               ICONV = 1;  ISAVE = 1;  GO TO 130
           ELSE     $(8034:  ICONV1)
               ICONV2 = 0
C     Convergence with f, a, N free and m fixed failed. Try fixing "a" and m:
 8070          CALL ENERGY(ICONV2,.....
 8072          IF (ICONV2.EQ.1) THEN
C     Convergence with f, N free and a, m fixed succeeded now free "a":
                   F00 = F;  A00 = AL;  M00 = M;     N0 = N
C     Re-solve the nonlinear problem using the f, a, m formulation in NEWTON:
                   CALL BLOCK(IA, 8080, 8090)
                   ICONV3 = 0
C     We have a new solution for f, a, m from NEWTON. Now go to the
C     four-variable theory, but do it first with slope m fixed because
C     convergence failed with m free in the initial call to ENERGY:
 8100              CALL ENERGY(ICONV3,.....
 8102              IF (ICONV3.EQ.0) THEN
C     Convergence with f, a, N free and m fixed failed. Accept the
C     converged solution from the previous application of NEWTON.
                       F = F00;  AL = A00;  M = M00;  N = N0;  ICONV = 1;  GO TO 130
                   ELSE     $(8102:  ICONV3)
C     Convergence with f, a, N free and m fixed succeeded. Next, free m.
                       F00 = F;  A00 = AL;  M00 = M;  N0 = N
C     Re-solve the nonlinear problem using the f, a, m formulation in NEWTON:
                       CALL BLOCK(IA, 8110, 8120)
                       ICONV4 = 0
C     We have a new solution for f, a, m from NEWTON. Now go to the
C     four-variable theory, this time with all four variables f, a, m, N free:
 8130                  CALL ENERGY(ICONV4,.....
                       IF (ICONV4.EQ.0) THEN
```

Table A.1 (Continued)

```
C     Convergence with f, a, m, N free failed. Accept the last converged
C     solution from NEWTON.
                              F = F00;  AL = A00;  M = M00;  N = N0
                          ENDIF
                          ICONV = 1;  ISAVE = 1;  GO TO 130
                      ENDIF    $(8102:  ICONV3)
                  ELSE    $(8072:  ICONV2)
C     Convergence with f, N free and a, m fixed failed. Follow prescription
C     described after label 125.
                      ITRIP = 0;  FF00 = F00;  AA00 = A00;  FM00 = M00;  FN00 = N0
  125                 CONTINUE
                      ICONV5 = 0
C     Convergence with f, N free and a, m fixed failed. Now set the amplitude
C     of the local imperfection W0 to zero and attempt a solution in which
C     f**2 is expressed in terms of "a" and N, and "a" and N are free.
C     Slope m is still fixed:
 8140                 CALL ENERGY(ICONV5, . . . . . .
 8146                 IF (ICONV5.EQ.0) THEN
C     No convergence with f**2 expressed in terms of "a" and N and
C     "a" and N are free. If TRIP = 0 try an even simpler nonlinear problem.
                          F = F00;  AL = A00;  M = M00;  N = N0
                          IF (ITRIP.EQ.0) THEN
                              FN0SV = N0;  FNNEW = N0;  ICONV6 = 0
  127                         CONTINUE
C     Keep the amplitude of the local imperfection W0 at zero and attempt
C     a solution in which F**2 is expressed in terms of N. "a" and m are
C     fixed:
 8150                         CALL ENERGY(ICONV6, . . . . . .
                              IF (ICONV6.EQ.0) THEN
C     No convergence with use of SUBROUTINE ENERGY. Accept previously
C     converged solution in which N was fixed, that is, accept the
C     previously converged solution from SUBROUTINE NEWTON.
                                  F = F00;  AL = A00;  M = M00;  FNNEW = 1.2*FNNEW
                                  N0 = FNNEW;  N = N0
                                  IF (FNNEW.LT.5.*FN0SV) GO TO 127
                                  N0 = FN0SV;  N = N0;  ICONV = 0;  GO TO 130
                              ELSE    $(ICONV6)
C     Convergence of the simplest possible nonlinear problem was achieved.
C     Now free "a" and go back to statement label 125.
                                  F00 = F;  A00 = AL;  M00 = M;  N0 = N;  ITRIP = 1
                                  GO TO 125
                              ENDIF    $(ICONV6)
                          ENDIF    $(ITRIP.EQ.0)
                          F00 = FF00;  A00 = AA00;  M00 = FM00;  N0 = FN00;  ICONV = 0
                          GO TO 130
                      ELSE    $(8146:    ICONV5)
C     Convergence was achieved with f**2 expressed in terms of "a" and N and
C     "a" and N free.
                          F00 = F;  A00 = AL;  M00 = M;  N0 = N
C     Re-solve the nonlinear problem using the f, a, m formulation in NEWTON:
                          CALL BLOCK(IA, 8160, 8170)
                          ICONV6 = 0
```

Table A.1 (Continued)

```
C     Convergence succeeded in NEWTON. Next, try the four-variable
C     formulation with slope m fixed and f, a, N free:
 8180                 CALL ENERGY(ICONV6,.............
 8182                 IF (ICONV6.EQ.0) THEN
C     Convergence with f, a, N free and m fixed failed. Accept the previously
C     converged solution and proceed.
                        F = F00;  AL = A00;  M = M00;  N = N0;  ICONV = 1
                        GO TO 130
                     ELSE    $(8182:    ICONV6)
C     Convergence with f, a, N free and m fixed succeeded.
                        F00 = F;  A00 = AL;  M00 = M;  N0 = N
C     Re-solve the nonlinear problem using the f, a, m formulation in NEWTON:
                          CALL BLOCK(IA, 8190, 8200)
                          ICONV7 = 0
C     Convergence with f, a, N free and m fixed successful. Now free m and
C     try again:
 8210                   CALL ENERGY(ICONV7,.............
                        IF (ICONV7.EQ.0) THEN
C     Convergence with f, a, m, N free failed. Accept the previously
C     converged solution and proceed.
                            F = F00;  AL = A00;  M = M00;  N = N0
                        ENDIF
                            ICONV = 1;  ISAVE = 1;  GO TO 130
                        ENDIF    $8182:    ICONV6)
                     ENDIF    $(8146:    ICONV5)
                  ENDIF    $(8072:    ICONV2)
               ENDIF    $(8034:    ICONV1)
  130          CONTINUE
               IF (IMOD.EQ.0) ICONVS = ICONV
               IF (ICONV.EQ.0) THEN
                  F = F00;  AL = A00;  M = M00;  N = N0
               ENDIF    $(ICONV.EQ.0)
 8236          IF (ICONV.EQ.1) THEN
                  F00 = F;  A00 = AL;  M00 = M;  N0 = N
C     Now f, a, m are free. Fix N at new value found in ENERGY and refine
C     the three-variable solution f, a, m via NEWTON. Use current values
C     of f, a, m as initial values, and use given value W0 for amplitude
C     of the initial local imperfection amplitude.
C
 8240           CALL NEWTON(.............
               ENDIF    $(8236:    ICONV.EQ.1)
            ENDIF    $(8005:    (ABS(EKOITR).LT.1.AND.ISTIF(1).NE.5 .... etc)
C
C     END CALCULATION OF POST-LOCAL-BUCKLING EQUILIBRIUM STATE FROM
C     KOITER THEORY
```

```
                SUBROUTINE BLOCK(IA, LABL1, LABL2 . . .)
C
C     Purpose is to use SUBROUTINE NEWTON to obtain a new solution to the
C     nonlinear problem with use of the three-variable (f, a, m) formulation.
C     IA is a control integer. With IA = 0 the "flattening" parameter"a"
C     is considered to be one of the unknowns.
```

Table A.1 (Continued)

```
                    IF (IA.EQ.0) THEN
                        AL = 0.;   F = 0.;   NOCONV = 0
C       Now f, a, m are free. Fix N at new value found in ENERGY and refine
C       the three-variable solution f, a m via NEWTON. Use current value of
C       slope, m, as initial value and start with f = 0 and a = 0 and local
C       imperfection amplitude W0 = 0:
LABL1               CALL NEWTON(. . . . . .
                    IF (IMOD.EQ.0.AND.IIIA.EQ.1) THEN
                        F = F00;   AL = A00;   M = M00;   N = N0;   IIIA = 0;   NOCONV = 0
                    ENDIF
C       Continue with the three-variable (f, a, m) problem with W0 = given value:
LABL2               CALL NEWTON(. . . . . .
                    IF (F.EQ.0.) THEN
                        WRITE(IFILE, 8051)
 8051                   FORMAT(/ '************ RUN ABORT ************'/
     1                  ' THERE APPEARS TO BE NO SOLUTION TO THE NONLINEAR'/
     1                  ' POST-LOCAL-BUCKLING PROBLEM FOR THIS GEOMETRY'/
     1                  ' AND LOADING. USE "CHANGE" TO CHANGE DIMENSIONS'/
     1                  ' AND TRY AGAIN.'/
     1                  ' *************** RUN ABORT ***************'/)
                        CALL ERREX
                    ENDIF     $(F.EQ.0)
                    IF (ABS(F/F00).LT.0.5.OR.ABS(F/F00).GT.2.0) THEN
C       Latest solution from NEWTON is too different from the previously
C       converged solution. Discard the latest NEWTON solution and replace
C       it was the previously converged solution.
                        F = F00;   AL = A00;   M = M00;   N = N0
                    ENDIF
                    F00 = F;   A00 = AL;   M00 = M;   N0 = N
                ENDIF     $(IA.EQ.0)
            RETURN
            END
```

Table A.2
Results from postbuckling analysis of unstiffened isotropic flat plate with in-plane loading Nx = −500 lb/in, Nxy = 100 lb/in. Properties of plate: width = 10 inches, length = 50 inches, thickness = 0.05 inches, elastic modulus, E = 10**7 psi, Poisson ratio = 0.3. Bifurcation buckling load factor: 0.0882

NONLINEAR POST-LOCAL BUCKLING BEHAVIOR WITH
INITIAL LOCAL IMPERFECTION IGNORED (Wo = 0):
SUBROUTINE NEWTON CALLED FROM KOIT2 AT LABEL = 8002 (f, a, m can vary)
NEWTON ITERATIONS BEGIN; SLOPE = 9.78883E − 02; a = 0.0000E + 00; f = 0.0000E + 00

ITER	SLOPE	DSLOPE	a	da	f	df
1	6.7694E − 01	5.7905E − 01	−2.8333E − 01	−2.8333E − 01	5.7455E − 01	1.8252E − 01
2	8.2478E − 01	1.4784E − 01	−4.1872E − 01	−1.3539E − 01	7.7836E − 01	1.4503E − 01
3	8.1235E − 01	−1.2438E − 02	−4.8590E − 01	−6.7184E − 02	8.8803E − 01	8.9583E − 02
4	7.9780E − 01	−1.4549E − 02	−5.0509E − 01	−1.9186E − 02	9.1558E − 01	2.5920E − 02
5	7.9625E − 01	−1.5417E − 03	−5.0654E − 01	−1.4517E − 03	9.1717E − 01	1.9073E − 03
6	7.9624E − 01	−9.8175E − 06	−5.0655E − 01	−8.2181E − 06	9.1718E − 01	1.0765E − 05

Table A.2 (Continued)

NONLINEAR POST-LOCAL BUCKLING BEHAVIOR WITH
INITIAL LOCAL IMPERFECTION INCLUDED (Wo = 5.0000E − 03):
SUBROUTINE NEWTON CALLED FROM KOIT2 AT LABEL = 8004 (f, a, m van vary)
NEWTON ITERATIONS BEGIN; SLOPE = 7.9624E − 01; a = −5.0655E − 01; f = 9.1718E − 01

ITER	SLOPE	DSLOPE	a	da	f	df
1	8.0557E − 01	9.3219E − 03	−5.0890E − 01	−2.3502E − 03	9.1266E − 01	−4.5151E − 03
2	8.0562E − 01	5.0984E − 05	−5.0890E − 01	−2.1028E − 06	9.1250E − 01	−1.6804E − 04
3	8.0562E − 01	5.1220E − 07	−5.0890E − 01	3.6318E − 07	9.1249E − 01	−1.1010E − 06

CONVERGENCE OF LOCAL STATE SUCCESSFUL!

NEWTON ITERATIONS BEGIN IN SUBROUTINE ENERGY
CALLED FROM SUBROUTINE KOIT2 AT LABEL = 8010. (f, a, m, N can all vary)
PURPOSE IS TO OBTAIN NEW SOLUTION ALLOWING THE AXIAL
HALFWAVELENGTH OF THE LOCAL POSTBUCKLED PATTERN TO CHANGE.

ITER. NO.	UNKNOWNS IN THE LOCAL POSTBUCKLING PROBLEM				
	AMPLITUDE f	FLATTENING a	NODAL LINE SLOPE, m	PI**2*n**2/4L**2 N	AXIAL HALFWAVELENGTH OF BUCKLES, (L/n)
0	9.12494E − 01	−5.08902E − 01	8.05619E − 01	2.46740E − 02	9.99999E + 00
1	8.14281E − 01	−5.29183E − 01	7.38945E − 01	3.15989E − 02	8.83657E + 00
2	8.00339E − 01	−5.29882E − 01	7.29213E − 01	3.41666E − 02	8.49803E + 00
3	7.82939E − 01	−5.32213E − 01	7.18150E − 01	3.58483E − 02	8.29631E + 00
4	7.82320E − 01	−5.32276E − 01	7.17679E − 01	3.59654E − 02	8.28280E + 00
5	7.82241E − 01	−5.32289E − 01	7.17624E − 01	3.59741E − 02	8.28180E + 00

CONVERGENCE SUCCESSFUL!

NONLINEAR POST-LOCAL BUCKLING BEHAVIOR WITH
INITIAL LOCAL IMPERFECTION INCLUDED (Wo = 5.0000E − 03):
SUBROUTINE NEWTON CALLED FROM KOIT2 AT LABEL = 8240 (f, a, m can vary)
NEWTON ITERATIONS BEGIN; SLOPE = 7.1762E − 01; a = −5.3229E − 01; f = 7.8224E − 01

ITER	SLOPE	DSLOPE	a	da	f	df
1	7.1763E − 01	1.9892E − 06	−5.3229E − 01	5.7157E − 07	7.8210E − 01	−1.4078E − 04
2	7.1763E − 01	4.4612E − 07	−5.3229E − 01	3.5048E − 07	7.8210E − 01	−1.4541E − 06
3	7.1763E − 01	8.6120E − 08	−5.3229E − 01	−8.8573E − 08	7.8210E − 01	2.0005E − 07

CONVERGENCE OF LOCAL STATE SUCCESSFUL!

LOCAL DEFORMATION CHARACTERISTICS:

Average axial strain,	EXAVE = −5.2512E − 03
Initial local imperfection amplitude,	Wo = 5.0000E − 03
Slope of local buckling nodal lines in skin	M = 7.1763E − 01
Parameter "a" in the expression f*(phi + a*phi**3)	= −5.3229E − 01
Amplitude f in the expression f*(phi + a*phi**3)	= 7.8210E − 01
Normal displacement amplitude between stringers	W = 3.6589E − 01
Number of axial halfwaves at local bifurcation	= 5
Number of axial halfwaves in postbuckled regime	= 6.0373E + 00

Table A.3
Results from postbuckling analysis of unstiffened isotropic flat plate with in-plane loading Nx = −500 lb/in, Nxy = 20 lb/in. Bifurcation buckling load factor: 0.0899

NONLINEAR POST-LOCAL BUCKLING BEHAVIOR
INITIAL LOCAL IMPERFECTION IGNORED (Wo = 0):
SUBROUTINE NEWTON CALLED FROM KOIT2 AT LABEL = 8002 (f, a, m can vary)
NEWTON ITERATIONS BEGIN; SLOPE = 1.9991E − 02; a = 0.0000E + 00; F = 0.0000E + 00

ITER	SLOPE	DSLOPE	a	da	f	df
1	1.5163E − 01	1.3164E − 01	−2.3309E − 01	−2.3309E − 01	4.9858E − 01	1.1405E − 01
2	1.9021E − 01	3.8579E − 02	−3.8860E − 01	−1.5551E − 01	6.6636E − 01	1.3088E − 01
3	1.8569E − 01	−4.5249E − 03	−4.7719E − 01	−8.8585E − 02	7.9749E − 01	1.0462E − 01
4	1.7835E − 01	−7.3381E − 03	−5.0944E − 01	−3.2252E − 02	8.4362E − 01	4.0788E − 01
5	1.7714E − 01	−1.2106E − 03	−5.1355E − 01	−4.1123E − 03	8.4798E − 01	4.9963E − 03
6	1.7712E − 01	−1.9673E − 05	−5.1362E − 01	−6.2875E − 05	8.4803E − 01	7.5686E − 05
7	1.7712E − 01	3.4112E − 08	−5.1362E − 01	4.1686E − 07	8.4803E − 01	−5.0172E − 07

NONLINEAR POST-LOCAL BUCKLING BEHAVIOR WITH
INITIAL LOCAL IMPERFECTION INCLUDED (Wo = 5.0000E − 03):
SUBROUTINE NEWTON CALLED FROM KOIT2 AT LABEL = 8004 (f, a, m can vary)
NEWTON ITERATIONS BEGIN; SLOPE = 1.7712E − 01; a = −5.1362E − 01; f = 8.4803E − 01

ITER	SLOPE	DSLOPE	a	da	f	df
1	1.7969E − 01	2.5676E − 03	−5.1663E − 01	−3.0190E − 03	8.4369E − 01	−4.3394E − 03
2	1.7971E − 01	2.0424E − 05	−5.1665E − 01	−1.4316E − 05	8.4351E − 01	−1.8148E − 04
3	1.7971E − 01	−2.3226E − 08	−5.1665E − 01	1.9497E − 08	8.4351E − 01	−3.8313E − 07

CONVERGENCE OF LOCAL STATE SUCCESSFUL!

NEWTON ITERATIONS BEGIN IN SUBROUTINE ENERGY
CALLED FROM SUBROUTINE KOIT2 AT LABEL = 8010. (f, a, m, N can all vary)

ITER. NO.	UNKNOWNS IN THE LOCAL POSTBUCKLING PROBLEM AMPLITUDE f	FLATTENING a	NODAL LINE SLOPE, m	PI**2*n**2/4L**2 N	AXIAL HALFWAVELENGTH OF BUCKLES, (L/n)
0	8.43513E − 01	−5.16650E − 01	1.79706E − 01	2.46740E − 02	9.99999E + 00
1	6.94983E − 01	−5.55049E − 01	1.53797E − 01	3.20762E − 02	8.77057E + 00
2	7.33335E − 01	−5.36473E − 01	1.60566E − 01	3.94784E − 02	7.90569E + 00

ITERATIONS IN "ENERGY" FAIL TO CONVERGE
NEGATIVE AXIAL WAVELENGTH. F, A, M, N = 1.32155 −0.488666 0.244518 −3.12714E − 02

NEWTON ITERATIONS BEGIN IN SUBROUTINE ENERGY (f, a, N can vary; m constant)
CALLED FROM SUBROUTINE KOIT2 AT LABEL = 8030.

ITER. NO.	UNKNOWNS IN THE LOCAL POSTBUCKLING PROBLEM AMPLITUDE f	FLATTENING a	NODAL LINE SLOPE, m	PI**2*n**2/4L**2 N	AXIAL HALFWAVELENGTH OF BUCKLES, (L/n)
0	8.43513E − 01	−5.16650E − 01	1.79706E − 01	2.46740E − 02	9.99999E + 00
1	6.95716E − 01	−5.54365E − 01	1.79706E − 01	3.20762E − 02	8.77057E + 00
2	7.32441E − 01	−5.36566E − 01	1.79706E − 01	3.94784E − 02	7.90569E + 00

ITERATIONS IN "ENERGY" FAIL TO CONVERGE
NEGATIVE AXIAL WAVELENGTH. F, A, M, N = 1.50681 −0.472680 0.179706 −5.26305E − 02

NEWTON ITERATIONS BEGIN IN SUBROUTINE ENERGY (f, N can vary; a, m constant)
CALLED FROM SUBROUTINE KOIT2 AT LABEL = 8070.

Table A.3 (Continued)

ITER. NO.	UNKNOWNS IN THE LOCAL POSTBUCKLING PROBLEM AMPLITUDE f	FLATTENING a	NODAL LINE SLOPE, m	PI**2*n**2/4L**2 N	AXIAL HALFWAVELENGTH OF BUCKLES, (L/n)
0	8.43513E − 01	−5.16650E − 01	1.79706E − 01	2.46740E − 02	9.99999E + 00
1	6.90135E − 01	−5.16650E − 01	1.79706E − 01	3.20762E − 02	8.77057E + 00
2	6.92953E − 01	−5.16650E − 01	1.79706E − 01	3.86457E − 02	7.99041E + 00
3	5.69367E − 01	−5.16650E − 01	1.79706E − 01	5.11808E − 02	6.94330E + 00
4	5.89899E − 01	−5.16650E − 01	1.79706E − 01	5.18703E − 02	6.89700E + 00
5	5.93111E − 01	−5.16650E − 01	1.79706E − 01	5.10229E − 02	6.95403E + 00
6	5.92693E − 01	−5.16650E − 01	1.79706E − 01	5.10976E − 02	6.94895E + 00
7	5.92673E − 01	−5.16650E − 01	1.79706E − 01	5.11006E − 02	6.94875E + 00

CONVERGENCE SUCCESSFUL!

NONLINEAR POST-LOCAL BUCKLING BEHAVIOR WITH
INITIAL LOCAL IMPERFECTION IGNORED (Wo = 0):
SUBROUTINE NEWTON CALLED FROM KOIT2 AT LABEL = 8080 (f, a, m can vary)
NEWTON ITERATIONS BEGIN; SLOPE = 1.7971E − 01; a = 0.0000E + 00; f = 0.0000E + 00

ITER	SLOPE	DSLOPE	a	da	f	df
1	1.7726E − 01	−2.4421E − 03	−2.4543E − 01	−2.4543E − 01	3.2616E − 01	8.4068E − 02
2	1.6937E − 01	−7.8943E − 03	−4.1248E − 01	−1.6704E − 01	4.7701E − 01	1.0405E − 01
3	1.5382E − 01	−1.5554E − 02	−5.1062E − 01	−9.8142E − 02	5.8564E − 01	8.9763E − 02
4	1.4448E − 01	−9.3320E − 03	−5.4997E − 01	−3.9353E − 02	6.2500E − 01	3.8138E − 02
5	1.4267E − 01	−1.8150E − 03	−5.5641E − 01	−6.4394E − 03	6.2828E − 01	5.7295E − 03
6	1.4261E − 01	−6.2876E − 05	−5.5659E − 01	−1.7838E − 04	6.2828E − 01	1.5488E − 04
7	1.4261E − 01	4.3519E − 08	−5.5659E − 01	4.5062E − 08	6.2828E − 01	−3.9108E − 08

NONLINEAR POST-LOCAL BUCKLING BEHAVIOR WITH
INITIAL LOCAL IMPERFECTION INCLUDED (Wo = 5.0000E − 03):
SUBROUTINE NEWTON CALLED FROM KOIT2 AT LABEL = 8090 (f, a, m can vary)
NEWTON ITERATIONS BEGIN; SLOPE = 1.4261E − 01; a = −5.5659E − 01; f = 6.2828E − 01

ITER	SLOPE	DSLOPE	a	da	f	df
1	1.4261E − 01	−5.9563E − 08	−5.5659E − 01	−1.7313E − 07	6.2828E − 01	1.9284E − 07
2	1.4261E − 01	5.1651E − 09	−5.5659E − 01	1.9636E − 08	6.2828E − 01	−1.5653E − 07
3	1.4261E − 01	8.5590E − 09	−5.5659E − 01	3.9676E − 08	6.2828E − 01	1.2373E − 08

CONVERGENCE OF LOCAL STATE SUCCESSFUL!

NEWTON ITERATIONS BEGIN IN SUBROUTINE ENERGY
CALLED FROM SUBROUTINE KOIT2 AT LABEL = 8100. (f, a, N can vary; m constant)

ITER. NO.	UNKNOWNS IN THE LOCAL POSTBUCKLING PROBLEM AMPLITUDE f	FLATTENING a	NODAL LINE SLOPE, m	PI**2*n**2/4L**2 N	AXIAL HALFWAVELENGTH OF BUCKLES, (L/n)
0	6.28275E − 01	−5.56588E − 01	1.42606E − 01	5.11006E − 02	6.94875E + 00
1	5.97346E − 01	−5.60637E − 01	1.42606E − 01	5.66818E − 02	6.59778E + 00
2	5.94910E − 01	−5.60781E − 01	1.42606E − 01	5.75797E − 02	6.54613E + 00
3	5.94446E − 01	−5.60822E − 01	1.42606E − 01	5.76754E − 02	6.54070E + 00

CONVERGENCE SUCCESSFUL!

NONLINEAR POST-LOCAL BUCKLING BEHAVIOR WITH
INITIAL LOCAL IMPERFECTION IGNORED (Wo = 0):
SUBROUTINE NEWTON CALLED FROM KOIT2 AT LABEL = 8110 (f, a, m can vary)

Table A.3 (Continued)

NEWTON ITERATIONS BEGIN; SLOPE = 1.4261E − 01; a = 0.0000E + 00; f = 0.0000E + 00

ITER	SLOPE	DSLOPE	a	da	f	df
1	1.5862E − 01	1.6012E − 02	−2.4719E − 01	−2.4719E − 01	3.1053E − 01	7.9262E − 02
2	1.5895E − 01	3.3399E − 04	−4.1526E − 01	−1.6807E − 01	4.4980E − 01	9.9058E − 02
3	1.4672E − 01	−1.2229E − 01	−5.1412E − 01	−9.8858E − 02	5.5379E − 01	8.5888E − 02
4	1.3821E − 01	−8.5124E − 03	−5.5405E − 01	−3.9926E − 02	5.9136E − 01	3.6662E − 02
5	1.3646E − 01	−1.7537E − 03	−5.6071E − 01	−6.6624E − 03	5.9445E − 01	5.5842E − 03
6	1.3639E − 01	−6.3168E − 05	−5.6090E − 01	−1.9040E − 04	5.9444E − 01	1.5541E − 04
7	1.3639E − 01	−2.2949E − 08	−5.6090E − 01	−3.1660E − 07	5.9444E − 01	2.5816E − 07

NONLINEAR POST-LOCAL BUCKLING BEHAVIOR WITH
INITIAL LOCAL IMPERFECTION INCLUDED (Wo = 5.0000E − 03):
SUBROUTINE NEWTON CALLED FROM KOIT2 AT LABEL = 8120 (f, a, m can vary)
NEWTON ITERATIONS BEGIN; SLOPE = 1.3639E − 01; a = −5.6090E − 01; f = 5.9444E − 01

ITER	SLOPE	DSLOPE	a	da	f	df
1	1.3639E − 01	−6.4583E − 08	−5.6090E − 01	−4.2594E − 07	5.9444E − 01	7.3915E − 07
2	1.3639E − 01	−1.8880E − 09	−5.6090E − 01	4.3998E − 09	5.9444E − 01	7.6121E − 09
3	1.3639E − 01	−1.8880E − 09	−5.6090E − 01	4.3998E − 09	5.9444E − 01	7.6121E − 09

CONVERGENCE OF LOCAL STATE SUCCESSFUL!

NEWTON ITERATIONS BEGIN IN SUBROUTINE ENERGY
CALLED FROM SUBROUTINE KOIT2 AT LABEL = 8130. (f, a, m, N can all vary)

ITER. NO.	UNKNOWNS IN THE LOCAL POSTBUCKLING PROBLEM				
	AMPLITUDE f	FLATTENING a	NODAL LINE SLOPE, m	PI**2*n**2/4L**2 N	AXIAL HALFWAVELENGTH OF BUCKLES, (L/n)
0	5.94438E − 01	−5.60899E − 01	1.36394E − 01	5.76754E − 02	6.54070E + 00
1	5.93869E − 01	−5.60968E − 01	1.36288E − 01	5.77943E − 02	6.53397E + 00
2	5.93861E − 01	−5.60967E − 01	1.36286E − 01	5.77959E − 02	6.53387E + 00
3	5.93872E − 01	−5.60969E − 01	1.36287E − 01	5.77944E − 02	6.53396E + 00

CONVERGENCE SUCCESSFUL!

NONLINEAR POST-LOCAL BUCKLING BEHAVIOR WITH
INITIAL LOCAL IMPERFECTION INCLUDED (Wo = 5.0000E − 03):
SUBROUTINE NEWTON CALLED FROM KOIT2 AT LABEL = 8240 (f, a, m can vary)
NEWTON ITERATIONS BEGIN; SLOPE = 1.3629E − 01; a = −5.6097E − 01; f = 5.9387E − 01

ITER	SLOPE	DSLOPE	a	da	f	df
1	1.3629E − 01	1.0022E − 06	−5.6096E − 01	5.8107E − 06	5.9386E − 01	−9.6806E − 06
2	1.3629E − 01	4.2861E − 08	−5.6096E − 01	3.6331E − 07	5.9386E − 01	−6.5867E − 07
3	1.3629E − 01	−6.7616E − 08	−5.6096E − 01	−2.5038E − 07	5.9386E − 01	1.6044E − 07

CONVERGENCE OF LOCAL STATE SUCCESSFUL!

LOCAL DEFORMATION CHARACTERISTICS:

Average axial strain,	EXAVE = −4.7204E − 03
Initial local imperfection amplitude,	Wo = 5.0000E − 03
Slope of local buckling nodal lines in skin	M = 1.3629E − 01
Parameter "a" in the expression f*(phi + a*phi**3)	= −5.6096E − 01
Amplitude f in the expression f*(phi + a*phi**3)	= 5.9386E − 01
Normal displacement amplitude between stringers	W = 2.6081E − 01
Number of axial halfwaves at local bifurcation	= 5
Number of axial halfwaves in postbuckled regime	= 7.6523E + 00

Table A.4
Runstream of PANDA2 processors for generation of optimum design, test simulation of optimum design, and evaluation of the optimum design via STAGS

COMMAND	PURPOSE OF COMMAND
BEGIN	Establish the starting design, material properties, boundary conditions. Configuration shown in Fig. 8.
SETUP	PANDA2 prepares certain banded matrix templates.
DECIDE	Choose decision variables, lower and upper bounds, linked variables, inequality constraints.
	Analysis type 1 = Optimization
MAINSETUP	Establish loading, factors of safety, strategy, global and local imperfections, type of analysis.
PANDAOPT	Launch the first batch run for optimization.
PANDAOPT	Launch the second batch run for optimization.
PANDAOPT	Launch the third batch run for optimization.
PANDAOPT	Launch the fourth batch run for optimization.
PANDAOPT	Launch the fifth batch run for optimization.
PANDAOPT	Launch the sixth batch run for optimization.
CHANGE	Change values of the decision variables.
SETUP	PANDA2 re-establishes matrix templates.
PANDAOPT	Launch the seventh batch run for optimization.
PANDAOPT	Launch the eighth batch run for optimization.
CHOOSEPLOT	Plot objective, decision variables, and design margins vs. design iterations.
DIPLOT	Obtain hard copies of plots (Figs. 9–14).
	Analysis type 3 = test simulation of optimized panel
MAINSETUP	Establish test simulation for Load Set 1.
PANDAOPT	Launch batch run for test simulation, Load Set 1.
CHOOSEPLOT	Choose which quantities to plot.
DIPLOT	Obtain hard copies of plots (Figs. 15–19).
MAINSETUP	Establish test simulation for Load Set 2.
PANDAOPT	Launch batch run for test simulation, Load Set 2.
CHOOSEPLOT	Choose which quantities to plot.
DIPLOT	Obtain hard copies of plots (Fig. 20).
MAINSETUP	Establish test simulation for Load Set 3.
PANDAOPT	Launch batch run for test simulation, Load Set 3.
CHOOSEPLOT	Choose which quantities to plot.
DIPLOT	Obtain hard copies of plots (Figs. 21–26).
	Evaluation of optimized panel with the STAGS computer program
Load Set 1 (Single-module model; axial comp.; negative bowing):	
STAGSMODEL	Generate STAGS input files for nonlinear bifurcation buckling corresponding to Load Set 1. Purpose of this run is to obtain initial imperfection shape.
Run STAGS	[22, 23, 52–56]
Get Plot	[57] (Fig. 27)
STAGSMODEL	Generate STAGS input files for nonlinear collapse of imperfect panel corresponding to Load Set 1.

Table A.4 (Continued)

Run STAGS	[22, 23, 52–56]. NOTE: Several runs may be required.
Get Plots	[57, 58] (Figs. 28–32).
Load Set 2	(Single-module model; axial comp.; positive bowing):
STAGSMODEL	Generate STAGS input files for nonlinear bifurcation buckling corresponding to Load Set 2. Purpose of this run is to obtain initial imperfection shapes.
Run STAGS	[22, 23, 52–56]
Get Plot	[57] (Fig. 33)
STAGSMODEL	Generate STAGS input files for nonlinear collapse of imperfect panel corresponding to Load Set 2.
Run STAGS	[22, 23, 52–56]. NOTE: Several runs may be required.
Get Plots	[57, 58] (Figs. 34–38).
Load Set 3	(Six-module model, YES in-plane warping of generators):
STAGSMODEL	Generate STAGS input files for nonlinear bifurcation buckling corresponding to Load Set 3. Purpose of this run is to obtain initial imperfection shape(s).
Run STAGS	[22, 23, 52–56]
Get Plot	[57] (Fig. 40)
STAGSMODEL	Generate STAGS input files for nonlinear collapse of imperfect panel corresponding to Load Set 3.
Run STAGS	[22, 23, 52–56]. NOTE: Several runs may be required.
Get Plots	[57, 58] (Figs. 39 and 41–54).
Load Set 3	(Six-module model, NO in-plane warping of generators):
STAGSMODEL	Generate STAGS input files for nonlinear bifurcation buckling corresponding to Load Set 3. Purpose of this run is to obtain initial imperfection shape(s).
Run STAGS	[22, 23, 52–56]
STAGSMODEL	Generate STAGS input files for nonlinear collapse of imperfect panel corresponding to Load Set 3.
Run STAGS	[22, 23, 52–56]. NOTE: Several runs may be required.
Get Plots	[57, 58] (Fig. 55)

Table A.5
Summary of state of the design with each iteration

RUN NO.	ITERATION NO.	WEIGHT OF PANEL	LOAD SET NO. -> DESIGN IS . . .	FOR EACH LOAD SET . . . . (IQUICK; NO. OF CRITICAL MARGINS) 1	2	3	4	5
1	1	1.7430E + 01	NOT FEASIBLE	(0; 10)	(0; 5)	(0; 3)		
	2	1.9228E + 01	NOT FEASIBLE	(0; 9)	(0; 6)	(0; 3)		
	3	2.1040E + 01	NOT FEASIBLE	(0; 4)	(0; 5)	(0; 2)		
	4	2.1288E + 01	NOT FEASIBLE	(0; 3)	(0; 5)	(0; 1)		
	5	2.1216E + 01	NOT FEASIBLE	(0; 2)	(0; 5)	(0; 1)		
	6	2.1106E + 01	NOT FEASIBLE	(0; 2)	(0; 4)	(0; 2)		
2	7	2.1106E + 01	NOT FEASIBLE	(0; 2)	(0; 4)	(0; 2)		
	8	2.4089E + 01	ALMOST FEASIBLE	(0; 1)	(0; 0)	(0; 0)		
	9	2.1836E + 01	ALMOST FEASIBLE	(0; 0)	(0; 2)	(0; 2)		
	10	2.0932E + 01	NOT FEASIBLE	(0; 1)	(0; 2)	(0; 2)		
	11	2.0460E + 01	ALMOST FEASIBLE	(0; 0)	(0; 1)	(0; 2)		
	12	2.0171E + 01	ALMOST FEASIBLE	(0; 0)	(0; 1)	(0; 2)		

Table A.5 (Continued)

3	13	2.0171E + 01	ALMOST FEASIBLE	(0; 0)	(0; 1)	(0; 2)	
	14	1.9074E + 01	NOT FEASIBLE	(0; 1)	(0; 1)	(0; 2)	
	15	1.8845E + 01	ALMOST FEASIBLE	(0; 2)	(0; 1)	(0; 2)	
	16	1.8700E + 01	ALMOST FEASIBLE	(0; 3)	(0; 1)	(0; 1)	
	17	1.8660E + 01	ALMOST FEASIBLE	(0; 3)	(0; 1)	(0; 2)	
	18	1.8670E + 01	ALMOST FEASIBLE	(0; 1)	(0; 1)	(0; 2)	
4	19	1.8670E + 01	ALMOST FEASIBLE	(0; 1)	(0; 1)	(0; 2)	
	20	1.8634E + 01	ALMOST FEASIBLE	(0; 3)	(0; 1)	(0; 2)	
	21	1.8621E + 01	ALMOST FEASIBLE	(0; 3)	(0; 1)	(0; 2)	
	22	1.8680E + 01	ALMOST FEASIBLE	(0; 1)	(0; 1)	(0; 2)	
	23	1.8664E + 01	FEASIBLE	(0; 3)	(0; 1)	(0; 2)	
	24	1.8632E + 01	ALMOST FEASIBLE	(0; 2)	(0; 1)	(0; 2)	
5	25	1.8632E + 01	ALMOST FEASIBLE	(0; 2)	(0; 1)	(0; 2)	
	26	1.8658E + 01	FEASIBLE	(0; 3)	(0; 1)	(0; 2)	
	27	1.8617E + 01	ALMOST FEASIBLE	(0; 3)	(0; 1)	(0; 2)	
	28	1.8669E + 01	ALMOST FEASIBLE	(0; 1)	(0; 1)	(0; 2)	
	29	1.8635E + 01	FEASIBLE	(0; 3)	(0; 1)	(0; 2)	
	30	1.8614E + 01	ALMOST FEASIBLE	(0; 3)	(0; 1)	(0; 2)	
6	31	1.8614E + 01	ALMOST FEASIBLE	(0; 3)	(0; 1)	(0; 2)	
	32	1.8657E + 01	ALMOST FEASIBLE	(0; 1)	(0; 1)	(0; 2)	
	33	1.8627E + 01	ALMOST FEASIBLE	(0; 2)	(0; 1)	(0; 2)	
	34	1.8610E + 01	ALMOST FEASIBLE	(0; 3)	(0; 1)	(0; 2)	
	35	1.8655E + 01	ALMOST FEASIBLE	(0; 1)	(0; 1)	(0; 2)	
	36	1.8634E + 01	FEASIBLE	(0; 2)	(0; 1)	(0; 2)	CHANGE
7	37	1.8520E + 01	ALMOST FEASIBLE	(0; 0)	(0; 1)	(0; 1)	
	38	1.8324E + 01	FEASIBLE	(0; 0)	(0; 1)	(0; 2)	
	39	1.8297E + 01	FEASIBLE	(0; 0)	(0; 1)	(0; 2)	
	40	1.8288E + 01	FEASIBLE	(0; 0)	(0; 1)	(0; 2)	
	41	1.8300E + 01	FEASIBLE	(0; 0)	(0; 1)	(0; 2)	
	42	1.8305E + 01	FEASIBLE	(0; 0)	(0; 1)	(0; 2)	
8	43	1.8305E + 01	FEASIBLE	(0; 0)	(0; 1)	(0; 2)	
	44	1.8290E + 01	FEASIBLE	(0; 0)	(0; 1)	(0; 2)	
	45	1.8286E + 01	FEASIBLE	(0; 0)	(0; 1)	(0; 2)	
	46	1.8307E + 01	FEASIBLE	(0; 0)	(0; 1)	(0; 2)	
	47	1.8313E + 01	FEASIBLE	(0; 0)	(0; 1)	(0; 2)	
	48	1.8317E + 01	FEASIBLE	(0; 0)	(0; 1)	(0; 2)	(optimum)

Acknowledgment

The author wishes to express his appreciation for the continuing support of Mr. Stan Simson and Mr. Bill Sable, Stress and Fractural Mechanics Department in Lockheed Missiles and Space Company's Satellite Systems Division, under whose sponsorship most of the development of PANDA2 was funded and who supported the production of this paper. The author is indeed grateful to Frank Brogan and Charles Rankin, the developers of STAGS, for their quick responses to requests for modifications in STAGS, and for their patience in teaching the author how to use STAGS and how to write the processor STAGSMODEL in

order to avoid possible numerical difficulties, especially those associated with boundary conditions. The author also wishes to thank W.D. Bushnell and Harold Cabiness for their contributions to the creation of the STAGS postprocessor STAGSPP, by means of which figures such as Figs. 44 and 55 were generated. W.D. Bushnell also modified the PANDA2 plot package DIPLOT to produce figures such as Figs. 9–26. He also performed most of the work required to port PANDA2 to UNIX based operating systems. Ms. Mary Ellen Hasbrouck was responsible for producing the figures in their final forms.

References

[1] A.W. Leissa, Buckling of laminated composite plates and shell panels, AFWAL-TR-85-3069, Air Force Wright Aeronautical Laboratories, Wright-Patterson AFB, Ohio 45433, June 1985.

[2] J.F.M. Wiggenraad, Postbuckling of thin-walled composite structures – Design, analysis, and experimental verification, National Aerospace Laboratory (NLR), The Netherlands, Memorandum SC-86-013 U, 28 February 1986.

[3] R.R. Arnold and J.C. Parekh, Buckling, postbuckling, and failure of flat and shallow-curved, edge-stiffened composite plates subject to combined axial compression and shear loads, AIAA Paper AIAA-86-1027-CP, 27th AIAA Structures, Structural Dynamics and Materials Conference (1986) 769–782.

[4] D. Bushnell, PANDA-Interactive program for minimum weight design of stiffened cylindrical panels and shells, Comput. & Structures 16 (1983) 167–185.

[5] D. Bushnell, Theoretical basis of the PANDA computer program for preliminary design of stiffened panels under combined in-plane loads, Comput. & Structures 27 (1987) 541–563.

[6] D. Bushnell, Computerized Buckling Analysis of Shells (Martinus Nijhoff, Amsterdam, 1985); reprinted by (Kluwer, Dordrecht, 1989).

[7] M. Baruch and J. Singer, Effect of eccentricity of stiffeners on the general instability of stiffened cylindrical shells under hydrostatic pressure, J. Mech. Engrg. Sci. 5 (1963) 23–27.

[8] J.H. Starnes, Jr., N.F. Knight, Jr. and M. Rouse, Postbuckling behavior of selected flat stiffened graphite-epoxy panels loaded in compression, AIAA J. 23 (1985) 1236–1246.

[9] E.E. Spier, On experimental versus theoretical incipient buckling of narrow graphite/epoxy plates in compression, AIAA Paper 80-0686-CP, 21st AIAA Structures, Dynamics and Materials Conference, 1980.

[10] E.E. Spier, Local buckling, postbuckling, and crippling behavior of graphite-epoxy short thin-walled compression members, NASC-N00019-80-C-0174, Naval Air Systems Command, Washington, DC, July 1981.

[11] M.P. Renieri and R.A. Garrett, Investigation of the local buckling, postbuckling and crippling behavior of graphite epoxy short thin-walled compression members, MDC-A7091, McDonnell Douglas Corporation, St. Louis, Missouri, July 1981.

[12] M.P. Renieri and R.A. Garrett, Postbuckling fatigue behavior of flat stiffened graphite/epoxy panels under shear loading, NADC-81-168-60, Naval Air Development Center, Warminster, PA, July 1982.

[13] L.W. Rehfield and A.D. Reddy, Observations on compressive local buckling, post-buckling, and crippling of graphite/epoxy airframe structure, AIAA Paper 86-0923-CP, 27th AIAA Structures, Dynamics and Materials Conference, 1986.

[14] T. Weller, G. Messer and A. Libai, Repeated buckling of graphite epoxy shear panels with bonded metal stiffeners, TAE No. 546, Department of Aeronautic Engineering, Technion, Haifa, Israel, August 1984.

[15] B.L. Agarwal, Postbuckling behavior of composite, stiffened, curved panels loaded in compression, Experimental Mech. 22 (1982).

[16] C. Blaas and J.F.M. Wiggenraad, Development and test verification of the ARIANE 4 interstage 2/3 in CFRP, AIAA 27th Structures, Structural Dynamics and Materials Conference, Part 1 (1986) 307–313.

[17] J.M.T. Thompson, J.D. Tulk and A.C. Walker, An experimental study of imperfection-sensitivity in the interactive buckling of stiffened plates, in: B. Budiansky, ed., Buckling of Structures (Springer, Berlin, 1976) 149–159.

[18] D. Bushnell, A.M.C. Holmes, D.L. Flaggs and P.J. McCormick, Optimum design, fabrication, and test of

graphite-epoxy, curved, stiffened, locally buckled panels loaded in axial compression, in: I. Elishakoff et al., eds., Buckling of Structures (Elsevier, Amsterdam, 1988) 61–131.
[19] N.R. Bauld, Jr. and N.S. Khot, A numerical and experimental investigation of the buckling behavior of composite panels, Comput. & Structures 15 (1982) 393–403.
[20] N.S. Khot and N.R. Bauld, Jr., Further comparison of the numerical and experimental buckling behaviors of composite panels, Comput. & Structures 17 (1983) 61–68.
[21] Y. Zhang and F.L. Matthews, Postbuckling behavior of anisotropic laminated plates under pure shear and shear combined with compressive loading, AIAA J. 22 (1984) 281–286.
[22] B.O. Almroth and F.A. Brogan, The STAGS Computer Code, NASA CR-2950, NASA Langley Research Center, Hampton, VA, 1978.
[23] C.C. Rankin, P. Stehlin and F.A. Brogan, Enhancements to the STAGS computer code, NASA CR 4000, NASA Langley Research Center, Hampton, VA, November 1986.
[24] G.A. Thurston, F.A. Brogan and P. Shehlin, Postbuckling analysis using a general purpose code, AIAA J. 24 (1986) 1013–1020.
[25] T.R. Graves-Smith and S.A. Sridharan, Finite strip method for the post-locally-buckled analysis of plate structures, Internat. J. Mech. Sci. 20 (1978) 833–843.
[26] F. Stoll and Z. Gürdal, Nonlinear analysis of compressively loaded linked-plate structures, AIAA Paper 90-0968-CP, 31st AIAA Structures, Structural Dynamics, and Materials Conference (1990) 903–913.
[27] F. Stoll, Z. Gürdal and J. Starnes, Jr., A method for the geometrically nonlinear analysis of compressively loaded prismatic composite structures, Rept CCMS-91-03 (VPI-E-91-01), VPISU Center for Composite Materials and Structures, February 1991.
[28] D.K. Shin, Z. Gürdal and O.H. Griffin, Jr., Minimum weight design of laminated composite plates for postbuckling performance, AIAA Paper 91-9069-CP, 32nd AIAA Structures, Structural Dynamics, and Materials Conference (1991) 257–266.
[29] E. Riks, A finite strip method for the buckling and postbuckling analysis of stiffened panels in wing box structures, Report NLR CR 89383 L, National Aerospace Laboratory (NLR), The Netherlands, November 1989.
[30] M.S. Anderson and W.J. Stroud, General panel sizing computer code and its application to composite structural panels, AIAA J. 17 (1979) 892–897.
[31] W.J. Stroud and M.S. Anderson, PASCO: Structural panel analysis and sizing code, capability and analytical foundations, NASA TM-80181, NASA Langley Research Center, Hampton, VA, 1981.
[32] W.J. Stroud, W.H. Greene and M.S. Anderson, Buckling loads of stiffened panels subjected to combined longitudinal compression and shear: Results obtained with PASCO, EAL, and STAGS computer programs, NASA TP 2215, NASA Langley Research Center, Hampton, VA, January 1984.
[33] J.N. Dickson, R.T. Cole and J.T.S. Wang, Design of stiffened composite panels in the post-buckling range, in: E.M. Lenoe, D.W. Oplinger and J.J. Burke, eds., Fibrous Composites in Structural Design (Plenum, New York, 1980) 313–327.
[34] J.N. Dickson, S.B. Biggers and J.T.S. Wang, Preliminary design procedure for composite panels with open-section stiffeners loaded in the post-buckling range, in: A.R. Bunsell et al., eds., Advances in Composite Materials (Pergamon, Oxford, 1980) 812–825.
[35] J.N. Dickson and S.B. Biggers, POSTOP: Postbuckled open-stiffened optimum panels, theory and capability, NAS1-15949, NASA Langley Research Center, Hampton, VA, May 1982.
[36] R. Butler and F.W. Williams, Optimum design features of VICONOPT, an exact buckling program for prismatic assemblies of anisotropic plates, AIAA Paper 90-1068-CP, 31st AIAA Structures, Structural Dynamics, and Materials Conference (1990) 1289–1299.
[37] F.W. Williams, D. Kennedy and M.S. Anderson, Analysis features of VICONOPT, an exact buckling and vibration program for prismatic assemblies of anisotropic plates, AIAA Paper 90-0970-CP, 31st AIAA Structures, Structural Dynamics, and Materials Conference (1990) 920–929.
[38] M.-P. Peng and S. Sridharan, Optimized design of stiffened panels subject to interactive buckling, AIAA Paper 90-1067-CP, 31st AIAA Structures, Structural Dynamics, and Materials Conference (1990) 1279–1288.
[39] D. Bushnell, PANDA2–Program for minimum weight design of stiffened, composite, locally buckled panels, Comput. & Structures 25 (1987) 469–605.
[40] G.N. Vanderplaats, CONMIN – A FORTRAN program for constrained function minimization, NASA TM X 62-282, version updated in March 1975, Ames Research Center, Moffett Field, CA, August 1973.

[41] G.N. Vanderplaats and F. Moses, Structural optimization by methods of feasible directions, Comput. & Structures 3 (1973) 739–755.
[42] G.N. Vanderplaats, ADS – A FORTRAN program for automated design synthesis, Version 2.01, Engineering Design Optimization, Inc, Santa Barbara, CA, January 1987.
[43] G.N. Vanderplaats and H. Sugimoto, A general-purpose optimization program for engineering design, Comput. & Structures 24 (1986) 13–21.
[44] D. Bushnell, BOSOR4: Program for stress, buckling, and vibration of complex shells of revolution, in: N. Perrone and W. Pilkey, eds., Structural Mechanics Software Series, Vol. 1 (Univ. Press of Virginia, Charlottesville, 1977) 11–131. See also: Comput. & Structures 4 (1974) 399–435; AIAA J. 9 (1971) 2004–2013; A. Niku-Lari, ed., Structural Analysis Systems, Vol. 2 (Pergamon, Oxford, 1986) 25–54; Comput. & Structures 18 (1984) 471–536.
[45] W.T. Koiter, Het Schuifplooiveld by Grote Overshrijdingen van de Knikspanning, National Luchtvaart Laboratorium, The Netherlands, Report X295, November 1946 (in Dutch).
[46] D. Bushnell, Improvements to PANDA2, Vol. 1; Vol. 2, Part 1; Vol. 2, Part 2, December 1991–January 1992. Unpublished literature distributed with the PANDA2 computer program.
[47] D. Bushnell, PANDA2.NEWS, November 1991, Unpublished literature distributed with PANDA2, also a PANDA2 file that is kept up-to-date.
[48] D. Bushnell, Truss-core sandwich design via PANDA2, AIAA Paper 90-1070-CP, 31st AIAA Structures, Structural Dynamics, and Materials Conference (1992) 1313–1332; Comput. & Structures 44 (1992) 1091–1119.
[49] D. Bushnell and W.D. Bushnell, Minimum-weight design of a stiffened panel via PANDA2 and evaluation of the optimized panel via STAGS, AIAA Paper AIAA-92-2316, 33rd AIAA Structures, Structural Dynamics and Materials Conference (1992) 2586–2618; submitted to Comput. & Structures.
[50] D. Bushnell, Nonlinear equilibrium of imperfect, locally deformed stringer-stiffened panels under combined in-plane loads, Comput. & Structures 27 (1987) 519–539.
[51] D. Bushnell, Use of PANDA2 to optimize composite, imperfect, stiffened, locally buckled panels under combined in-plane loads and normal pressure, in: D. Hui and T.J. Kozik, eds., Design and analysis of composite materials vessels, PVP Vol. 121 (ASME, New York, 1987) 21–42.
[52] C.C. Rankin et al., STAGS user's manual (Latest version, on which the work reported here is based, has not yet been released.).
[53] C.C. Rankin and F.A. Brogan, An element independent corotational procedure for the treatment of large rotations, J. Pressure Vessel Technology 108 (1986) 165–174.
[54] G.M. Stanley, Continuum-based shell elements, PhD Dissertation, Stanford University, Stanford, CA, 1985.
[55] K.C. Park and G.M. Stanley, A curved C_0 shell element based on assumed natural coordinate strains, J. Appl. Mech. 108 (1986) 278–290.
[56] G.M. Stanley, K.C. Park and H. Cabiness, The computational structural mechanics testbed structural element processor ES7: Revised ANS shell elements, NASA CR 4360, NASA Langley Research Center, May 1991.
[57] PATRAN-Plus User Manual, Release 2.4, PDA Engineering, Costa Mesa, California, September 1989.
[58] F.A. Brogan, W.D. Bushnell, H. Cabiness and C.C. Rankin, STAGSPP, A postprocessor for STAGS (not released as of this writing).
[59] E. Riks, Some computational aspects of the stability analysis of nonlinear structures, Comput. Methods Appl. Mech. Engrg. 47 (1984) 219–259.
[60] S. Fan, B. Kröplin and B. Geier, Buckling, postbuckling and failure behavior of composite-stiffened panels under axial compression, AIAA Paper AIAA-92-2285, 33rd AIAA Structures, Structural Dynamics and Materials Conference (1992) 264–273.
[61] C. Rankin, E. Riks and F.A. Brogan, Unpublished work on solution of the mode jumping problem by mixed static and dynamic nonlinear continuation (1992).